FZD-481

Construction and execution of experiments at the multi-purpose thermal hydraulic test facility TOPFLOW for generic investigations of two-phase flows and the development and validation of CFD codes

Final Report

H.-M. Prasser, D. Lucas, M. Beyer, C. Vallée,
E. Krepper, T. Höhne, A. Manera, H. Carl,
H. Pietruske, P. Schütz, A. Zaruba, S. Al Issa, J.-M. Shi, F.-P. Weiß

September 2007

Wissenschaftlich-Technische Berichte
FZD-481 2007 · ISSN 1437-322X

WISSENSCHAFTLICH-TECHNISCHE BERICHTE

Forschungszentrum
Dresden Rossendorf

Wissenschaftlich-Technische Berichte
FZD-481
September 2007

H.-M. Prasser, D. Lucas, M. Beyer, C. Vallée,
E. Krepper, T. Höhne, A. Manera, H. Carl,
H. Pietruske, P. Schütz, A. Zaruba, S. Al Issa,
J.-M. Shi, F.-P. Weiß

Construction and execution of experiments at the multi-purpose thermal hydraulic test facility TOPFLOW for generic investigations of two-phase flows and the development and validation of CFD codes

Final Report

Forschungszentrum
Dresden Rossendorf

Abschlussbericht

Final Report

Reaktorsicherheitsforschung-Vorhaben-Nr./
Reactor Safety Research-project No.: 150 1265

Vorhabenstitel: **Aufbau und Durchführung von Experimenten an der Mehrzweck-Thermohydraulikversuchsanlage TOPFLOW für generische Untersuchungen von Zweiphasenströmungen und die Weiterentwicklung und Validierung von CFD-Codes**

Project Title: **Construction and execution of experiments at the multi-purpose thermal hydraulic test facility TOPFLOW for generic investigations of two-phase flows and the development and validation of CFD codes**

Autoren / Author(s): **H.-M. Prasser, D. Lucas, M. Beyer, C. Vallée, E. Krepper, T. Höhne, A. Manera, H. Carl, H. Pietruske, P. Schütz, A. Zaruba, S. Al Issa, J.-M. Shi, F.-P. Weiß**

Dienststelle der Autoren / Performing Organisation: **Forschungszentrum Dresden-Rossendorf e.V. Institut für Sicherheitsforschung**

Berichtsdatum / Publication Date: **September 2007**

Berichts-Nr. / Report-No.: **FZD-481**

Das diesem Bericht zugrunde liegende Vorhaben wurde mit Mitteln des Bundesministeriums für Wirtschaft und Technologie unter dem Förderkennzeichen 150 1265 gefördert. Die Verantwortung für den Inhalt dieser Veröffentlichung liegt bei den Autoren.

Berichtsblatt

1. ISBN oder ISSN	2. Berichtsart Abschlussbericht
3a. Titel des Berichts Aufbau und Durchführung von Experimenten an der Mehrzweck-Thermohydraulikversuchsanlage TOPFLOW für generische Untersuchungen von Zweiphasenströmungen und die Weiterentwicklung und Validierung von CFD-Codes	
3b. Titel der Publikation	
4a. Autoren des Berichts (Name, Vorname(n)) H.-M. Prasser, D. Lucas, M. Beyer, C. Vallée, E. Krepper, T. Höhne, A. Manera, H. Carl, H. Pietruske, P. Schütz, A. Zaruba, S. Al Issa, J.-M. Shi, F.-P. Weiß	5. Abschlussdatum des Vorhabens 30.09.2006
	6. Veröffentlichungsdatum September 2007
4b. Autoren der Publikation (Name, Vorname(n))	7. Form der Publikation Broschüre
8. Durchführende Institution(en) (Name, Adresse) Forschungszentrum Dresden-Rossendorf e.V. Institut für Sicherheitsforschung Postfach 510119 01314 Dresden	9. Ber.Nr. Durchführende Institution
	10. Förderkennzeichen *) 150 1265
	11a. Seitenzahl Bericht 103
	11b. Seitenzahl Publikation
13. Fördernde Institution (Name, Adresse) Bundesministeriums für Wirtschaft und Technologie (BMWi) 11019 Berlin	12. Literaturangaben 62
	14. Tabellen 3
	15. Abbildungen 74
16. Zusätzliche Angaben	
17. Vorgelegt bei (Titel, Ort, Datum)	

18. Kurzreferat

Ziel der Arbeiten war die Weiterentwicklung und Validierung von Modellen in CFD-Codes. Hierzu wurde am FZD die thermohydraulische Versuchsanlage TOPFLOW aufgebaut und mit räumlich und zeitlich hochauflösenden Gittersensoren ausgestattet. Vertikale Teststrecken mit Nenndurchmessern von DN50 bzw. DN200 für Luft-Wasser- sowie Dampf-Wasser-Strömungen lieferten Ergebnisse zur Entwicklung von Strömungsformen, zum Verhalten der Zwischenphasengrenzfläche sowie zum Wärme- und Impulsaustausch zwischen den Phasen. Die Validierung des CFD-Codes in komplexen Geometrien erfolgte anhand von 3D Gasgehalts- und Geschwindigkeitsfeldern, die bei Umströmung eines asymmetrischen Hindernisses auftreten, das in der Teststrecke DN200 eingebaut war. Im Hinblick auf Strömungen mit freier Oberfläche untersuchte das FZD in zwei horizontalen Acrylglas-Kanälen geschichtete Zweiphasenströmungen im Gleich- bzw. Gegenstrom sowie Schwallströmungen. Bei den Nachrechnungen dieser Versuche gelang die Simulation der Schwallentstehung.

Entsprechend des Projektziels wurden die experimentellen Ergebnisse zur Modellentwicklung genutzt. Bei vertikalen Strömungen stand die Wirkung der lateralen Blasenkräfte (z.B. Liftkraft) im Vordergrund. Zum Test unterschiedlicher Modellansätze wurde hierzu ein Mehrblasenklassen-Testsolver entwickelt und genutzt. Darauf aufbauend wurde ein neues Konzept für ein Mehrblasenklassenmodell, das Inhomogene MUSIG Modell erarbeitet und in den kommerziellen CFD Code CFX (ANSYS) implementiert. Bei Validierungsrechnungen zeigte sich, dass vor allem die Blasenkoaleszenz- und –zerfallsmodelle weiter optimiert werden müssen. Untersuchungen zu Einzeleffekten, wie z.B. die Abschätzung von Turbulenzkoeffizienten und die Analyse der Trajektoren von Einzelblasen in unmittelbarer Wandnähe, lieferten weitere wichtige Ergebnisse des Projekts.

19. Schlagwörter

Zweiphasenströmung, 3D-Gasgehaltsverteilung, 3D-Geschwindigkeitsfeld, CFD-Simulationen

20. Verlag	21. Preis

Document Control Sheet

1. ISBN or ISSN	2. Type of Report Final Report
3a. Report Title Construction and execution of experiments at the multi-purpose thermal hydraulic test facility TOPFLOW for generic investigations of two-phase flows and the development and validation of CFD codes	
3b. Title of Publication	
4a. Author(s) of the Report (Family Name, First Name(s)) H.-M. Prasser, D. Lucas, M. Beyer, C. Vallée, E. Krepper, T. Höhne, A. Manera, H. Carl, H. Pietruske, P. Schütz, A. Zaruba S. Al Issa, J.-M. Shi, F.-P. Weiß	5. End of Project 30.09.2006
	6. Publication Date September 2007
4b. Author(s) of the Publication (Family Name, First Name(s))	7. Form of Publication Booklet
8. Performing Organisation(s) (Name, Address) Forschungszentrum Dresden-Rossendorf e.V. Institut für Sicherheitsforschung Postfach 510119 01314 Dresden	9. Originator's Report No.
	10. Reference No.*) 150 1265
	11a. No. of Pages Report 103
	11b. No. of Pages Publication
13. Sponsoring Agency (Name, Address) Bundesministeriums für Wirtschaft und Technologie (BMWi) 11019 Berlin	12. No. of References 62
	14. No. of Tables 3
	15. No. of Figures 74
16. Supplementary Notes	
17. Presented at (Title, Place, Date)	

18. Abstract

The works aimed at the further development and validation of models for CFD codes. For this reason, the new thermal-hydraulic test facility TOPFLOW was erected and equipped with wire-mesh sensors with high spatial and time resolution. Vertical test sections with nominal diameters of DN50 and DN200 operating with air-water as well as steam-water two-phase flows provided results on the evaluation of flow patterns, on the behaviour of the interfacial area as well as on interfacial momentum and heat transfer. The validation of the CFD-code for complex geometries was carried out using 3D void fraction and velocity distributions obtained in an experiment with an asymmetric obstacle in the large DN200 test section. With respect to free surface flows, stratified co- and counter-current flows as well as slug flows were studied in two horizontal test channels made from acrylic glass. Post-test calculations of these experiments succeeded in predicting the slug formation process. Corresponding to the main goal of the project, the experimental data was used for the model development. For vertical flows, the emphasis was put on lateral bubble forces (e.g. lift force). Different constitutive laws were tested using a Multi Bubble Size Class Test Solver that has been developed for this purpose. Basing on the results a generalized inhomogeneous Multiple Size Group (MUSIG) Model has been proposed and implemented into the CFD code CFX (ANSYS). Validation calculations with the new code resulted in the conclusion that particularly the models for bubble coalescence and fragmentation need further optimisation.

Studies of single effects, like the assessment of turbulent dissipation in a bubbly flow and the analysis of trajectories of single bubbles near the wall, supplied other important results of the project.

19. Keywords

Two-phase flow, 3D-void fraction distribution, 3D-velocity distribution, CFD-simulation

20. Publisher	21. Price

This report is part of a series, which comprise following reports:

- Construction and execution of experiments at the multi-purpose thermal hydraulic test facility TOPFLOW for generic investigations of two-phase flows and the development and validation of CFD codes (Final project report), FZD-481,
- Experiments on upwards gas-liquid flow in vertical pipes, FZD-482,
- Experiments on two-phase flow in a vertical tube with a moveable obstacle, FZD-483,
- Experimental investigation of stratified air/water flows in a horizontal channel, FZD-484,
- Experimental investigation and CFD simulation of slug flow in horizontal channels, FZD-485,
- CFD models for polydispersed bubbly flows, FZD-486,
- Turbulent Dispersion of Bubbles in Poly-dispersed Gas-Liquid Flows in a Vertical Pipe, FZD-487,
- Validation of the Multiple Velocity Multiple Size Group (CFX10.0 N x M MUSIG) Model for Poly-dispersed Multiphase Flows, FZD-487.

All these reports are published as reports of the Forschungszentrum Dresden-Rossendorf.

Dieser Bericht ist Teil einer Serie, die folgende Einzelberichte umfasst:

- Aufbau und Durchführung von Experimenten an der Mehrzweck-Thermohydraulikversuchsanlage TOPFLOW für generische Untersuchungen von Zweiphasenströmungen und die Weiterentwicklung und Validierung von CFD-Codes (Abschlussbericht), FZD-480,
- Experimente zu aufwärtsgerichteten Gas-Flüssig Strömungen in vertikalen Rohren, FZD-482,
- Experimente zur Zweiphasenströmung in einem vertikalen Rohr mit verschiebbarem Hindernis, FZD-483,
- Experimentelle Untersuchung von geschichteten Luft/Wasser Strömungen in einem horizontalen Kanal, FZD-484,
- Experimentelle Untersuchung und CFD-Simulation von Schwallströmung in horizontalen Kanälen, FZD-485,
- CFD Modelle für polydisperse Blasenströmungen, FZD-486,
- Turbulente Blasendispersion in einer polydispersen Rohrströmung, FZD-487,
- Validierung des N x M MUSIG Modells für polydisperse Mehrphasen-strömungen, FZD-487.

Alle Berichte sind als Berichte des Forschungszentrums Dresden-Rossendorf veröffentlicht.

Contents

1. Introduction

1.1 Background

The present report summarizes the main scientific results of the research project "Construction and execution of experiments at the multi-purpose thermal hydraulic test facility TOPFLOW for generic investigations of two-phase flows and the development and validation of CFD codes". The project was funded by the Federal Ministry Economics and Technology of Germany under the topic of reactor safety research. It is embedded into the German CFD alliance, which unites research centres, university groups, code developers, nuclear utilities under the umbrella of the GRS. The coordinated research activities aim at the development and validation of CFD codes for the modelling of safety related three-dimensional single-phase and two-phase flows in nuclear reactors. The long-term goal is the substitution of thermal hydraulic system codes by advanced CFD modelling. From the side of the application, the contributions of FZD concern the thermal fluid-dynamics of the primary circuit. The general focus of the research is the safety of existing nuclear power plants.

The growing interest in CFD in the field of reactor safety is explained by the necessity to increase the independence of accident and transient analyses from empirical correlations, scaling effects and the influence of geometry factors. CFD is based on a numerical solution of the conservation equations for the phases and components of the flow on a grid of calculation nodes that represents the discretized geometry of the flow domain. Indispensable ingredients for a two-phase flow CFD (except in case of DNS) are empirical closure laws describing

- the dynamics of turbulence parameters (also for single-phase flows),
- the interaction of the participating phases (mass, momentum and energy exchange at the gas-liquid interface),
- the dynamics of the gas-liquid interface (i.e. bubble coalescence and breakup, free surfaces etc.)
- and the modulation of turbulence due to the presence of two phases (in case of a continuous liquid phase the enhancement or damping of the liquid turbulence due to the presence of gas bubbles).

Compared to 1D thermal hydraulics, the new quality is given by the fact, that empirical relations in CFD models are geometry independent. The closure laws have to be formulated for the calculation cell, and no more for a specific component with a particular geometry, like T-junctions, valves, fuel rod bundles, pumps etc.

Beside the fact that specific instrumentation is necessary to access to such microscopic processes, the generalizing abilities of CFD have also a consequence for the strategy of experiments. It is no more necessary to keep strict geometric similarity to plant components of interest, since the mesh generation allows a flexible adaptation of the geometry. Therefore, the design of experiments can be much more oriented to the phenomena to be studied. More attention can be paid to the specifics of available instrumentation during the planning of the experimental set-up with the goal to optimise the utilizable output. It is of course a necessary condition, that the phenomena to be studied are present in the experiment, but more freedom in choosing experiment geometry and scenarios can help to provoke the interesting

phenomena in a more pronounced and selective way. These considerations were the basis for choosing the experiments performed in the frame of the present project.

Within the CFD alliance, the TOPFLOW test facility of FZD plays the central role of a multi-purpose experiment for model development and code validation. It belongs to the merits of this thermal fluid dynamic test facility to offer the opportunity of studying a gas-liquid two-phase flow in large scales in a wide range of void fractions and fluid parameters up to close-to-power-plant conditions. The project accomplished by FZD addresses the modelling of gas-liquid flow under conditions where the liquid phase is continuous. This is the application domain of most of the high resolution instrumentation developed by FZD, which is a deciding factor in the project.

The TOPFLOW project is both theory and experiment oriented. The work programme comprised experiments for the development and validation of the aforementioned geometry-independent closure relations necessary for the upgrade of CFD codes, validation tests for both two-fluid models and models for the description of dynamic free surfaces, as well as for the derivation of the model equations themselves and the validation of the code after the implementation of the models. The code chosen by the CFD alliance for application to reactor safety issues is the commercial product CFX developed and distributed by ANSYS. For an efficient execution of the project, FZD concluded a bilateral co-operation contract with ANSYS in order to regulate the mutual exchange of information, the code licensing issues and the co-ordination of joint code validation efforts. This co-operation, which was installed parallel to the co-ordination within the CFD alliance, was one of the main driving factors for the successful accomplishing of the present project.

The present synthesis report gives an overview of the most important results achieved in the project. Most of the results were published in journals and at conferences.

1.2 Experimental work

The aforementioned model development and validation activities inevitably require new experiments using advanced measuring techniques with high resolution in space and time. For this reason, a new thermal-hydraulic, multi-purpose test facility TOPFLOW (Transient Two Phase Flow Test Facility) was erected by the Institute of Safety Research by middle of 2002 (Schaffrath et al., 2001, 2002). TOPFLOW allows two-phase flow experiments at a maximum of 286°C and 7 MPa with a steam mass flow up to 1.4 kg/s (4 MW heating power). A scheme of TOPFLOW is shown in Fig. 1.1, a summary is given by Prasser et al. (2005a and 2005d). An important feature of TOPFLOW is the availability of sensors and measuring techniques that allow a high-resolving characterisation of the shape and dimension of the gas-liquid interface.

The first experimental complex comprises two-phase flow experiments in vertical pipes. This geometry was chosen, because it is much suitable for studying the action of different constitutive relations characterizing the momentum exchange at the gas-liquid interface as well as the dynamic behaviour of the gas-liquid interface itself. The flow can be observed in its movement along the pipe and, in particular, within the velocity gradient close to the pipe wall over a considerable vertical distance and, consequently, over a comparatively long time without the immediate separation of gas and liquid characteristic for horizontal flows.

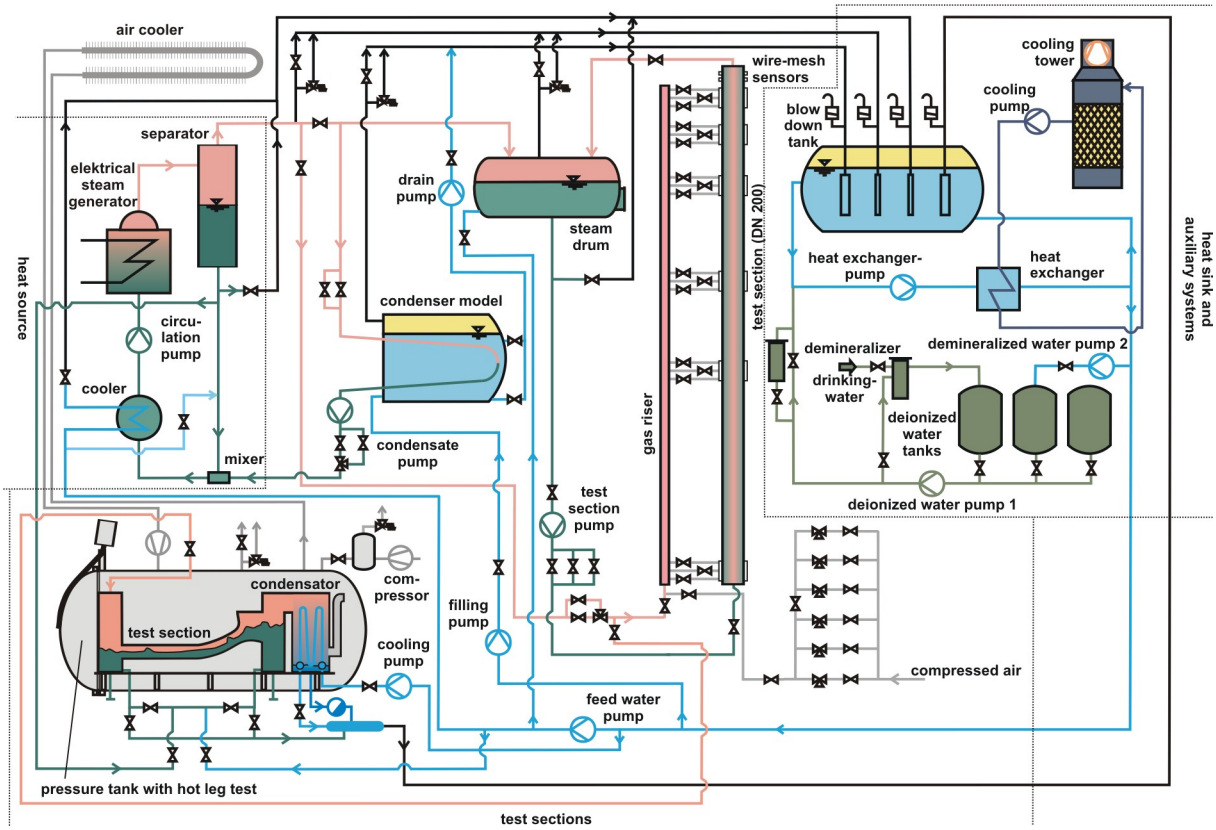

Fig. 1.1 General scheme of the thermal-hydraulic test facility TOPFLOW

The main flow regimes tackled were bubbly flow, slug flow and the transition towards churn-turbulent flow. These flow patterns are characterized by a gas phase that is represented by bubbles of different size and shape. The momentum exchange between gas and liquid is then described by so-called bubble forces, which act either in the main flow direction, like the drag force, or perpendicular to the main flow in the presence of a gradient of the liquid velocity field, which is due to the non-slip conditions at the pipe wall. The latter ones are the so-called non-drag forces. Correlations for the bubble forces are tested by measuring the change of radial gas-fraction profiles along the flow path and comparing them to the predictions of fluid dynamic models, containing the bubble-force correlations to be tested.

In the same time, the gas-liquid interface is changing along the flow direction. In case of the aforementioned flow regimes, the dynamics of the interface is caused by bubble coalescence and breakup. The interface is characterized by the bubble-size distribution, the evolution of which is measured to deliver the basis for the validation of bubble coalescence and breakup models.

A second series of experiments was dedicated to a pronounced three-dimensional flow field around an asymmetric obstacle put into a vertical test pipe. The purpose of these tests is the validation of the CFD code after implementation of new models as a whole against data from a complex flow situation. At the obstacle a number of phenomena are observed that are typical for the flow in components of the industrial installation, like stagnation points, flow separation, recirculation areas, jet formation etc. In these flow regions, the two-phase fluid shows strong spatial non-uniformities of nearly all interesting parameters, including those which characterise the structure of the gas-liquid interface and the turbulence. These are ideal prerequisites for a sensitive code validation. A novel technique was applied to record these parameters

from a domain as extensive as possible. It was achieved by moving the obstacle along the axis of the pipe, while the wire-mesh sensor used for the measurements remained at the same position.

The last class of experiments included in the project were dedicated to the problem of free gas-liquid surfaces often appearing when the time is sufficient for a segregation of gas and liquid. They may display a number of different flow patterns, like stratified, wavy and horizontal slug flow. The application chosen was the flow in the hot-leg of the primary circuit of a pressurized water reactor under counter-current flow conditions during a reflux condenser mode. For experimental studies of the dynamics of the free surface a test section representing the geometry of the hot-leg of a KONVOI type PWR in the scale of 1:3 was designed. In order to achieve a comprehensive optical access to the flow, the test section was designed as a channel with a rectangular cross-section and flat glass side walls, serving as large observation windows. The geometry reflects the reactor outlet, the horizontal part of the main circulation pipe, the bend towards the inlet chamber of the steam generator and, with certain simplifications, the inlet chamber itself. It was planned to execute experiments at saturation conditions with a pressure of up to 5 MPa.

For the hot-leg tests, extensive pre-test calculations were performed. The tests themselves were not able to be performed due to the later described problems in the commissioning of the test channel inside the pressure tank, which serves to maintain the pressure equilibrium.

Parallel to the preparation of the hot-leg tests, horizontal flow experiments with air-water at room temperature and ambient pressure were conducted in two different transparent flow channels. Both had a rectangular shape with a height being larger than the width. Such flow channels are very suitable for the investigation of waves and slug structures by an optical high-speed observation via the side wall. At the same test facilities, PIV measurements of the velocity distribution in the passing slug were performed. These experiments were widely used for the validation of free-surface models in CFX.

The latter measurements in non-pressurized horizontal ducts were not part of the initial project planning. They were included because of the good suitability for code validation. Thanks to these experiments, most of the theoretical project goals concerning the free-surface modelling were achieved despite of the unavailability of the hot-leg test facility.

Two more experimental activities were added to the work plan. In the vertical test section, a series of contact condensation tests was performed. A small sub-cooling of the liquid phase was achieved by throttling the flow downstream of the outlet of the large vertical test section of TOPFLOW. As a result, the injected steam condensed along the flow path. This process was recorded by wire-mesh sensors, which allowed obtaining bubble-size distributions evolving due to a combination of bubble interactions with the bubble shrinkage due to condensation caused by interfacial heat transfer. Furthermore, some small-scale air-water experiments in transparent vertical channels with and without forced convection of the liquid phase were performed, using a high-speed video system for the observation of the gaseous phase.

1.3 Theoretical work

It was the goal of the experiments in the vertical test sections to supply the basis for the theoretical work package, directed towards a multi-disperse two-fluid model for an adiabatic gas-liquid flow at a wide range of gas fractions. The result is presented in form of an extension of the so-called MUSIG model in CFX. In its previous state, the MUSIG model was describing the evolution of the bubble-size distribution due to coalescence and bubble breakup without being able to reflect the bubble-size dependency of most of the interfacial forces, especially that of the so-called non-drag forces, on the bubble diameter. The latter effect leads to a segregation of bubbles, depending on their diameter, which can only be described, if bubbles of different size classes can propagate with different velocities and in different directions. The solution was the implementation of the Inhomogeneous MUSIG model, which unites bubble-size groups into classes, disposing of their individual momentum equation. This model represents a nearly ideal compromise between the realisation of the necessary degrees of freedom to reflect the movement of bubbles of different shapes and a limitation of the arising calculational costs to a feasible extent. The Inhomogeneous MUSIG model, jointly proposed and developed by ANSYS and FZD, has been brought within reach for customers as a part of the code CFX starting from version 10. It is one of the most important results of the TOPFLOW project.

In the frame of the present project, the following theoretical activities were performed by FZD to achieve the aforementioned goal:

Interfacial momentum transfer

Different bubble-force correlations concerning both the drag force and the non-drag forces were tested against experimental data obtained at TOPFLOW in order to select the models with the best correspondence to the radial gas-fraction profiles and to their evolution along the flow path as well as to adjust model coefficients, if necessary. The work was carried out using a so-called simplified test solver, which allows predicting radial distributions for the comparison with the experiments in a very efficient way compared to full CFD simulations. Significant improvements were made, reflected by the fact that the set of validated constitutive equations can reproduce the change from wall-peaked to central-peaked void-fraction distributions if the bubble-size distribution is given. Furthermore, the modelling became scale independent within the range of scales from 50 mm to 200 mm inner diameter, represented by TOFLOW.

Dynamics of the gas-liquid interface

Model equations, available from literature for bubble coalescence and breakup, were checked against measured bubble-size distributions. For this purpose, the simplified test solver was extended to integrate the solution of a population balance. The resulting pre-validated constitutive equations were implemented into the Inhomogeneous MUSIG model of CFX-10. In the next step, post-test calculations of experiments at the vertical test sections were performed, which served for a further tuning of model coefficients.

Interfacial heat transfer

An important element is the modelling of the bubble transfer from one class into another by diameter changes caused by condensation or evaporation. This required a coupling of the population balance equations with an interfacial heat transfer model. As a first step, the contact condensation tests in the large vertical test pipe

were analysed by the help of the simplified test solver. As a result, a heat-transfer model from the literature was identified, which produces the best agreement with the measured void-fraction and bubble-size profiles.

Code validation

The experiments on the evolution of the flow structure along the vertical test sections as well as the measurements on the flow around the asymmetric movable obstacle were used for code validation purposes. The validation of the two-fluid model in CFX started from that of the mono-disperse model, which was successfully predicting the global three-dimensional velocity and void fraction fields around the obstacle. The available experiments were later used to validate CFX with the newly implemented Inhomogeneous MUSIG model.

A second field was the validation of CFX, applied to free-surface flows. The calculations were performed for the horizontal ducts and used the option of the so-called "compressive advective scheme" as an inherent surface sharpening algorithm. It was demonstrated that the code is able to predict spontaneous slug formation in a straight horizontal duct. Furthermore, pre-test calculations of the transient free-surface flow for the geometry of the hot-leg model during counter-current flow limitation revealed periodic slug structures at the steam generator inlet.

The success of the TOPFLOW project is based, to a significant extent, on a number of methodological innovations reported in the following section 2. Most of these novel approaches have a general relevance for research work in the field of two-phase flow modelling and experimentation and can be utilized in future projects.

The main result of the TOPFLOW project is represented by the progress made in the development of the CFD code CFX-10 by the implementation of new or improved models and the validation against experimental data with a high sensibility for the relevant fluid-dynamic phenomena.

2. Methodological innovations

2.1 Vertical test section with variable gas injection system

The choice of vertical pipes for two-phase flow studies was motivated by the fact that evolution of the structure of a gas-liquid flow with a dispersed gaseous phase can be studied over a comparatively long time, in case the flow structure is not changed by a too early phase-separation. This is only the case in straight vertical pipes, where bubbles can be studied in their axial and lateral motion in the bulk and in the shear field close to the wall. Furthermore, bubble coalescence and breakup can be characterized on the basis of the evolution of bubble-size distributions along the flow path. The flow patterns to be considered in vertical pipes are bubbly flow, vertical slug flow, churn-turbulent flow, wispy-annular flow, annular flow and finely-dispersed flow. All these flow regimes were addressed by experiments performed within the project.

For these reasons, vertical pipe flow has always been in the centre of the attention of thermal hydraulic two-phase flow research. The experiments at the vertical test sections of TOPFLOW distinguish themselves by a number of novel characteristics.

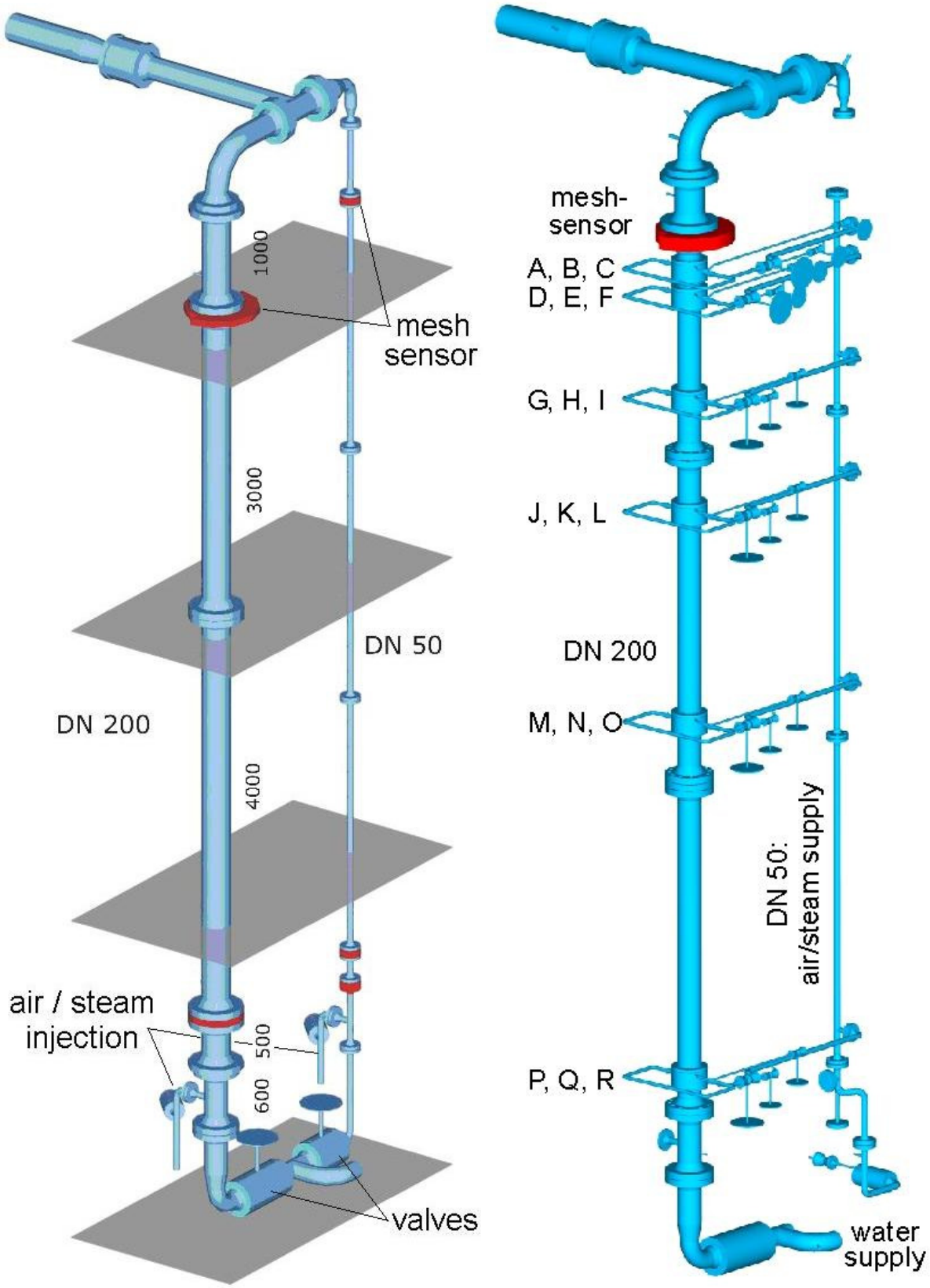

Fig. 2.1 Vertical test sections of the TOPFLOW facility; left: DN50: inner diameter ∅52.3 mm, DN200: inner diameter ∅193.7 mm, right: DN200 with variable gas injection system, inner diameter ∅195.3 mm, both systems: max. pressure: 7 MPa, max. temperature: 286 °C

For the first time, gas-liquid flows in large diameter pipes were studied at fluid parameters close to nuclear reactor conditions with instrumentation capable of characterizing the flow structure in the entire cross-section with a resolution in the range of millimetres and sampling frequencies in the range of some kHz. The combination of steam-water mixture at a pressure of up to 7 MPa with the world-wide leading resolution of the wire-mesh sensor and the pipe diameter of about 200 mm is unique in the field. An important feature of the experiments is furthermore the possibility to perform all tests for comparison also with an air-water mixture at room temperature to obtain information about the influence of the physical fluid properties, as well as the availability of a parallel small test section of 50 mm diameter that allows performing scaling studies (Fig. 2.1, left side).

At TOPFLOW, two vertical test sections with different flow diameters are available. This allowed studying the influence of the scaling on the flow structure. The small test section has a nominal diameter of DN50, while the large one is a DN200 pipe. It is well-known that there is a limit diameter, below which the average gas fraction is diameter dependent. At larger diameters, a further increase does no more cause a change of the void fraction, when the superficial velocities are kept constant. The dimensions of both vertical test sections were selected in the given way to perform measurements both below and above this diameter limit. Another important feature is the capability to run tests at high pressure and temperature which allows studying the influence of the fluid parameters on the flow patterns.

For the construction of the large test section with a nominal diameter of 200 mm (DN200) of TOPFLOW, a special design was chosen: The test pipe was equipped with a variable gas injection system (Prasser et al., 2005d), consisting of six injection units at different heights (Fig. 2.1, right side).

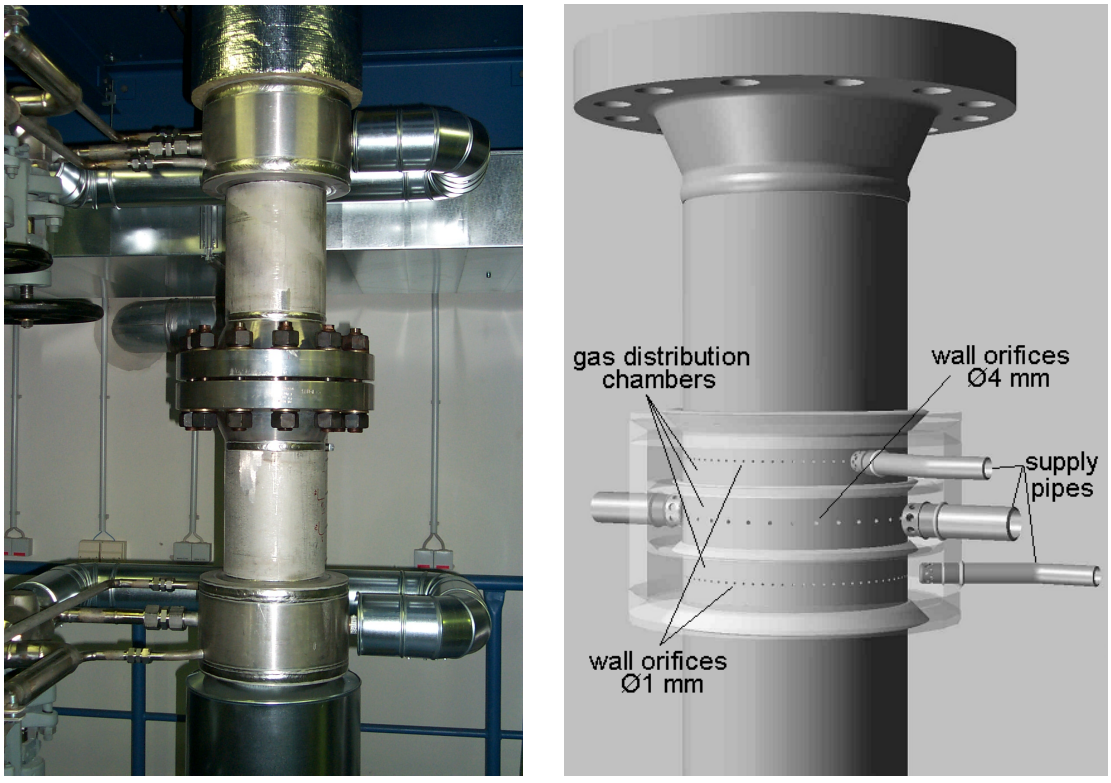

Fig. 2.2 Injection unit of the variable gas injection system at the vertical test section DN200 of TOPFLOW

Each unit has three annular distributing chambers, from which gas or steam enters the test section via a number of orifices in the pipe wall. In order to avoid an obstruction of the cross-section by the gas-injection device for the flow coming from another gas-injection port located upstream, there is no alternative to wall orifices. Injection devices that are accommodated in the pipe cross-section cannot be used here.

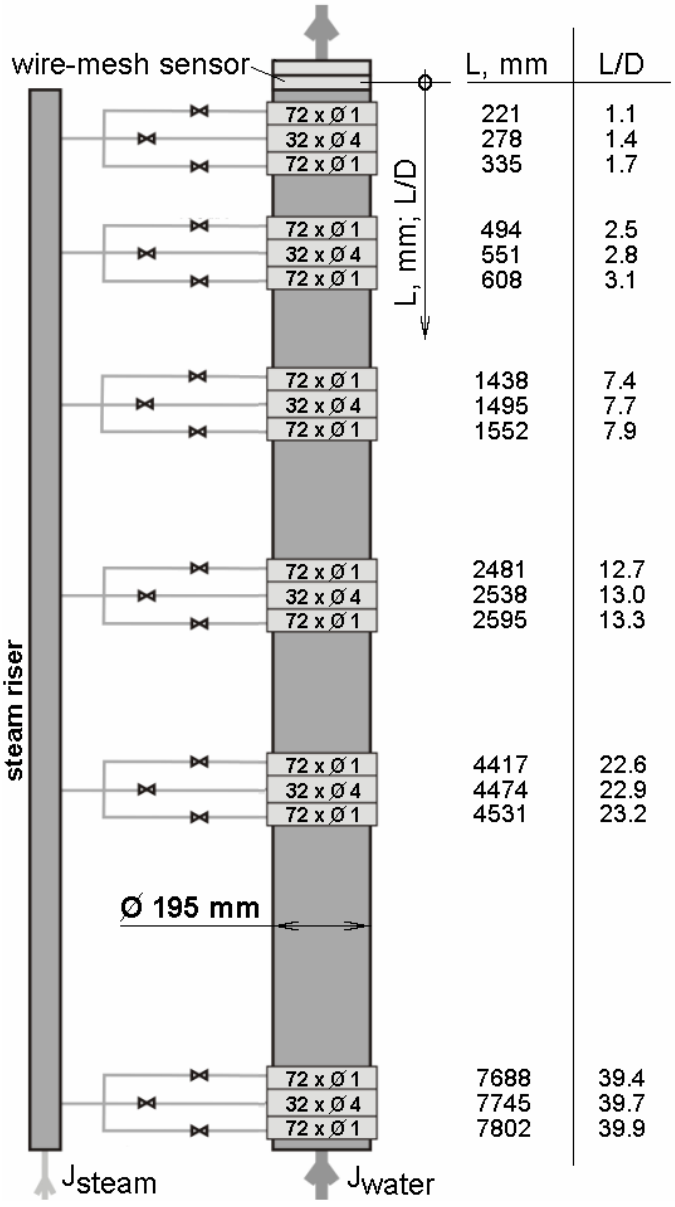

Fig. 2.3 Geometry parameters of the variable gas injection system at the vertical DN200 test section of TOPFLOW

Two different injection diameters allow to change the primary bubble size and to study its influence on the flow structure. The upper and the lower chambers have 72 orifices of 1 mm diameter; the central chamber has 32 orifices of 4 mm (Fig. 2.2). This solution enables to vary the distance between gas-injection and measuring position, the so-called "inlet length", in 6 steps for the orifices of 4 mm and in 12 steps for the small orifices of 1 mm diameter. The latter is an advantage especially close to the sensor position where the axial distance between two rings with 1 mm orifices in one and the same injection unit is still comparable to the distance of the unit from the sensor. For the lower injection units, the distance between both rings of 1 mm orifices becomes insignificant.

The axial positions of the units follow an approximately logarithmic function, namely the distance between neighbouring gas-injection units are increasing with growing distance from the sensor (Fig. 2.3). In this way, it is taken into account that the intensity of the changes of the flow structure decreases with growing distance downstream of the gas injection. Another important option offered by the presence of two rings with 1 mm orifices in each unit is that gas flow rates above the limit flow rate for one ring can be achieved by a parallel operation of both rings. The whole system is designed for an operation at 7 MPa and the corresponding saturation temperature, which allows performing both air-water and steam-water tests under identical boundary conditions.

The steam supply for the injection units comes from a riser pipe of 50 mm nominal diameter, which replaced the small test section. Experiments at the DN50 test section were therefore not possible during the use of the variable gas injection system. Details on the variable gas injection system are given in the separate report ”Experiments on upwards gas-liquid flow in vertical pipes” (see appendix: A 1).

2.2 Development of high-temperature wire-mesh sensors

At the start of the project, wire-mesh sensors were available only for moderate thermodynamic fluid parameters (Prasser et al., 1998). Most of the experiments in the predecessor project (Prasser et al., 2003a) were carried out with an air-water mixture at room temperature and at ambient pressure. For other projects, like the nationally funded water-hammer project accomplished in co-operation with Fraunhofer UMSICHT Oberhausen (Prasser et al., 1999), the EU FP5 projects NACUSP (stability of boiling water reactors) and WAHALoads (Giot & Seynhaeve, 2004), wire-mesh sensors were stepwise upgraded to withstand conditions with considerable shock loads and with higher pressures and temperatures. For water-hammer experiments, the working temperature was increased to 180 °C in a first step. Later, within the WAHALoads project, the first sensor applicable to close-to-reactor conditions was manufactured, which was used in spontaneous water-hammer tests at the PMK-2 test facility of KFKI Budapest. Both types of sensors were equipped with reinforced electrode rods instead of thin wires, which made them less applicable to detailed flow structure studies required in the frame of the TOPFLOW project. Mesh sizes of 16x16 were typical for the application in the aforementioned projects.

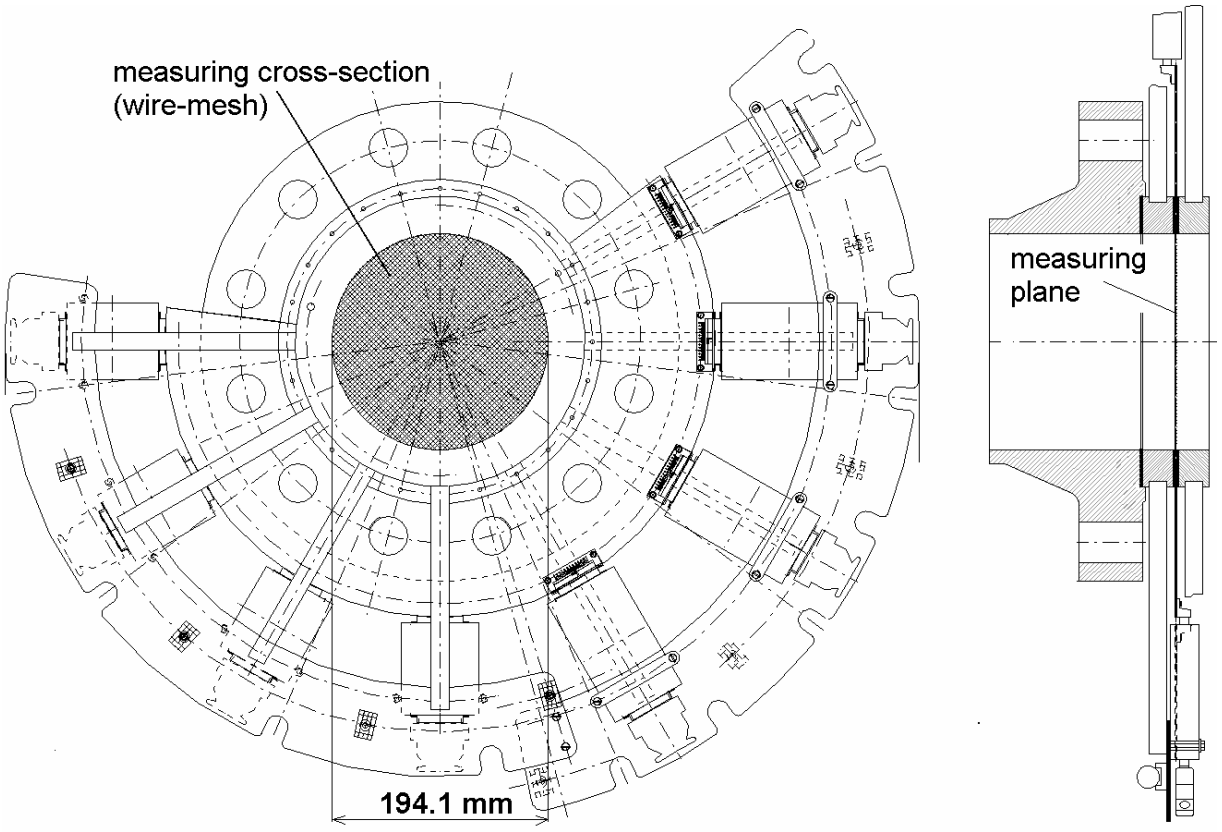

Fig. 2.4 Wire-mesh sensor for air-water tests in the DN200 test pipe with a measuring matrix of 64x64 points

This motivated the further upgrading of the sensors for the TOPFLOW project. For the first experimental series with an air-water flow in the large vertical test section, the development was focused on the increase of the mesh size. Parallel to the TOPFLOW project, the first sensors with a measuring matrix of 64x64 points, forming a grid of 3 mm lateral resolution within the entire cross section of the DN200 pipe was designed (Fig. 2.4). A parallel effort was directed to develop wire-mesh signal acquisition systems granting sufficient measuring frequencies for such large sensor matrices. This work was carried out in a close co-operation with TELETRONIC GmbH (Prasser et al., 2002b).

In the corresponding work package of the TOPFLOW project, it was foreseen to apply wire-mesh sensors in adiabatic steam-water flows under saturation conditions at up to 7 MPa. It was decided to follow the design lines of the sensors for elevated parameters developed for the mentioned water-hammer projects, which meant that compromises concerning the spatial resolution were to be accepted. The use of reinforced electrode rods - apparently the only solution to achieve the necessary mechanical stability of the sensor electrodes - would limit the lateral resolution to about 6 mm and the size of the measuring matrix to 32x32 in case of the DN200 test section.

During the execution of the TOPFLOW project, several new design solutions were developed, which allowed significantly increasing the specifications compared to the project application. The solutions put down in a corresponding patent (Pietruske et al., 2006) makes it feasible to use stainless steel wires as electrodes instead of reinforced profiled rods and to reduce the lateral distance down to 3 mm, achieved earlier in air-water tests. Three high-pressure sensors of this kind were successfully produced and applied, two of them in the DN50 test section and one in the DN200 test pipe. With these results, the requirements of the project description were significantly exceeded.

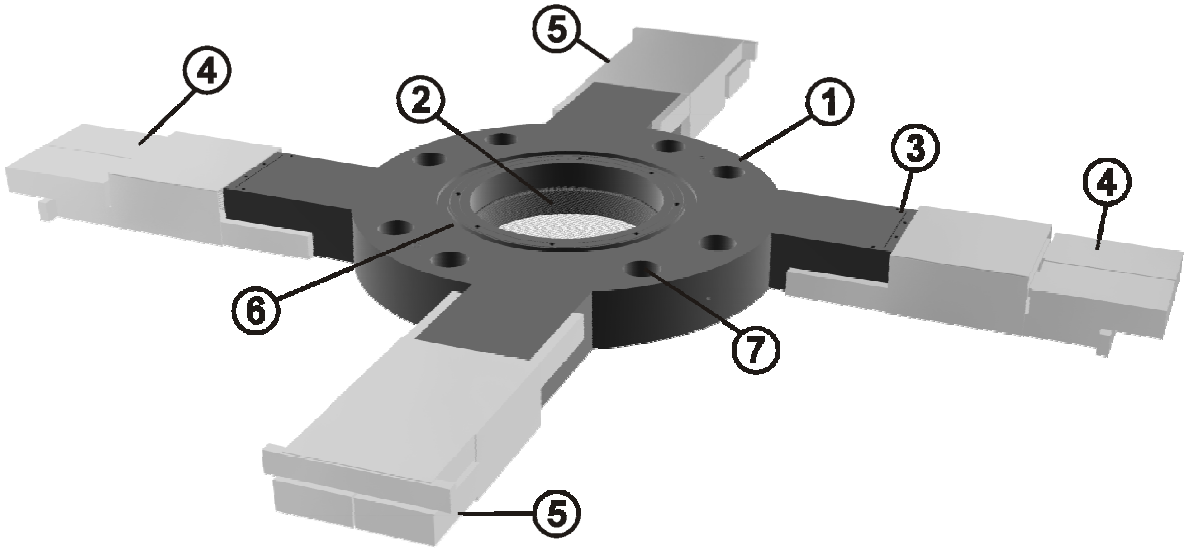

Fig. 2.5 CAD image of the complete sensor for DN200 pipe, 64x64 electrodes: 1 - sensor body, 2 - measuring plane with wires, 3 - location of sealed bushings ("ear"), 4 - driver unit, 5 - receiver pre-amplifier, 6 - cover ring, 7 - bolt hole of flange connection

The sensor for DN200 (Fig. 2.5) consists of 64 receiver- and 64 transmitter wires of 250 µm diameter. The electronic unit is able to perform 2500 samples per second. Since a measuring time of 10 s was chosen, each run resulted in 25000 two-dimensional gas fraction distributions consisting of 64x64 values, i.e. the data array of each measurement has the dimension of 25000x64x64. The inner diameter is identical with that of the test section. The lateral pitch of the wires and the axial distance between the two grids are 3 mm. For the steam-water experiments, the sensor has to withstand the high temperatures and, in particular, temperature changes. For this reason, the wires are suspended with steel springs, which have to be kept outside the measuring cross section in caverns milled into the sensor body (Fig. 2.6).

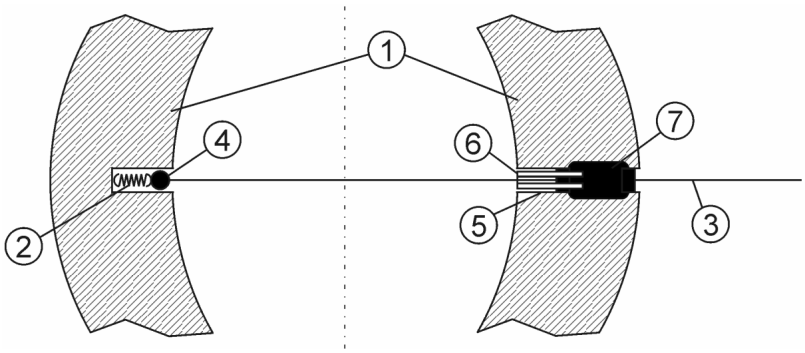

Fig. 2.6 Fixing of electrode wires in the sensor:
1 - sensor body, 2 - spring, 3 - electrode wire,
4 - ceramic insulation pearl, 5 - channel,
6 - ceramic tube, 7 - cavern with epoxy resin

The sealing of electrically through-contacted pressure and temperature resistant bushings for 128 electrode wires was another challenge. The entire construction is so complicated that the sensor body must be divided into two pieces in axial direction. Channels and caverns for bushings and springs are milled into the surface of these half-shells, which are afterwards joined together in a vacuum brazing step.

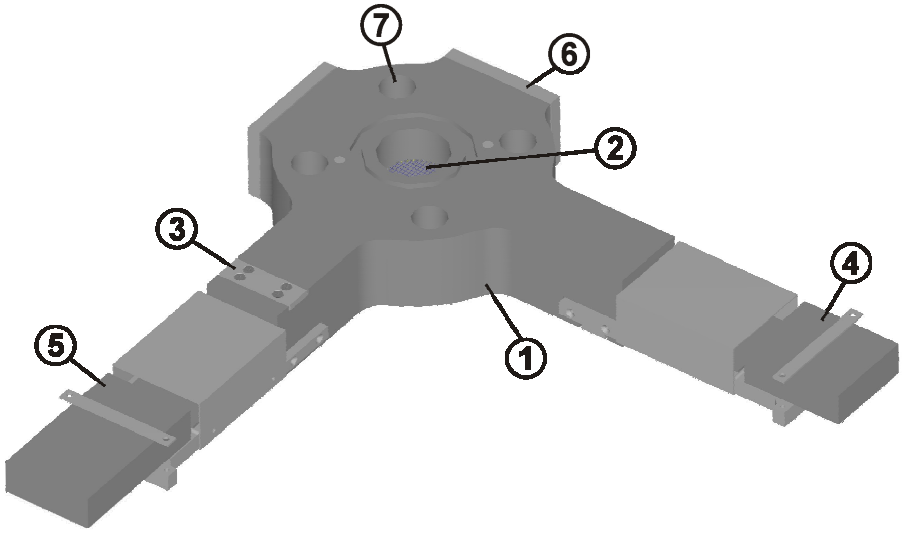

Fig. 2.7 CAD view of the complete sensor for DN50 pipe, 16x16 electrodes:
1 - sensor body, 2 - measuring plane with wires, 3 - location of sealed bushings ("ear"), 4 - driver unit, 5 - receiver pre-amplifier, 6 - cap,
7 - bolt hole of flange connection

A similar design was developed for the sensors of DN50, which dispose of a matrix of measuring points of the dimension of 16x16 (Fig. 2.7). Both sensors are described by Pietruske & Prasser (2005).

2.3 Measurement of complex three-dimensional two-phase flow fields

A novel technique was developed to perform three-dimensional measurements of a two-phase flow in a complicated geometry using a wire-mesh sensor. For this purpose, the large test section with a nominal diameter of DN200 was used to study the flow field around an asymmetric obstacle. The main characteristics distinguishing the experiments with the movable obstacle from earlier available data are:

- Complex flow field with a comparatively large scale,
- high spatial and temporal resolution of the two-phase instrumentation,
- wide range of flow boundary conditions,
- availability of experimental data for different fluid properties thank to a wide variation of the system pressure and temperature,
- acquisition of the gas-fraction and liquid velocity field in a large, three-dimensional domain upstream and downstream of a complex flow obstacle.

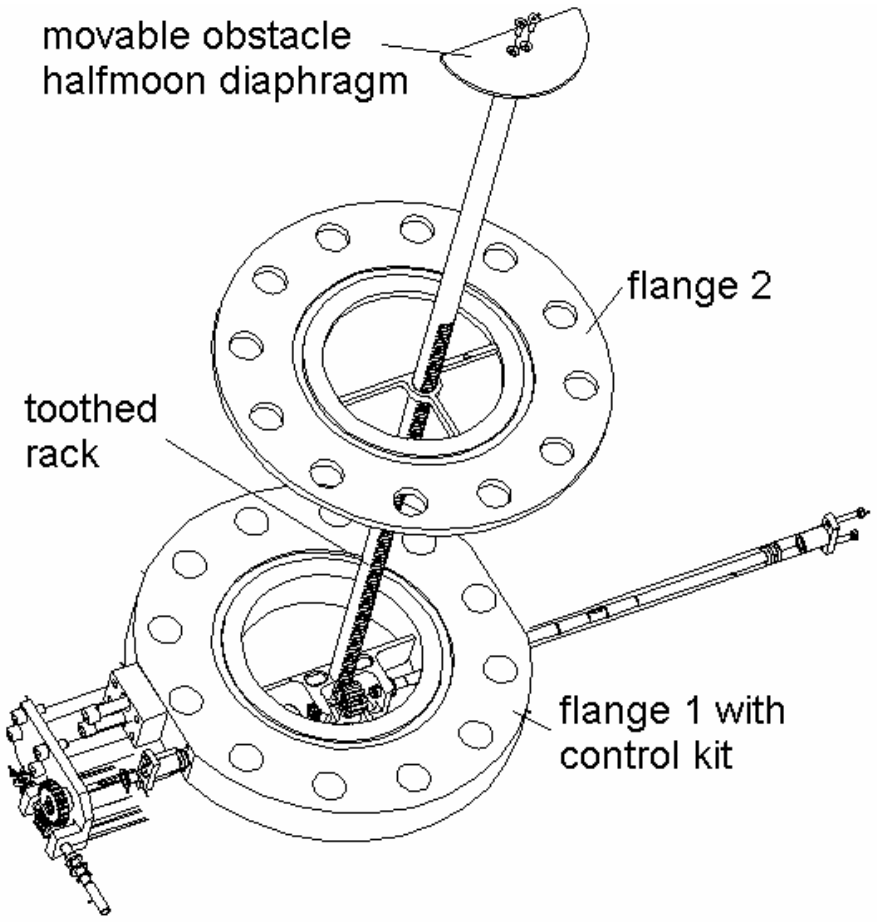

Fig. 2.8 Movable obstacle for the vertical test pipe DN200

The diaphragm used as an obstacle (Fig. 2.8) is a half-moon shaped disk, of which the straight edge is arranged along the diameter of the pipe while the circular edge is at a distance of 10 mm from the inner wall of the pipe. The disk is mounted on top of a toothed rod connected to a translation mechanism to change the axial position of the diaphragm. Both obstacle and moving mechanism can be inverted and mounted either up- or downstream of the wire-mesh sensor shown in Fig. 2.5.

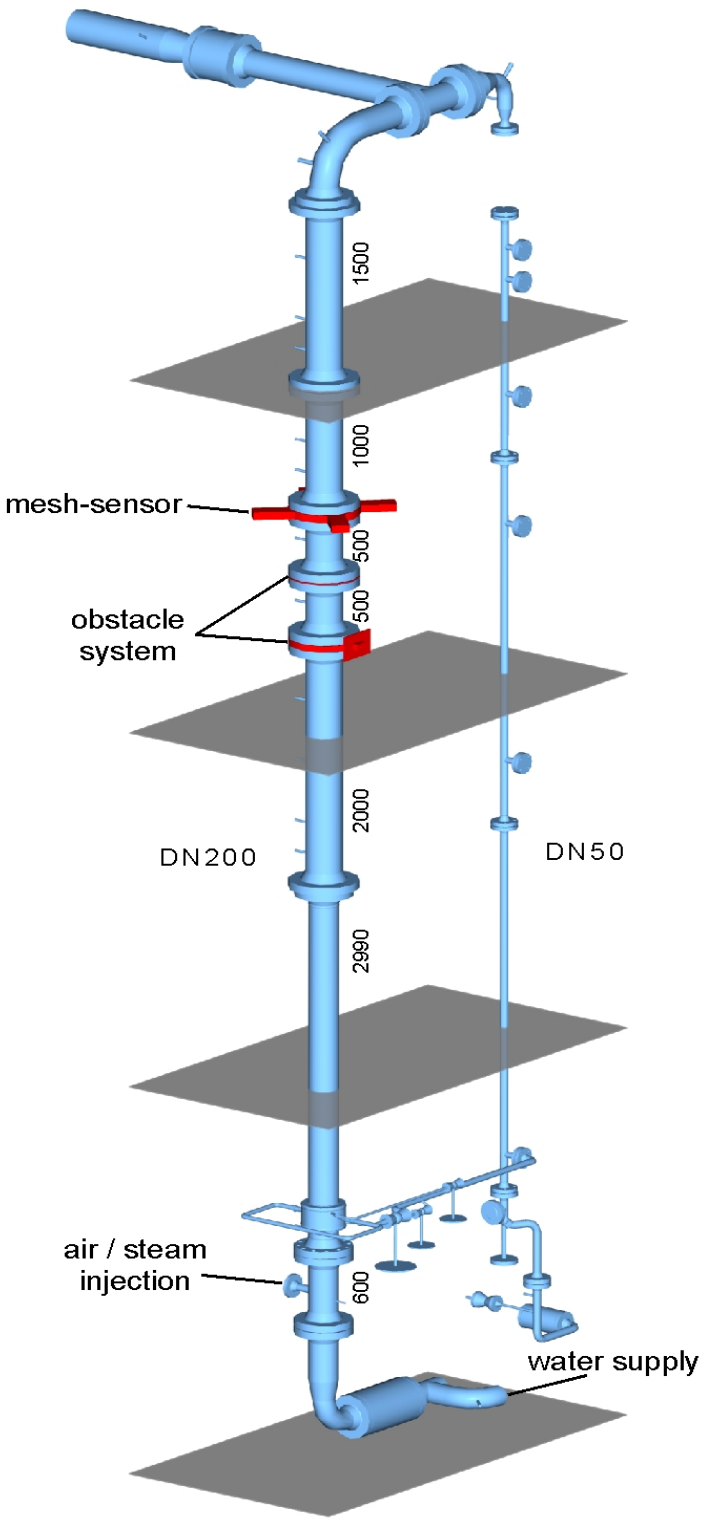

Fig. 2.9 Test section DN200 with sensor and obstacle

The described arrangement (Fig. 2.9) allows acquiring local instantaneous void-fractions from the full cross-section of the pipe with a spatial resolution of 3 mm and with a rate of 2.5 kHz within the three-dimensional flow field around the diaphragm. The distance between sensor and diaphragm can be varied from 10 mm to a maximum distance of 520 mm without moving the sensor position, which is essential to perform high-pressure experiments in an efficient way, i.e. without dismantling and rearranging the test facility each time the measuring position has to be changed (Prasser et al., 2006 a). Details are given in a separate report ”Experiments on two-phase flow in a vertical tube with a moveable obstacle” (see appendix: A 2).

2.4 Measurement of the turbulent dispersion of the gaseous phase

2.4.1 Use of wire-mesh sensor signals

It was demonstrated that a pair of wire-mesh sensors mounted in a short distance behind each other can be used to measure the time-averaged local velocity of the gaseous phase by calculating the cross-correlation function of the time histories of the local instantaneous gas-fraction at the identical location in the measuring plane of both sensors. The most probable time delay between the two sensors, characterized by the delay time of the maximum of the cross-correlation function is interpreted as the average travelling time of the gas bubbles. The velocity is obtained by dividing the distance between the sensors by the delay time (Prasser, 2000; Prasser et al., 2005a).

The action of the turbulence on the motion of bubbles along the flow path provokes a stochastic lateral displacement. Statistical information of this displacement can be obtained by a generalized cross-correlation technique. Instead of only cross-correlating the signals from a pair of identical crossing points of electrode wires in the two sensors, cross-correlation functions are also calculated with a lateral shift (Manera et al., 2005).

The cross-correlation calculated for two positions at a certain axial distance which is kept constant decreases with growing lateral shift. It finally vanishes completely, when a position in the second sensor is reached, which is not accessible for bubbles that crossed the fixed position in the first sensor. In the central region of the pipe, turbulent dispersion dominates over other non-drag forces. The width of the spatial correlation therefore characterizes the statistical movement of the bubbles in the lateral direction caused by turbulence. Since bubbles have a finite size, a cross-correlation of the signals coming from a fixed crossing point in the first sensor and a second, laterally shifted point in the same sensor has also a finite width, which characterizes the average bubble size (ACF in Fig. 2.10).

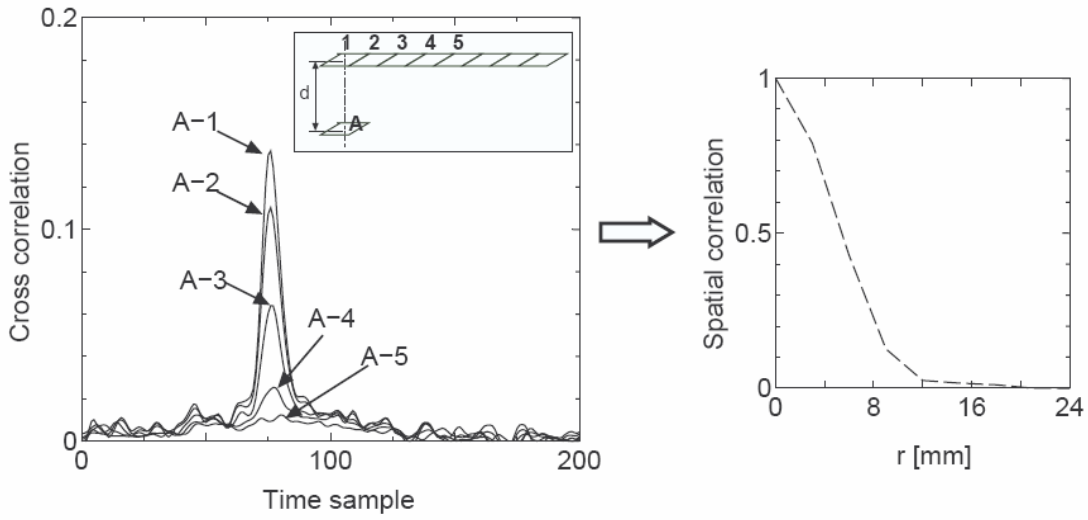

Fig. 2.10 Cross-correlation with an additional lateral shift between two successive wire-mesh sensors; left: time dependent cross-correlation functions, right: decrease of maximum with growing lateral shift

This effect is superposed to the action of the turbulence, which can be separated by deconvoluting the CCF with the ACF, i.e. by seeking a transfer function that converts the ACF into the CCF. For this, a Gaussian distribution of the transfer function was assumed and the dispersion was varied to match the measured CCF by a convolution of the ACF and the transfer function. The width of the Gaussian transfer function contains the information about the turbulent diffusion (Fig. 2.11).

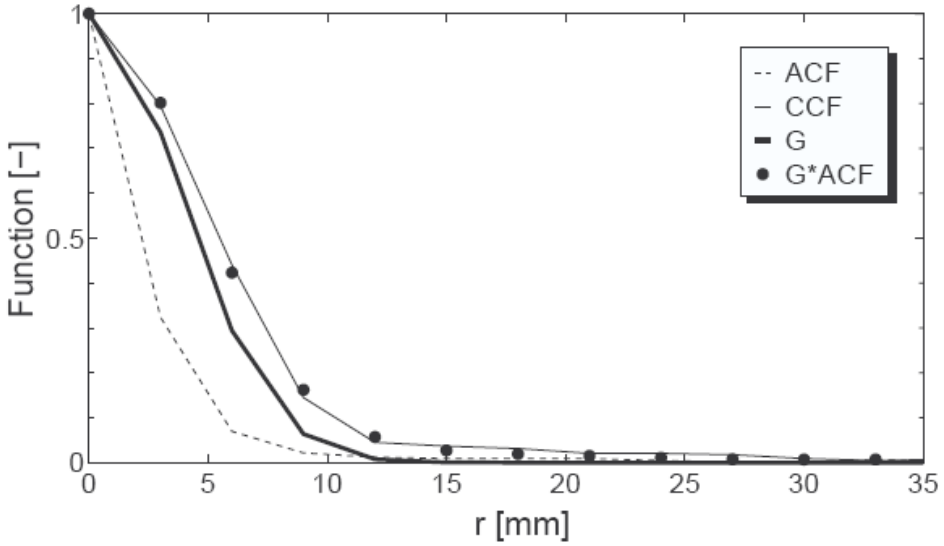

Fig. 2.11 Example for spatial cross (CCF) and auto (ACF) correlation functions, a result of a deconvolution (G) and a test convolution (G*ACF) to show the accuracy of the Gaussean fit

It was found that a turbulent enhancement takes place which is well described by the algebraic equation of Sato & Sekoguchi (1975 and 1981) even in the region of churn-turbulent flow, for which the Sato equation was not validated before (Fig. 2.12).

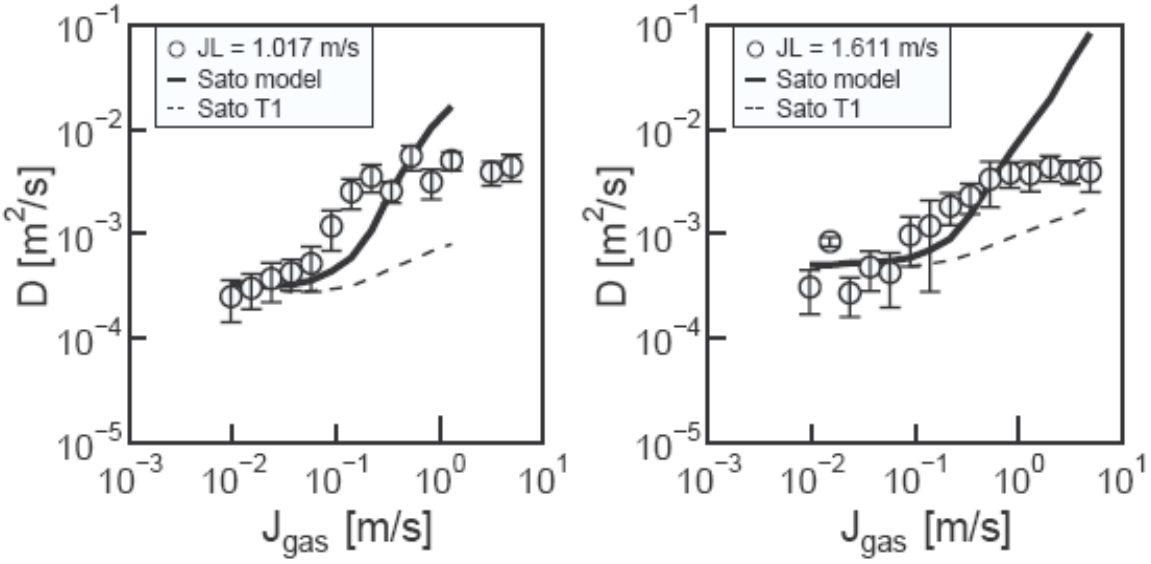

Fig. 2.12 Selected results of the turbulent diffusion coefficient as a function of the superficial air velocity, comparison to the Sato model (Sato et al., 1975 and 1981)

Note that Sato's equation may not be optimal for the application in CFD codes which use transport equations for turbulence quantities, where the aforementioned effects have rather to be reflected by additional source terms in the turbulence model. It was

shown that a sharp increase of the turbulent diffusion observed at a certain superficial gas velocity corresponds to the appearance of very large bubbles in the flow.

2.4.2 Evaluation of optical bubble tracking data

Parallel to the experimental work at TOPFLOW, a number of small-scale test facilities were used to study the motion of air bubbles in water at room temperature and ambient pressure using high-speed video equipment. Bubble tracking algorithms were applied to the captured sequences of the bitmaps recorded by the camera. They provide the coordinates of large ensembles of bubbles, mapped in the two dimensions orthogonal to the aspect direction (Fig. 2.13). Later, a stereo-observation was organized using a mirror system projecting both side-views of a channel with square cross-section to the objective of a single camera. In case of dilute bubbly flow, the extraction of three coordinates of the bubbles as a function of time was achieved.

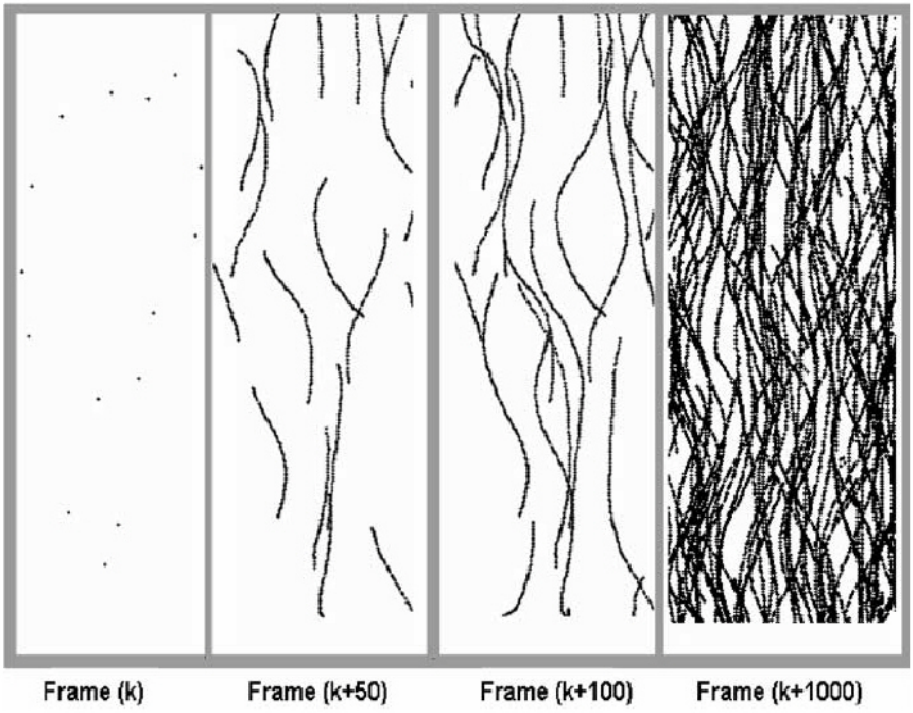

Fig. 2.13 Bubble trajectories obtained from sequences of high-speed camera images in a bubble column of 100x20 mm cross-section

The obtained data of a large number of bubble trajectories were used for a statistic evaluation of the lateral displacement of the bubbles due to the action of turbulence. This is done in the following way: The lateral position of a bubble was fixed when it crosses a horizontal control plane. When the bubble a certain number of camera frames later crosses a second control plane situated at a fixed distance above the first one, the lateral position is different due to the dissipation. The difference of both positions is evaluated statistically by integrating a large number of events in a histogram of the lateral displacement (Fig. 2.14).

The bubble displacement is well described by a Gaussian distribution, the width of which increases with growing axial distance between the pair of control planes. This is illustrated in Fig. 2.14. A pure diffusive dispersion process would lead to a growth of the standard deviation proportionally to the vertical distance.

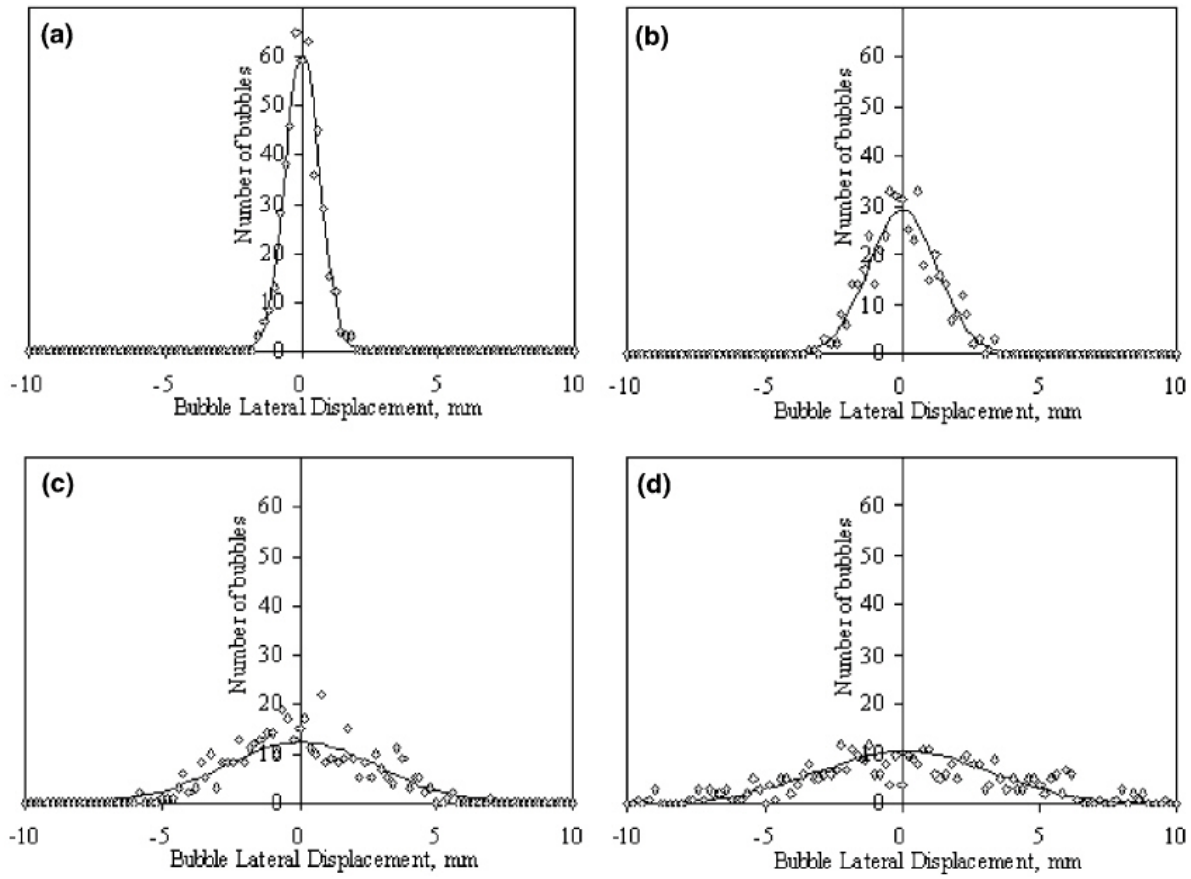

Fig. 2.14 Statistics of the lateral displacement of bubbles (points) and standard Gaussian distribution (solid lines), vertical distance of the control planes: (a) 5 mm, (b) 8 mm, (c) 12 mm, (d) 16 mm

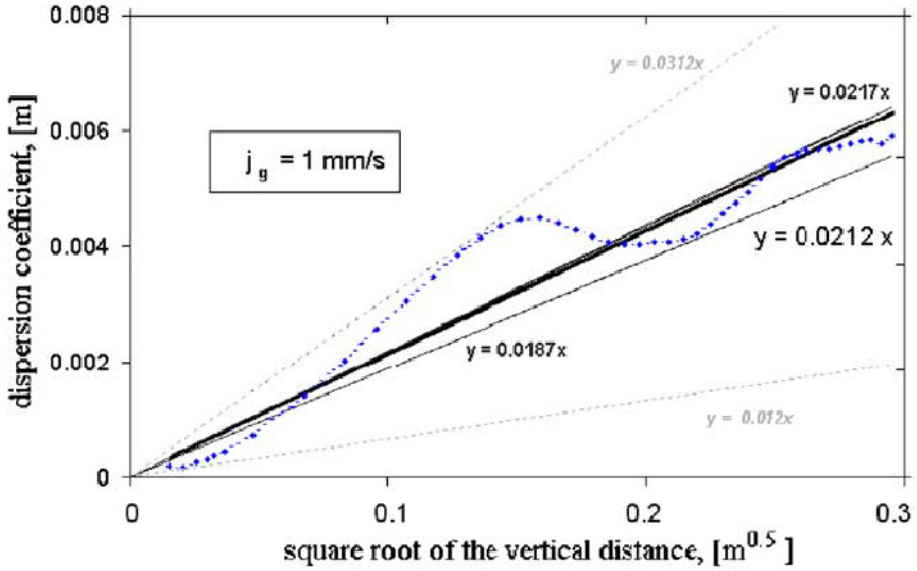

Fig. 2.15 Dispersion coefficients of the Gaussian PDF as a function of the square root of the vertical distance (thick solid line - best linear fit, dotted lines - tangents to points of maximum deviation from linear fit, thin solid lines - tangents to the last two available points of maximum deviation; superficial gas velocity J_G = 1 mm/s)

A linear fit in the co-ordinate system, used in Fig. 2.15, therefore delivers a slope from which the turbulent dispersion coefficient can be assessed. Oscillatory deviations from the linear behaviour are caused by the lateral oscillations of the bubbles. The local maxima and minima of the slope are used to obtain error bands for the dispersion coefficient (Zaruba et al., 2005a, 2005b).

Later, the method was generalized by evaluating both axial and lateral dispersion, which was done in the following way: At a certain instant, an initial position of all bubbles identified in the frame captured by the camera was fixed. The bubbles were tracked in order to determine how far they travel with respect to the fixed initial position. The lateral and axial distance was statistically evaluated by calculating probability density distributions (PDF). The distributions, obtained for the displacement in lateral and vertical directions, widen with growing time. The standard deviation of the distributions was found to be nearly proportional to the square-root of time, which supports the assumption of a stochastic dispersion process that can be nearly described by a diffusion equation.

An evaluation of the PDFs reveals turbulent diffusion coefficients that are close to the values predicted by models from literature. Some deviations of the widening of the PDFs from the square-root-of-time behaviour can be attributed to coherent oscillatory movements of the bubbles in lateral direction and differences in the rise velocity due to varying bubble-sizes.

The described optical method is complementary to the measurement of turbulent diffusion coefficients by cross-correlating wire-mesh sensor signals. The work was performed in the frame of a PhD thesis at FZD.

2.5 Bubble force validation on basis of a bubble trajectory evaluation

The application of the three-dimensional (stereoscopic) bubble tracking method was used to study the trajectories of individual bubbles in a vertically oriented, square channel with forced liquid circulation. The void-fraction was kept very small, so that bubbles moved more or less without mutual influence. It was found that small bubbles with a size of 2-3 mm perform a bouncing at the wall (see Fig. 2.16).

Fig. 2.16 Examples of sliding and bouncing bubbles along a vertical wall (turned by 90 deg), superposed series of high-speed camera frames:
(a): D_{eq} = 2.7 mm, J_L = 0.35 m/s; (b): D_{eq} = 2.4 mm, J_L = 0.4 m/s;
(c): D_{eq} = 2.4 mm, J_L=0.5 m/s

The bubbles move along a nearly parabolic trajectory between two bounces. The maximum distance from the wall as well as the distance between two bouncing

decrease due to energy dissipation. Finally, most of the bubbles reach an equilibrium distance at which they start sliding parallel to the wall. At some flow conditions, sliding bubbles may restart to bounce. This is caused either by an interaction of a vortex with the bubble, or by another bubble passing nearby. It can be assumed that such restart of bouncing becomes more frequent at higher gas fractions.

The trajectory of the bubbles during the bouncing motion was modelled on basis of a momentum equation considering all known forces acting on the bubble. The equation of the "ballistic flight" of the bubble was solved in Lagrangian coordinates. Fig. 2.17 shows the results which were compared to the measured trajectories.

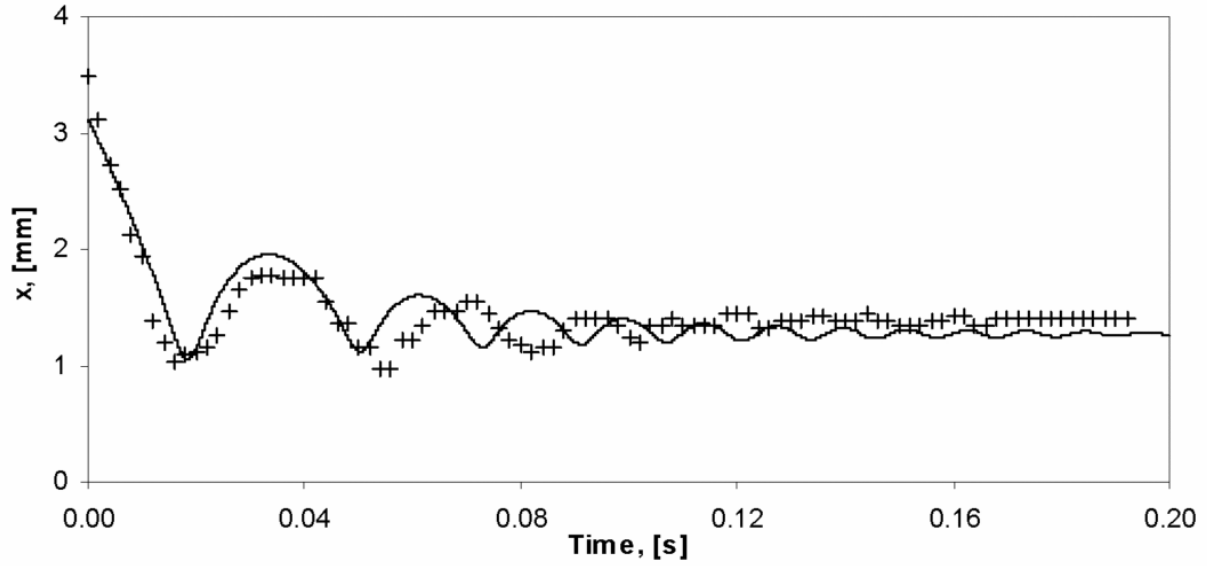

Fig. 2.17 Calculated (solid line) and recorded (separate signs) trajectory of a bubble; D_{eq} = 2.6 mm, J_L = 0.4 m/s

It was shown that the different features of the bubble trajectories depend on the coefficients of the different bubble forces in a characteristic way. This means that the identification of model constants by this comparison leads to a unique set of model parameters. It is found that some bubble-force models present in the literature have to be rejected, because the main characteristics of the bubble trajectory cannot be reproduced. The results are summarized in a paper (Zaruba et al., 2007), where the combination of models is given that results in the best agreement between model and experiment.

2.6 Measurement of the interfacial area in a gas-liquid flow by wire-mesh sensors

In the course of the TOPFLOW project, an algorithm to extract the interfacial area concentration from wire-mesh sensor data was developed (Prasser & Gregor, 2005c). The state of the art is defined to a large extent by the use of local void probes with multiple tips to measure the interfacial area density in a gas-liquid flow. The theoretical basis to use needle-shaped local probes was laid by Ishii (1975). Numerous papers were published by Ishii and his co-workers (eg. Fu & Ishii, 2002a, 2002b, Hibiki & Ishii, 1999, 2000, Kataoka et al., 1986, 1987, Kim et al., 2001, Kim & Ishii, 2001). In order to compare the novel method with those well-established measuring methods, a benchmark experiment with a four-tip electrical probe was carried out in an air-water flow in a 50 mm vertical test pipe at Purdue University, in

the laboratory of Prof. Ishii. The results have shown a good convergence of both approaches. A publication is in preparation (Manera et al., 2007).

Compared to local probes, the application of wire-mesh sensors has the advantage of delivering the total interfacial area in a duct as well as profiles of this quantity without cumbersome traversing of the probe. This opens opportunities to extensive screening experiments over large domains of superficial velocities of the participating phases.

The new method is based on a full reconstruction of the gas-liquid interface from the measured data that is represented by a three-dimensional matrix of local instantaneous gas fractions consisting of a time sequence of two-dimensional gas-fraction distributions. The interfacial area of each bubble is recovered as the sum of the surface area of all surface elements belonging to the given bubble.

Before the reconstruction of the gas-liquid interface is started, a run of the bubble recognition algorithm is executed. After this, each element of the distribution of local instantaneous gas fraction delivered by the sensor is assigned to an individual bubble, using a bubble identification number. This allows the reconstruction of the gas-liquid interface for each bubble individually by taking into account only those gas fractions which belong to the currently analysed bubble.

The full reconstruction is performed in two steps. In the first step, the contour of the bubble is found within the measuring plane for each time step. It is defined as a polygon uniting all points at which the interpolated instantaneous gas fraction is equal to a threshold that characterizes the boundary of the bubble. The interpolation is carried out at the rectangular grid, spanned out by the electrode wires of the sensor (Fig. 2.18).

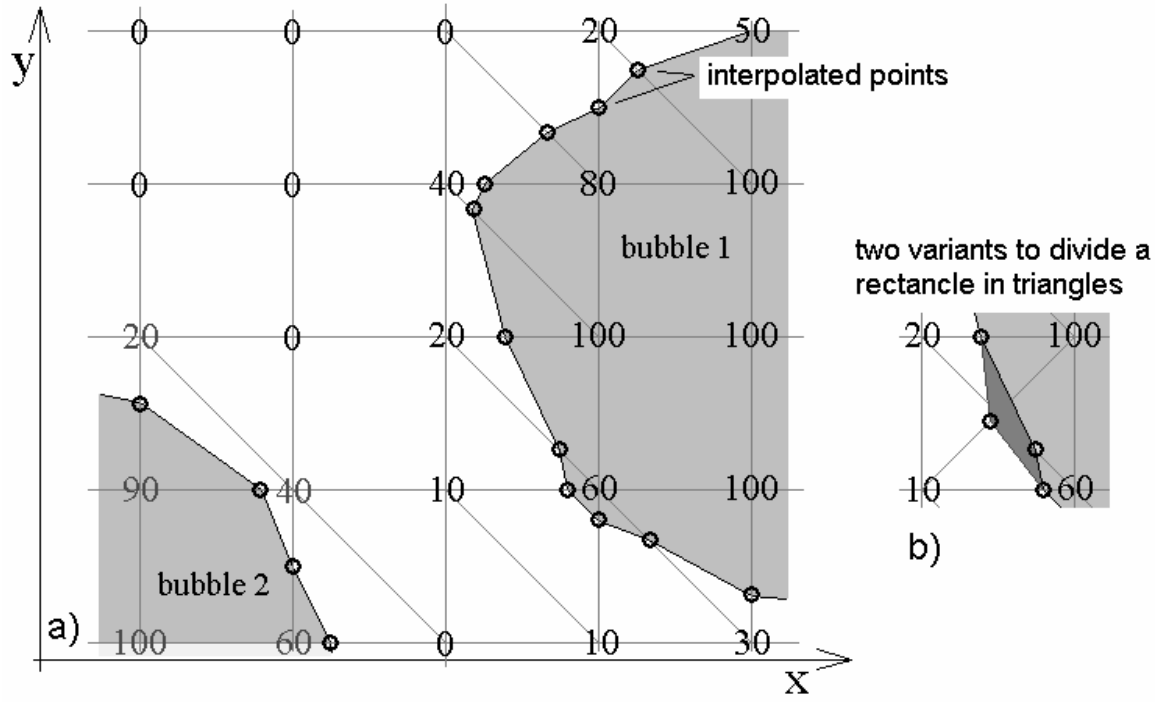

Fig. 2.18 Interpolation of the bubble boundary on the measuring grid for a given threshold

To avoid equivocal situations, each of the square meshes is subdivided in a pair of triangles and an interpolation is also performed at the diagonal. Since there are two

possibilities to define a diagonal, the one is taken, which results in the smaller length of the bubble contour within the mesh. This has proven to supply the best results. In meshes, in which the gas fraction in all four corners is either above or below the threshold, a contour is not found and the corresponding contribution to the contour length is zero.

The second step is carried out in cuboidal control elements formed by the square meshes extended in the axial direction (orthogonal to the measuring plane) by the distance the flow travels in the period between two sampling instants. The axial extension of the control cuboid is defined as the product of the sampling period times and the bubble velocity.

In this step, the area of each surface element of the bubble is calculated which unites the linear bubble boundaries found in the measuring plane in two successive sampling instants. This is done in an approximate way assuming a plain surface. The bubble surface is then the sum of the surface elements found in this way.

In parallel, the part of the area of the rectangular mesh that belongs to the bubble is calculated, too. The total area occupied by the reconstructed bubble, multiplied by the effective height of the control cuboid, supplies the volume of the reconstructed bubble. This is important, because the gas-fraction threshold has to be adapted for each bubble individually.

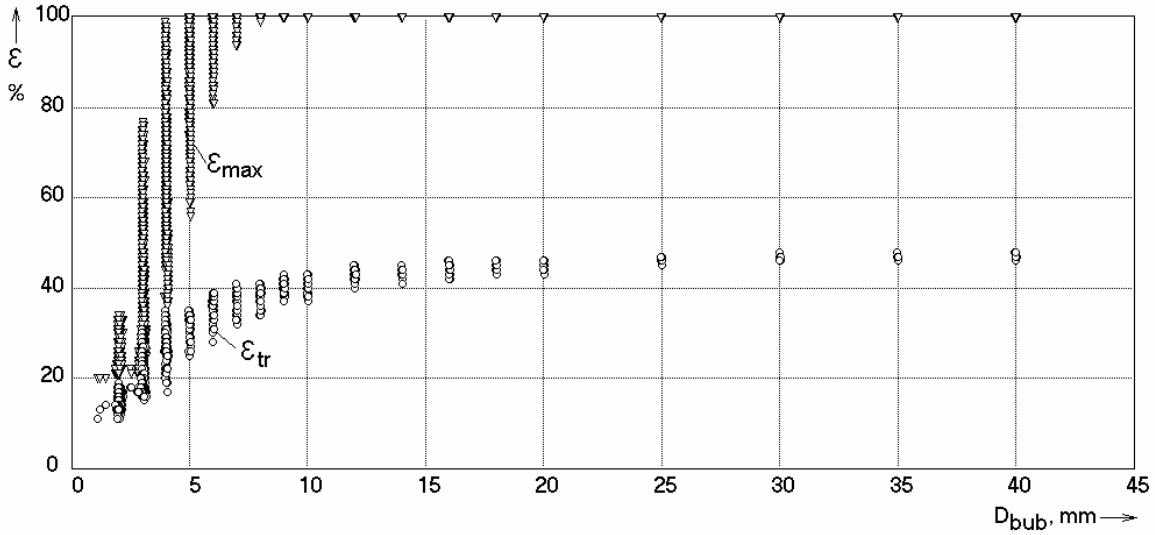

Fig. 2.19 Maximum local instantaneous gas fractions ε_{max} inside synthetic bubbles of selected diameters and the optimal threshold ε_{tr} for the determination of the gas-liquid interface

In fact, it was earlier described (Prasser et al., 2001), that the local instantaneous gas fraction inside a bubble during the passage through the measuring plane has not necessarily to reach unity. Small bubbles do not cover the control meshes completely and the maximum reached remains below 100 % significantly. In such a case, an a-priori chosen threshold may prove to be higher than the maximum of the gas fraction inside the bubble and the resulting interfacial area, but also the volume of the reconstructed bubble, become equal to zero, whereas the integration over the local instantaneous gas fractions in the elements identified to belong to the bubble by the bubble-recognition algorithm is bigger than zero. The problem was solved by iterating the threshold for the reconstruction for each individual bubble until the reconstructed volume becomes equal to the volume found by bubble recognition. It is observed that

the resulting threshold is around the expected value of 50 % for large bubbles, while it starts significantly to lower with decreasing bubble size (Fig. 2.19).

At the end, the interfacial area can be transformed into an area density by relating it to the total volume of the two-phase flow. In case the superficial gas and liquid velocities are known, the total volume of two-phase mixture that passes through the sensor plane is found by multiplying the sum of the superficial velocities by the pipe cross-section and the total measuring time. A combination with bubble size measurements allowed the decomposition of the interfacial area concentration into classes belonging to different bubble sizes.

As an alternative to the described method, it seemed to be convenient to discretize the gas-liquid interface into triangular elements by converting the measuring grid into a grid of tetrahedral elements, the angles of which are identical with the points in which local instantaneous gas fractions are given. This method was found to result in a significant overestimation of the surface area of synthetic bubbles when the height of the control cubiods is small compared to their area in the measuring plane, which is the case when the measuring frequency is high.

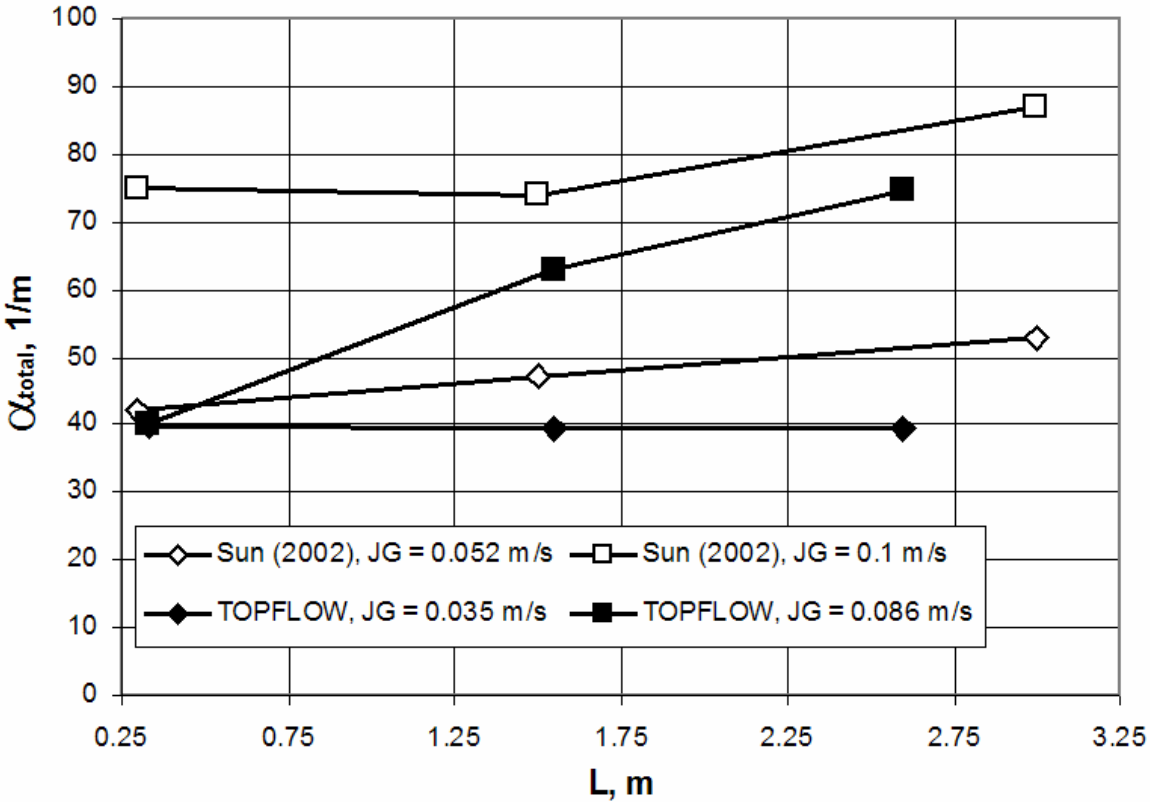

Fig. 2.20 Comparison of total interfacial area densities measured in the 195.3 mm pipe with results of Sun et al. (2002) obtained in a 101.6 mm diameter pipe using a four-sensor conductivity probe, J_L = 1 m/s

The method was applied to a vertical air-water flow (see section 5.2). Since the distance between the sensors and the gas injection was varied using the variable gas injection system, it was possible to characterize the change of the interfacial area concentration along the pipe. On Fig. 2.20 the data was compared with the measurements of Sun et al. (2002). This is the only available publication on interfacial area density measurements in a pipe of larger diameter. Unfortunately, the diameter of the pipe was 101.6 mm instead of 195.3 mm in case of TOPFLOW and the experiments

were performed at slightly different superficial velocities. Furthermore, a different gas injection device was used. On this account the comparison has to remain qualitative. In general, the measurements of Sun et al. (2002) resulted in larger values of the interfacial area, which can partially be explained by the slightly higher gas superficial velocities.

2.7 Pressure equilibrium method for high-pressure fluid-dynamic experiments

Often postulated accident scenarios in pressurized water reactors are connected with the occurrence of stratified flow conditions in the hot or cold legs of the primary circuit. A prominent example is the reflux condenser mode in the course of a small-break LOCA. The modelling of the dynamics of the free surface in case of stratified, wavy or slug flow conditions is therefore an important task for CFD codes applied to reactor safety. It was decided to support the development of free-surface models in CFX by experiments in simplified geometries which are representing the main characteristic geometrical features of the primary circuit hot-leg, while still accessible, to a large extent, to high-resolution instrumentation like high-speed video systems. In the same time, the experiments should be performed at fluid parameters close to the original ones.

A test section representing the geometry of the hot leg of a KONVOI type PWR in the scale of 1:3 was designed: a channel with a rectangular cross-section and flat glass side walls serving as large observation windows. The geometry reflects the reactor outlet, the horizontal part of the main circulation pipe, the bend towards the inlet chamber of the steam generator and, with certain simplifications, the inlet chamber itself.

As a flat model with a depth of 50 mm, the accurate reproduction of counter-current flow limitation (CCFL) maps cannot be expected. The function of the test is rather the characterisation of the dynamic free-surface during CCFL to supply a basis for the code validation. The final goal is the prediction of phenomena like CCFL out of first principles.

Large observation windows of the size shown in Fig. 2.21 are not suitable for high-pressure experiments, unless special solutions are applied. To this end, a completely novel experimental methodology was developed, called "Diving Chamber Technology" (Fig. 2.22). The test section is put in a pressure tank of 7 m length and 2.5 m diameter, which can be pressurized with air and after an upgrade, also with nitrogen, up to a pressure of 5 MPa. For this, the facility is equipped with a compressor station and a nitrogen storage system. The temperature of the inner atmosphere inside the tank is kept below 50 °C by an air circulation system, which is connected to an over-roof cooler. Nevertheless, the test section has of course to be equipped with a good thermal insulation. The identification of a thermal insulation material turned out to be a major problem, which was not solved within the project period. An incident during an insulation test caused signifi-

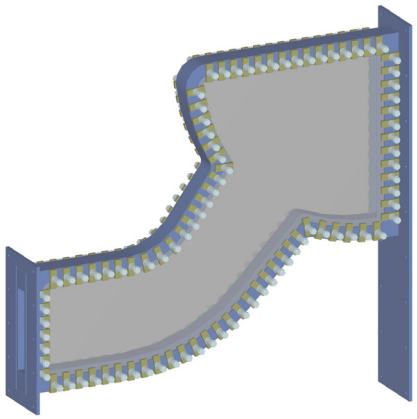

Fig. 2.21 Flat model of a part of the hot-leg of a PWR primary circuit with inlet chamber of the steam generator, equipped with side-walls from glass for video observation

cant damage to the test facility. In the consequence, the hot-leg tests were postponed.

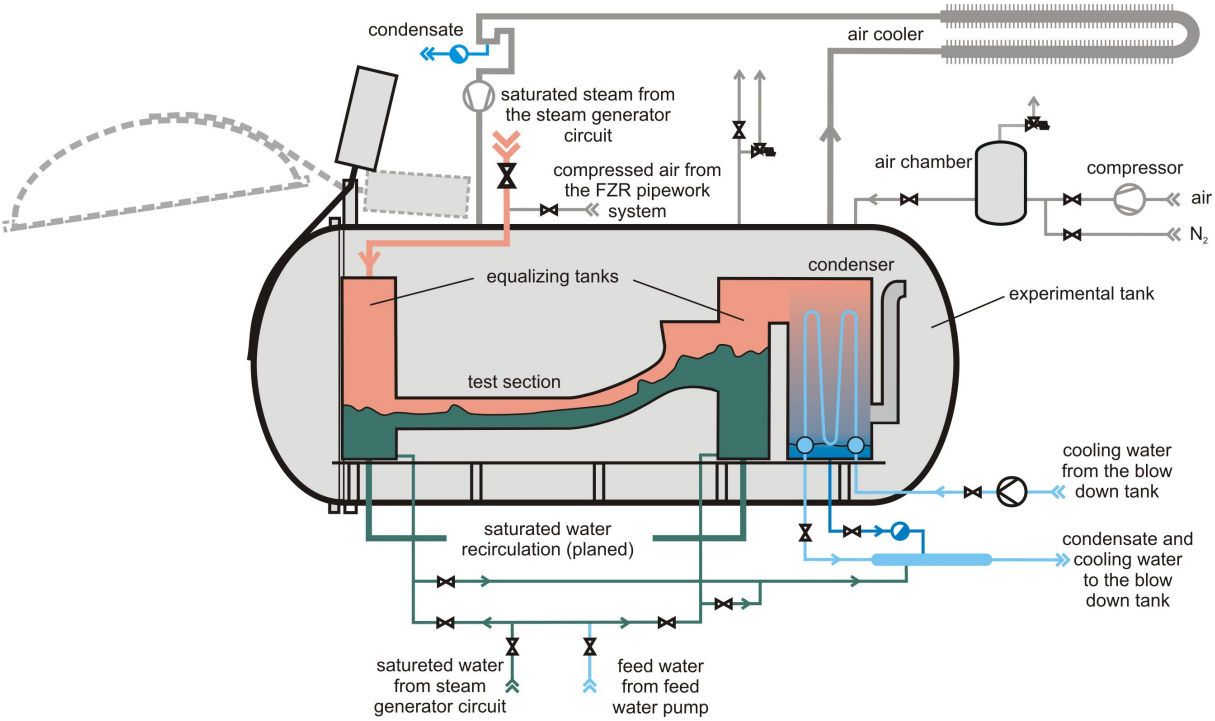

Fig. 2.22 Hot-leg test channel housed by a pressure vessel ("Diving Chamber") for operating test facilities in pressure equilibrium up to 5 MPa, together with the auxiliary systems for pressurization and cooling

A deciding innovation for the operation of the test section in pressure equilibrium is the development of a built-in condenser, which is directly accommodated inside the pressure tank. This condenser is in permanent connection with the exhaust duct of the test section via a large cross-section. Steam is condensed on a bundle of vertical heat exchanger pipes. The steam enters the condenser from the top and flows in the downwards direction while being condensed. In this way, stable density stratification is formed at the point where the steam is completely expired. The condenser is open at the bottom to the inner atmosphere of the pressure tank. In this way, the pressure in the test section is kept at the pressure level inside the tank.

During the commissioning experiments and the insulation tests, the function of the built-in condenser and the strategy of maintaining the pressure equilibrium were successfully demonstrated, together with the efficiency of the heat removal system. It was furthermore shown that counter-current flow-limitation can be reached with the available steam flow rates (Prasser et al., 2006b).

3. Scale dependency of flow patterns and influence of fluid properties

The availability of vertical test sections of two different diameters, equipped with wire-mesh sensors of identical resolution, makes it possible to study the effect of the geometrical scale on the flow pattern. It is well-known that the void fraction dependency from the pipe diameter in a vertical pipe flow vanishes at a certain critical diameter which is correlated by the capillary constant:

$$D_c = \sqrt{\frac{\sigma}{g \cdot (\rho_L - \rho_G)}} \qquad (1)$$

Consequently, it was assumed that at the critical diameter, which is a multiple of D_c, a characteristic transition in the flow structure has to be expected. Ohnuki et al. (1996) and (2000) indeed describe the qualitative observation that slug flow is no more found when the pipe diameter is large enough. In air-water experiments at 24 m tall vertical test pipes of 200 mm diameter the authors observed an immediate transition from bubbly to churn turbulent flow.

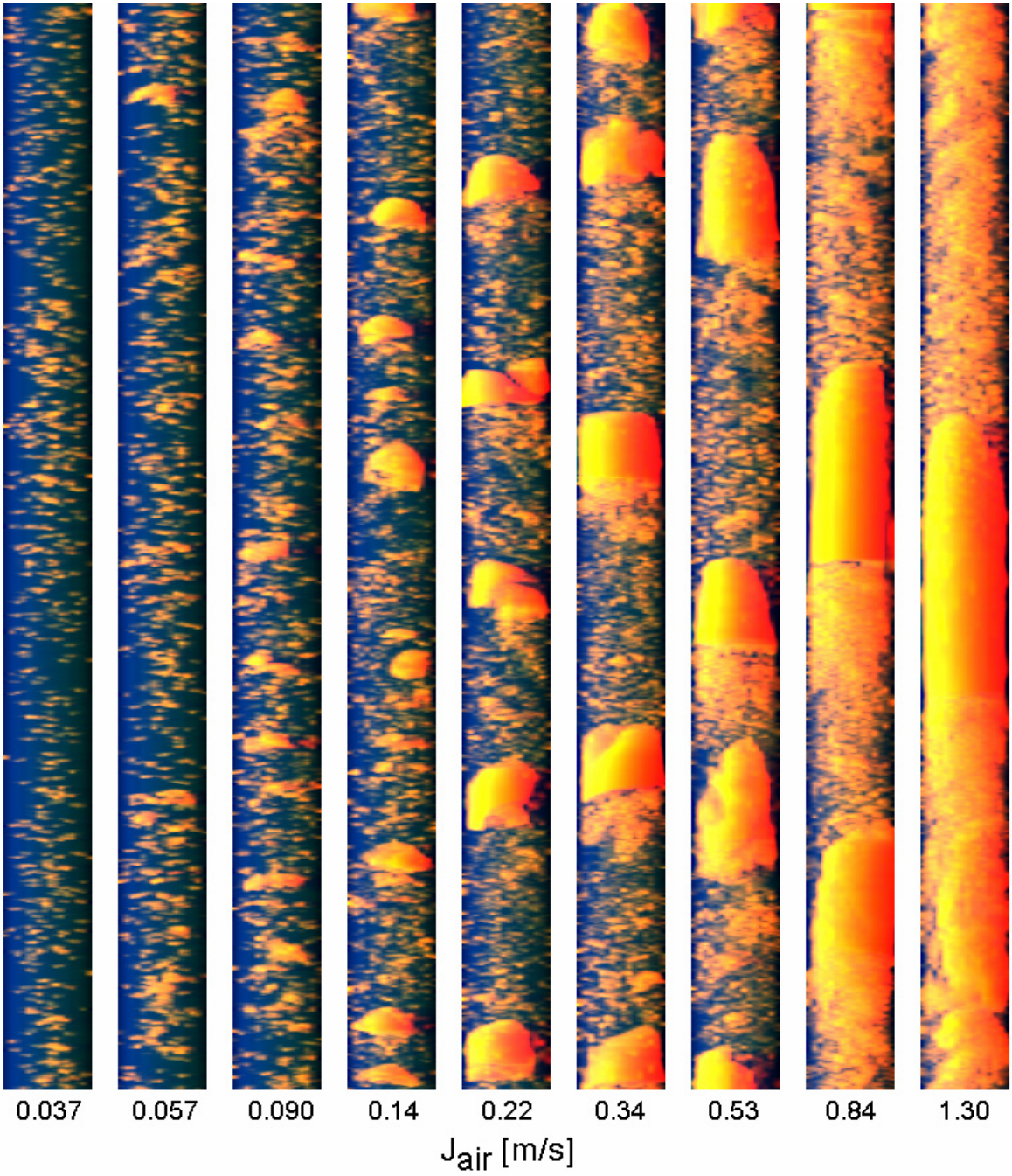

Fig. 3.1 Virtual side projections of the void distribution in the DN50 test section, J_L = 1.017 m/s, relation vertical to horizontal scale = 1:1, height scaled according to average gas phase velocity

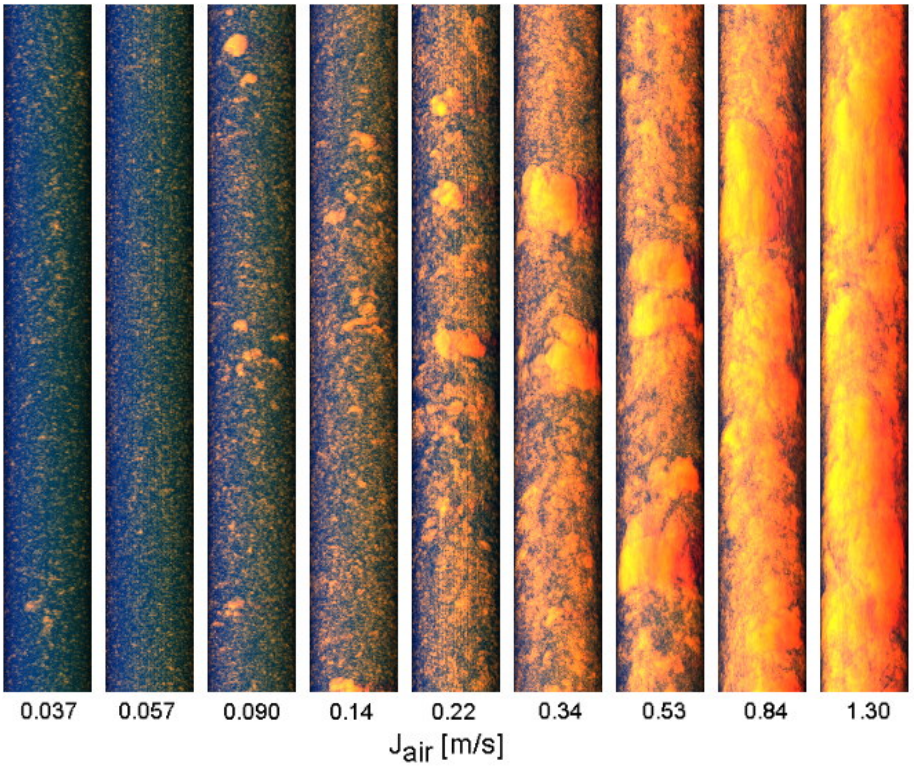

Fig. 3.2 Virtual side projections of the void (colour from red to yellow) distribution in the DN200 test section, J_L = 1.017 m/s, relation vertical to horizontal scale = 1:1, height scaled according to average gas phase velocity

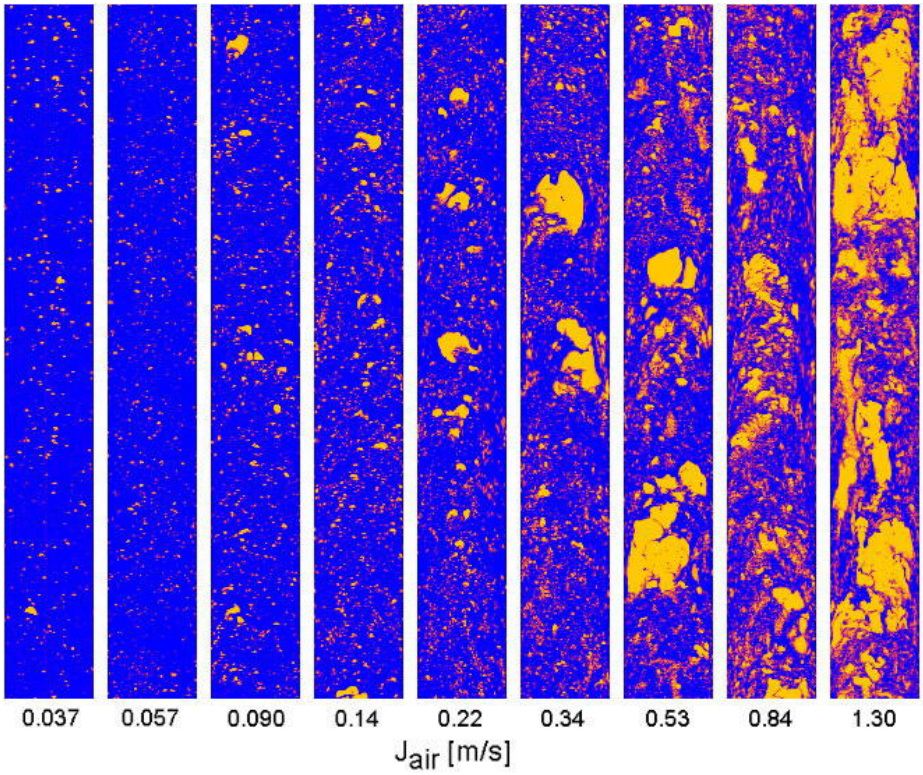

Fig. 3.3 Virtual sectional views of the void distribution in the DN200 test section, J_L = 1.017 m/s, relation vertical to horizontal scale = 1:1, height scaled according to average gas phase velocity (colours: air = yellow, water = blue)

In our experiments at the vertical test sections DN50 and DN200 of TOPFLOW as well as in comparison to earlier measurements at MTLoop this behaviour was confirmed. Large Taylor bubbles which are typically found under slug flow conditions in the test pipe DN50 (Fig. 3.1) are not present in the large DN200 pipe (Fig. 3.2 and Fig. 3.3). Nevertheless, an increase of the superficial gas velocity leads to the appearance of large bubbles also in the large pipe. The corresponding bubble-size distributions become bimodal (Fig. 3.4), but in contrast to the conditions in the small pipe, the large bubbles are much more deformed under the action of the stronger turbulence and due to the less pronounced confining effect of the pipe walls. The large bubble peak is much wider and less high in case of the larger pipe, but also the peak of the small bubble is wider in the large pipe. All in all, the bubble size distribution seems to be closer to an equilibrium distribution than in the small pipe, where the movement of large bubbles is very much determined by the confining action of the walls.

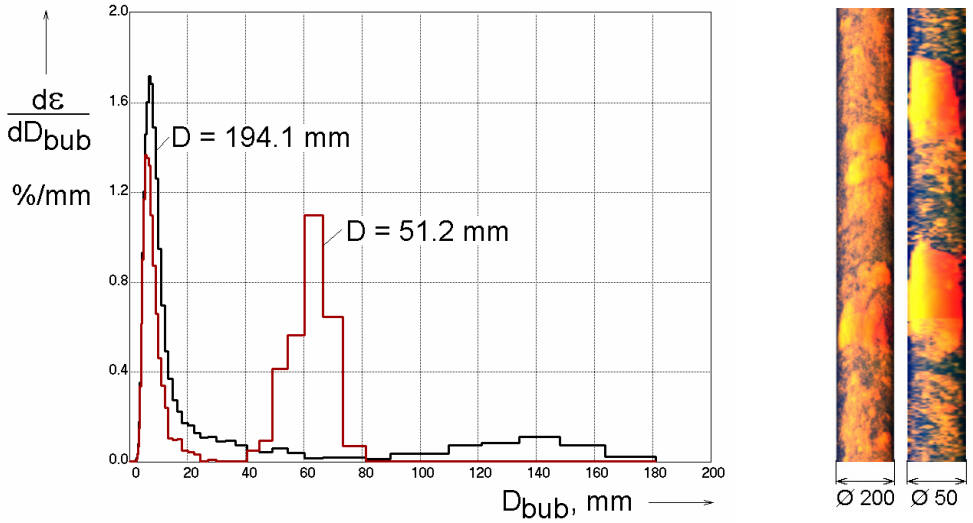

Fig. 3.4 Comparison of bubble size distributions in DN50 and DN200 test sections for an air flow rate typical for slug flow in pipes of small diameter; J_G = 0.534 m/s, J_L = 1.017 m/s

This effect was carefully studied in order to exclude that the findings are biased by a misinterpretation of the influence of the inlet length. It has to be questioned whether the relative inlet length L/D or rather the absolute inlet length is responsible for the establishing of the flow structure, since the latter defines the travelling time of a fluid element, in which the flow structure evolves, while the evolution of the radial profiles is dependent on L/D. As shown in Fig. 3.5, the scale dependency of the bubble-size distributions is observed independently of the fact whether L/D or L is kept constant, when the diameter is varied.

In the large pipes, large bubbles are much more freely distributed over the cross-section and the turbulence is able to deform them in a more intensive way. The resulting bubble sizes and shapes are far from the classical Taylor bubbles (Fig. 3.6 to Fig. 3.8, see Prasser et al., 2005a).

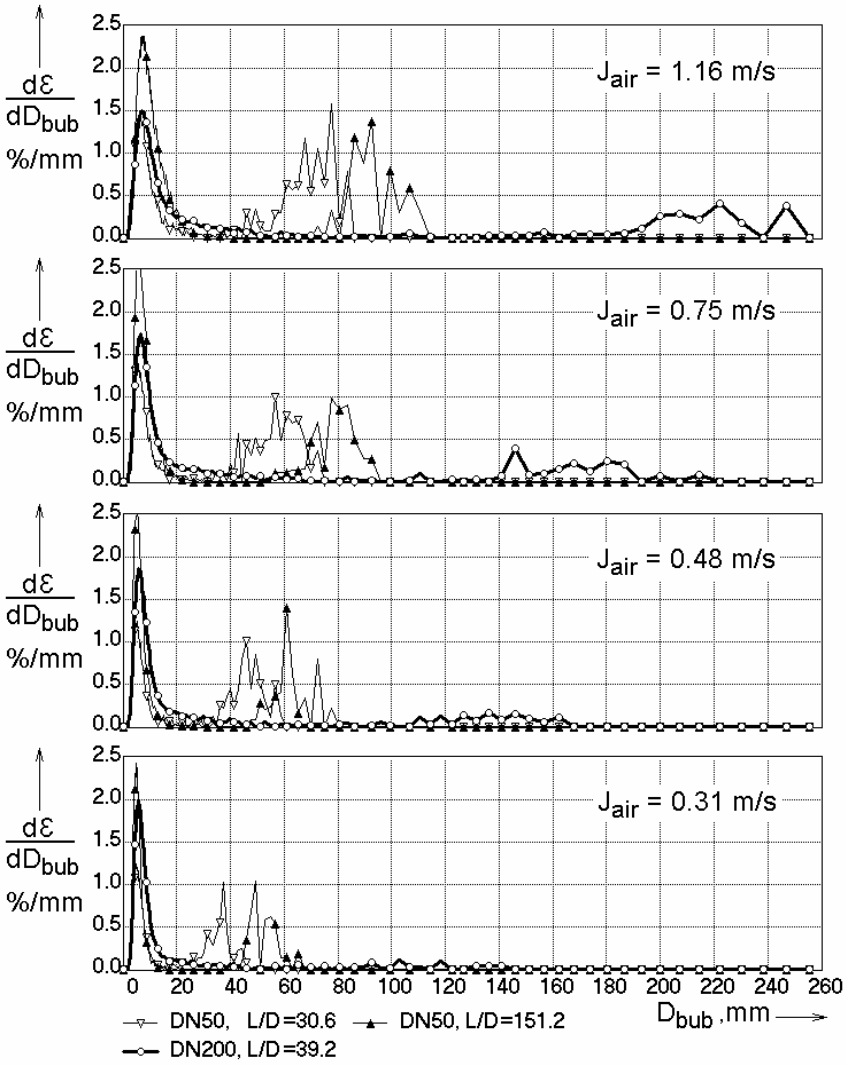

Fig. 3.5 Bubble size distributions in the test sections DN50 and DN200; J_L = 1.017 m/s, J_G > 0.2 m/s

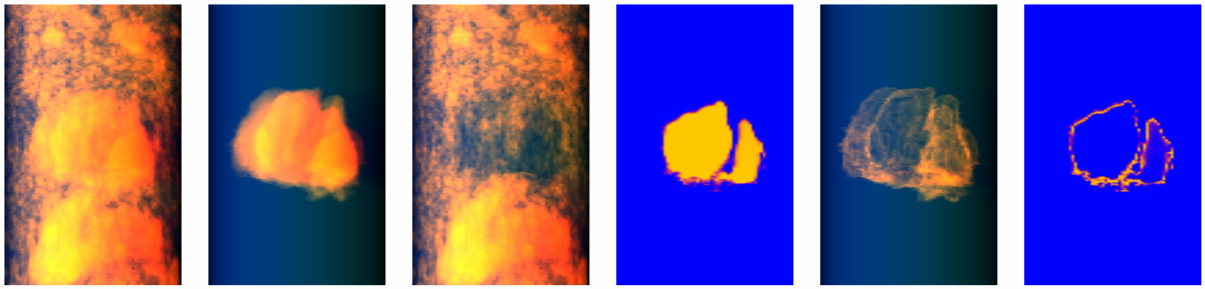

Fig. 3.6 Analysis of a large isolated bubble (flow see Fig. 3.2) extracted from the signal of the wire-mesh sensor (superficial velocities: J_G = 0.534 m/s and J_L = 1.017 m/s)

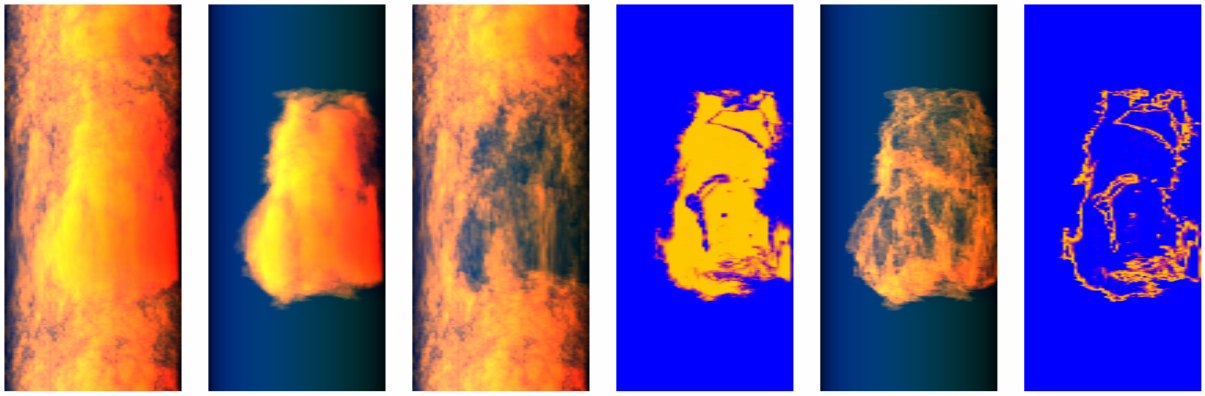

Fig. 3.7 Analysis of a large isolated bubble (flow see Fig. 3.2) extracted from the signal of the wire-mesh sensor (superficial velocities: J_G = 0.835 m/s and J_L = 1.017 m/s)

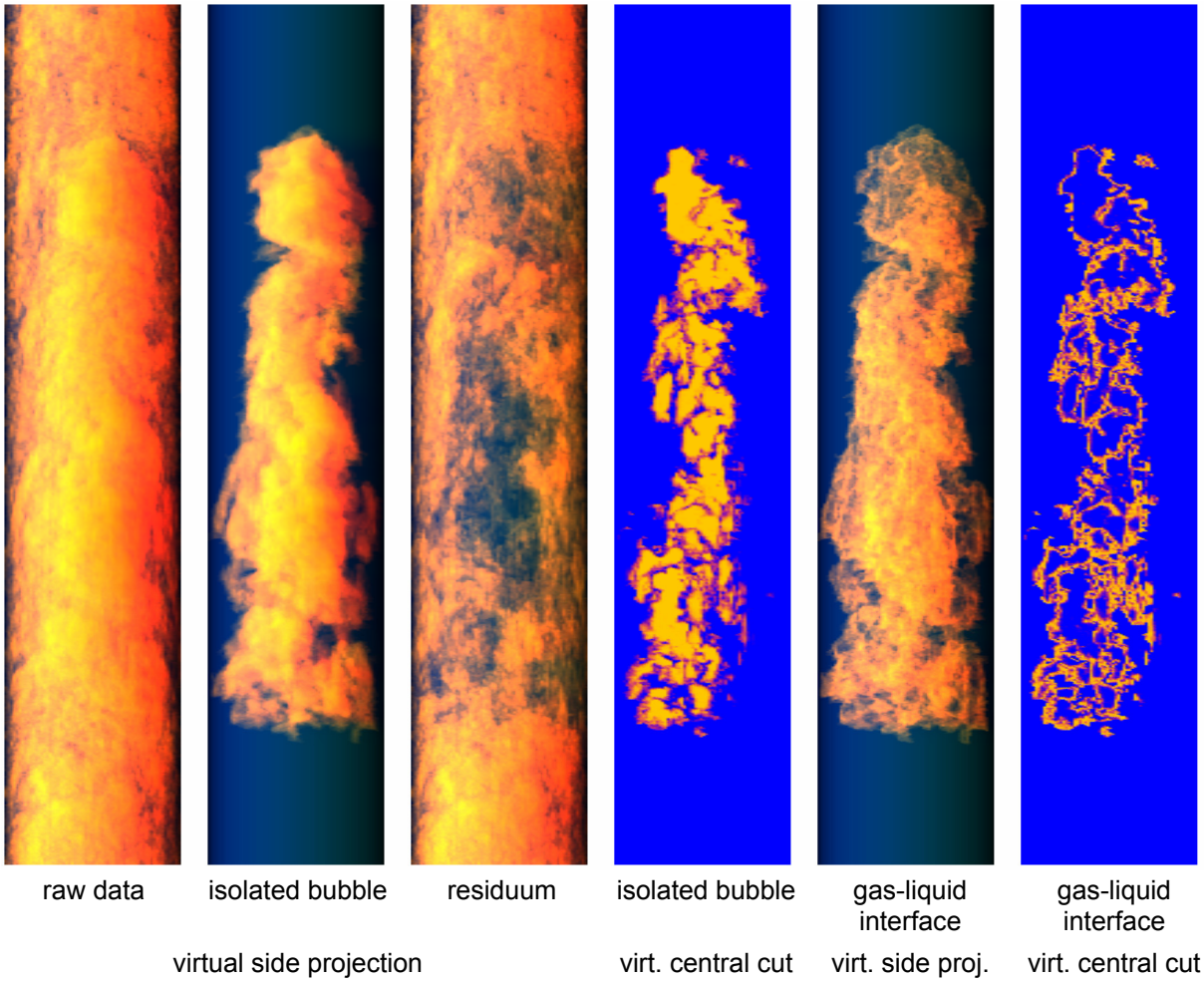

Fig. 3.8 Analysis of a large isolated bubble (flow see Fig. 3.2) extracted from the signal of the wire-mesh sensor (superficial velocities: J_G = 1.305 m/s and J_L = 1.017 m/s)

It has to be noted that the giant bubble shown in Fig. 3.8 has a pronounced internal structure, which was discovered by preparing virtual side views of the gas-liquid interface (Fig. 3.8, two right columns). The interface was made visible using the function $\varepsilon' = (1-\varepsilon)\cdot\varepsilon$ instead of the local instantaneous gas fractions, a function that has its maximum at a gas fraction of 50 %, i.e. those points are highlighted, which are semi-filled with the gaseous phase. The bubble contains large quantities of the liquid phase arranged in numerous lamellas. The voids between these liquid films are connected by gas containing holes, through which they are united by the bubble recognition algorithm. This is clearly visible, when the plane of the virtual cut is rotated. It remains open, whether these holes in the liquid lamellas are reality or if the films become invisible for the sensor due to a thickness below the resolution of the sensor. A final answer can only be given by increasing the resolution of the void measurement.

The fact, that the amount of liquid inside a large bubble increases with growing superficial gas velocity, supports the hypothesis of an increasing deformation of the gas-liquid interface as the cause of the complicated inner structure. The bubble in Fig. 3.6, for example, found at J_G = 0.534 m/s consists of two parts divided by a liquid film. Both parts are connected at the bottom of the bubble. With growing air flow the structure becomes more and more complicated.

The fluid properties have a significant influence on the established flow regime and the effects mentioned above (Prasser et al., 2005d). An increase of the thermodynamic parameters leads to an earlier appearance of the churn-turbulent flow regime even in the DN50 pipe (Fig. 3.9), whereas at atmospheric pressure and ambient temperature the flow is still dominated by Taylor bubbles. In the large DN200 pipe, the churn flow undergoes a gradual transition to smaller and more homogeneously distributed interface structures (Fig. 3.10). Both are attributed to the decrease of surface tension in eq. (1) as well as to the decrease of viscosity, which results in a growing Reynolds number.

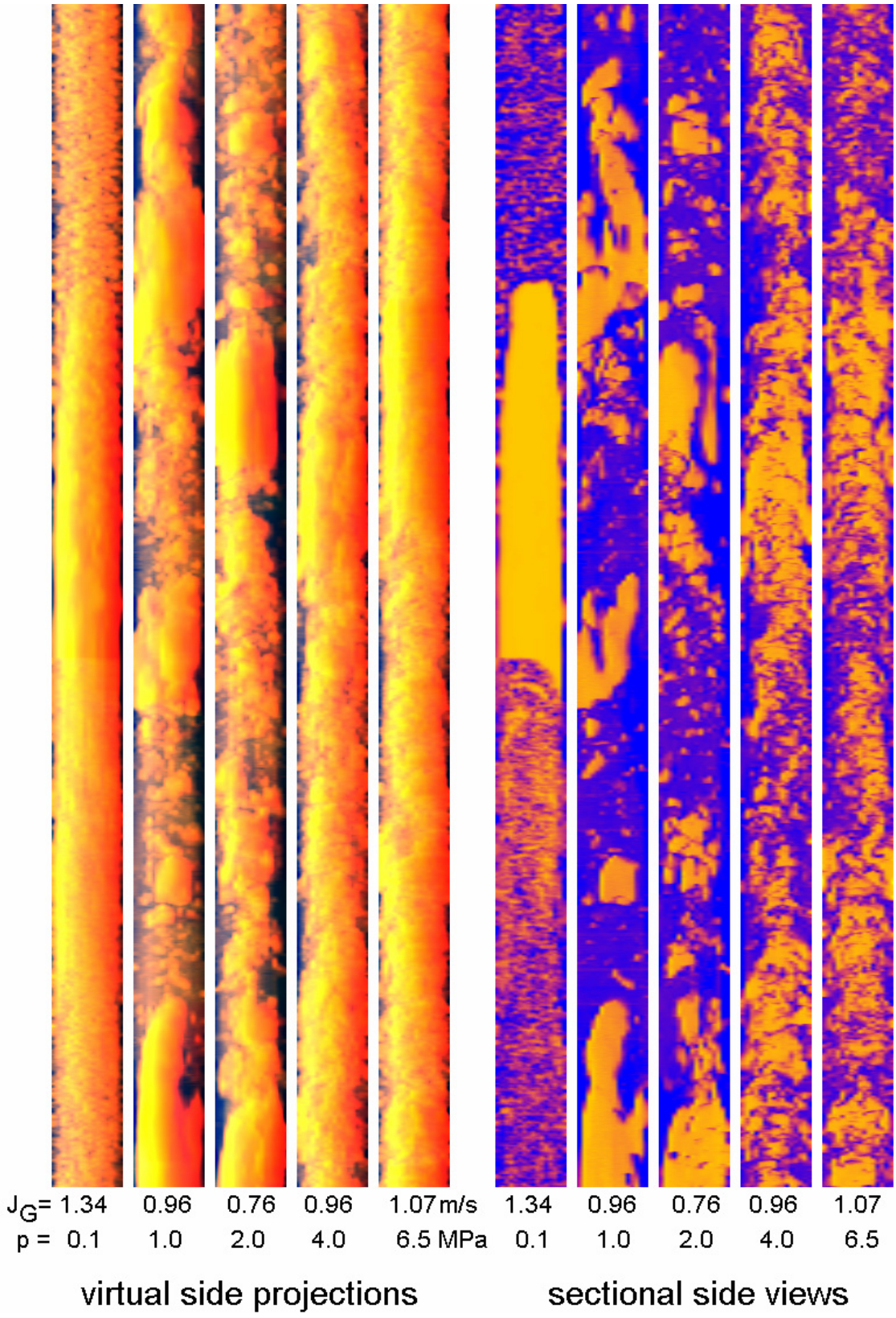

Fig. 3.9 Visualization of wire-mesh sensor data obtained in the pipe ∅52.3 mm, J_L = 1.017 m/s, L/D = 151.2

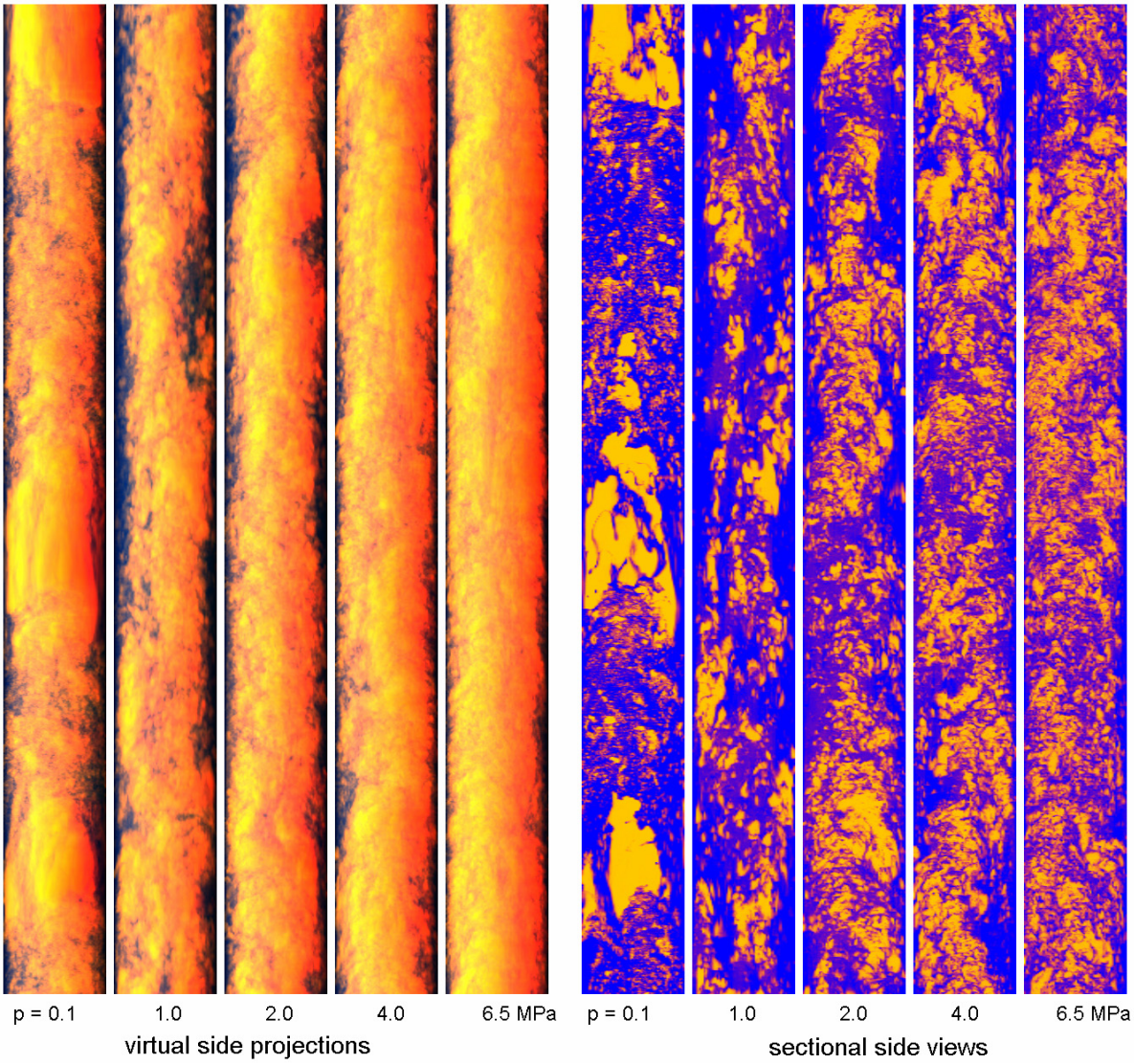

Fig. 3.10 Visualization of wire-mesh sensor data obtained in the pipe ∅195.3 mm, J_L = 1.017 m/s, $J_G \cong$ 0.84 m/s, L/D = 39.7

Another consequence of the aforementioned changes in the fluid properties is that the establishing of equilibrium bubble-size distributions is much accelerated at higher temperatures. While in case of air-water flow at ambient conditions the influence of the gas injector is still evident at the maximal available inlet length of the DN200 pipe (L/D = 39.7), at 6.5 MPa an equilibrium is already reached after about L/D = 7.7 (Fig. 3.11).

Beside the influence of the fluid properties, also the superficial gas velocity has a significant influence on the inlet length necessary to establish an equilibrium bubble-size distribution. As shown by Prasser (2004), the influence of different sparger geometries is still significant at L/D ≅ 40 at low gas flows, while at higher superficial gas velocities the flow structures converge. In a bubbly flow regime, the injection through orifices of 0.8 mm diameter resulted in a wall-peaked void distribution at L/D = 39.3 in the DN200 pipe, while an injection though 6 mm holes caused a central-peaked distribution. In the churn-turbulent regime, the radial profiles as well as the bubble-size distributions converged.

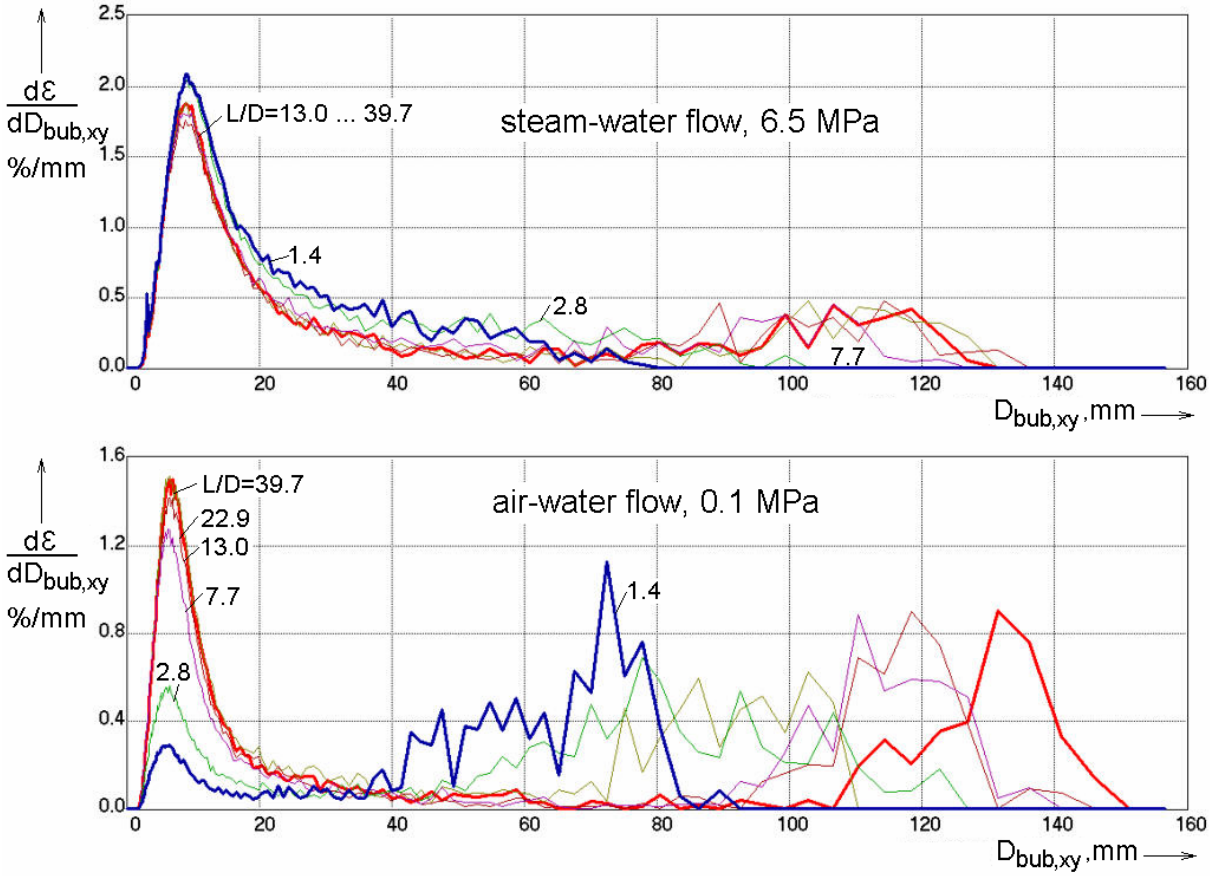

Fig. 3.11 Bubble size distributions in the test pipe DN200 at J_L = 1.017 m/s and J_G = 0.835 m/s, gas injection orifices: D_{inj} = 4 mm

The outlined results are extending the knowledge on scaling effects in two-phase flows. For the first time, the qualitative findings of Ohnuki on the direct transition from bubbly to churn-turbulent flow were confirmed by quantitative measurements and by a high-resolution characterization of the shape of large bubbles found in such flow structures. The fact that a comparison between air-water and steam-water experiments is available, the latter at pressures and temperatures typical for nuclear reactors, is of special value for two-phase flow research in the field of nuclear reactor safety. For more details see separate report ”Experiments on upwards gas-liquid flow in vertical pipes” (see appendix: A 1).

4. Momentum exchange between gaseous and liquid phases

4.1 Experimental basis

Experimental basis for the performed analytical work on the modelling of the momentum exchange between the gas and the liquid in a two-phase flow with the liquid being the continuous phase are to a large extend measurements of the evolution of the flow structure along the flow path performed in vertical test pipes. The work was started in the FLOWMAP project at the test facility MTLoop (Prasser et al., 2003a), the main part of which consisted in a vertical pipe of 51.2 mm inner diameter and a utilizable inlet length for varying the distance between the gas injection and the sensor of up to 3.5 m. At TOPFLOW, the opportunities for such experiments were largely extended by the two test section DN50 (52.3 mm inner

diameter) and DN200 (195.3 mm inner diameter), which are described in section 2.1. Other advantages of the TOPFLOW test sections are:

- larger inlet length of the small test pipe (L/D up to 151.2, both test sections are equally tall, their useable height is 9 m),
- much wider variations of fluid properties due to the possible steam-water operation at up to 7 MPa,
- the opportunity to study flows with phase transition (see section 7).

In case of the small test sections of MTLoop and TOPFLOW, the variation of the distance between gas injection and measuring position was done by dismantling the test pipe to rearrange pipe sections in order to achieve the desired inlet length. The large test section DN200 is equipped with the variable gas injection system that allows the variation of the inlet length by changing valves without the cumbersome reassembling of pipe segments (see section 2.1).

Wire-mesh sensors were available for both air-water- and pressurized steam-water experiments, with the difference that there were pairs of sensors for all experiments in the DN50 pipe, while for the DN200 pipe a pair of sensors was only available for cold air-water tests. For pressurized steam-water tests, only a single large sensor was available. The resolution was equally high for both cold and hot tests, i.e. all sensors were manufactured with a lateral pitch of the electrode wires of 3 mm (see section 2.2).

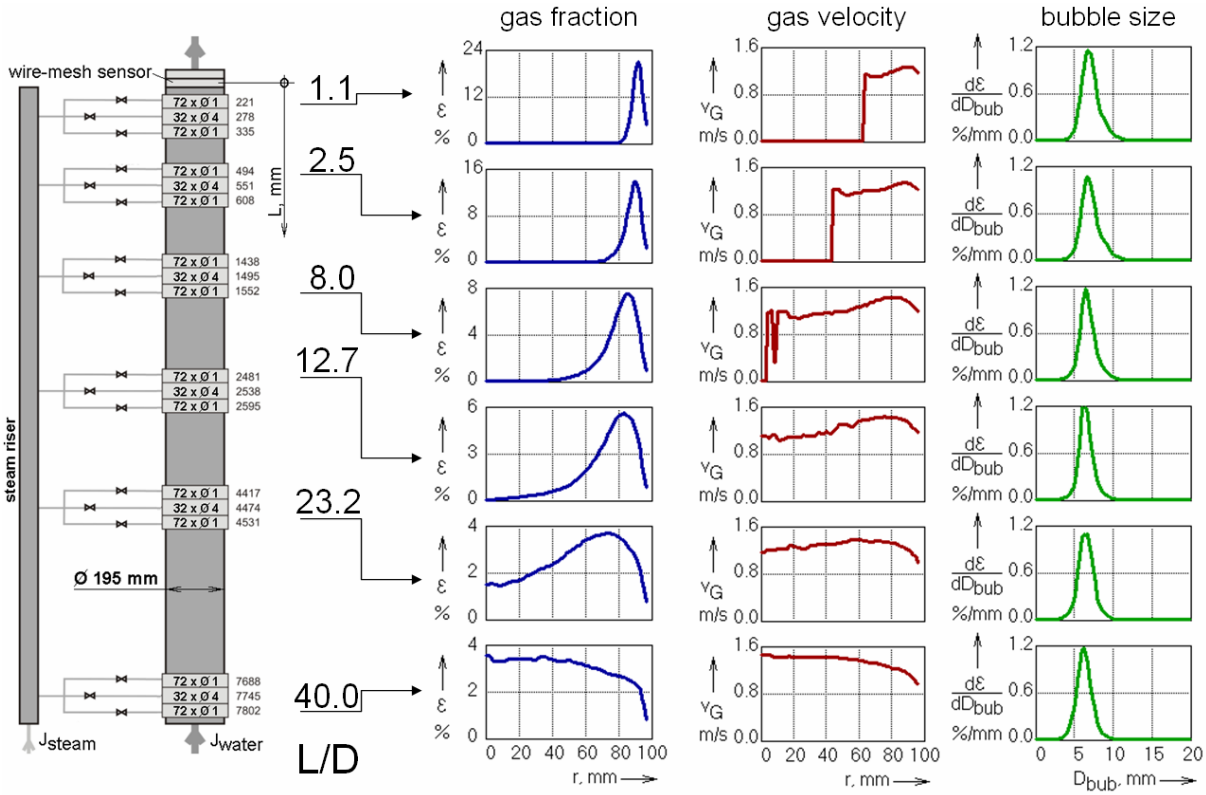

Fig. 4.1 Gas fraction and gas velocity profiles as well as bubble size distributions in the test pipe DN200 in an air-water experiment at J_L = 1.017 m/s and J_G = 0.037 m/s, T = 30 °C, p = 0.12 MPa at sensor position, gas injection orifices: D_{inj} = 1 mm

The experimental data basis for development and validation of closure relations for the interfacial momentum exchange consists in time-averaged radial profiles of flow

parameters as a function of the inlet length. These are above all profiles of the volumetric gas fraction (void fraction) and the gas phase velocity, the latter determined by a cross-correlation of signals from both sensors. Characteristic results are shown in the Fig. 4.1 and Fig. 4.2. The flow in Fig. 4.1 is characterized by a nearly constant bubble size distribution. The gas fraction profile close to the injection port has a forced wall peak which is later on transformed into a central peak due to the bubble migration towards the centre. At higher superficial gas velocities, bubble coalescence and breakup is observed (Fig. 4.2). In both cases, the gas velocity profiles show first a maximum close to the wall, which is caused by the local buoyancy in the gas fraction peak. Later, also the liquid velocity profiles become central peaked.

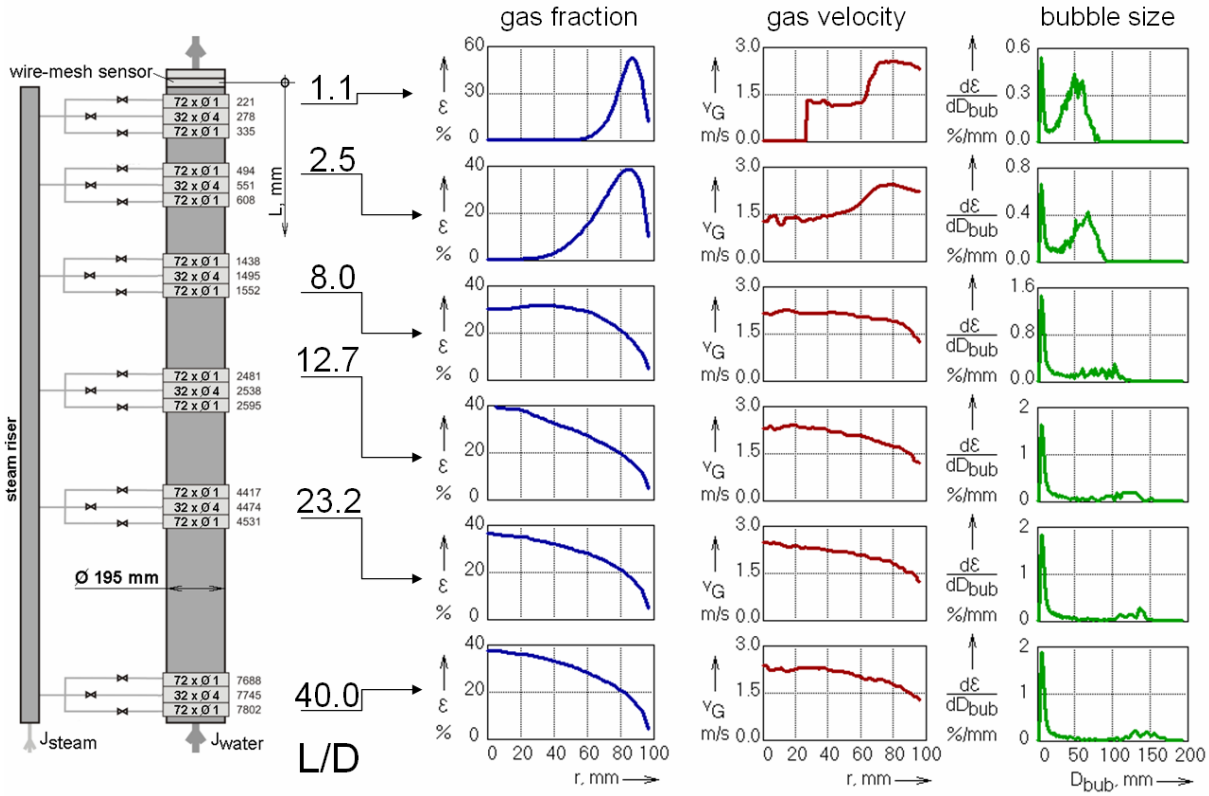

Fig. 4.2 Gas fraction and gas velocity profiles as well as bubble size distributions in the test pipe DN200 in an air-water experiment at J_L = 1.017 m/s and J_G = 0.534 m/s, T = 30 °C, p = 0.12 MPa at sensor position, gas injection orifices: D_{inj} = 1 mm

The void fraction profiles can be obtained decomposed into bubble-size classes, which is done on the basis of the bubble identification methods developed for wire-mesh sensor signals (Prasser et al., 2002a). Due to the variation of the inlet length, these decomposed profiles contain information about the lateral movement of bubbles in dependence on their size, which allows a very sensitive testing of bubble forces, which are in general depending on the bubble diameter.

It is evident that the decomposed radial gas fraction profiles show a wall peak for bubbles below the critical diameter of the lift force reverse even in case when the total gas fraction profile has a central peak (Fig. 4.3 and Fig. 4.4), while large bubbles always tend to migrate towards the centre of the pipe. Details on the variable gas injection system are given in a separate report ”Experiments on upwards gas-liquid flow in vertical pipes” (see appendix A 1).

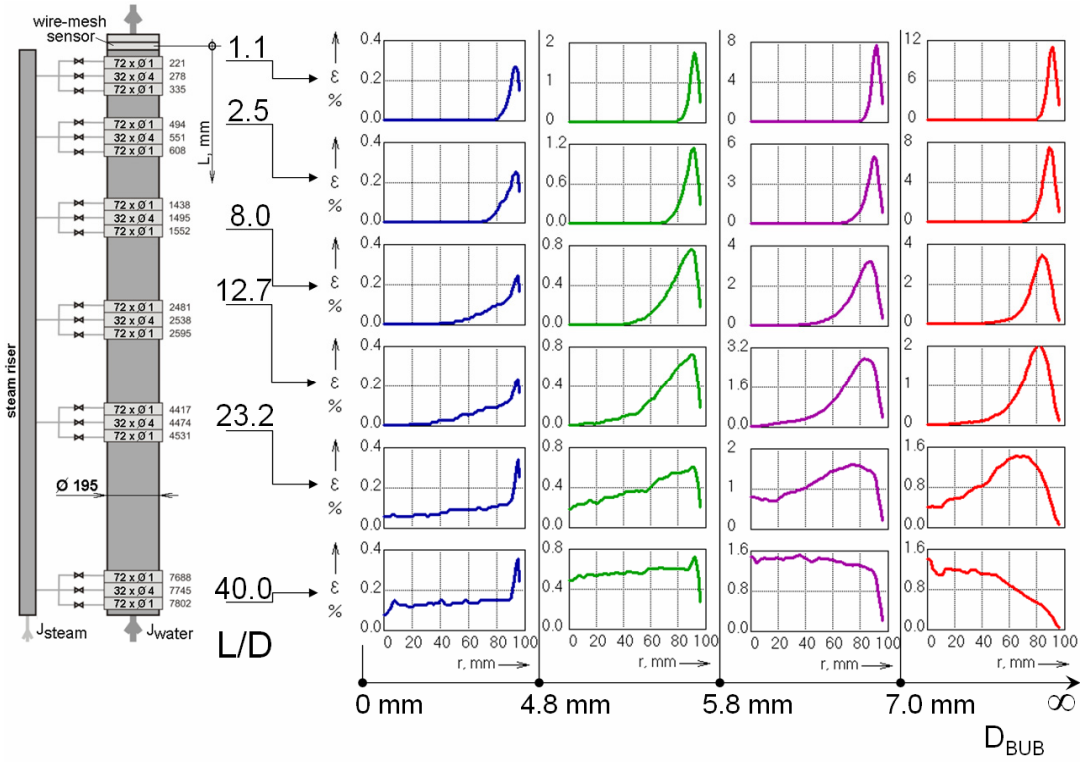

Fig. 4.3 Gas fraction profiles decomposed according to bubble size classes in the test pipe DN200 in an air-water experiment at J_L = 1.017 m/s and J_G = 0.037 m/s, T = 30 °C, p = 0.12 MPa at sensor position, gas injection orifices: D_{inj} = 1 mm

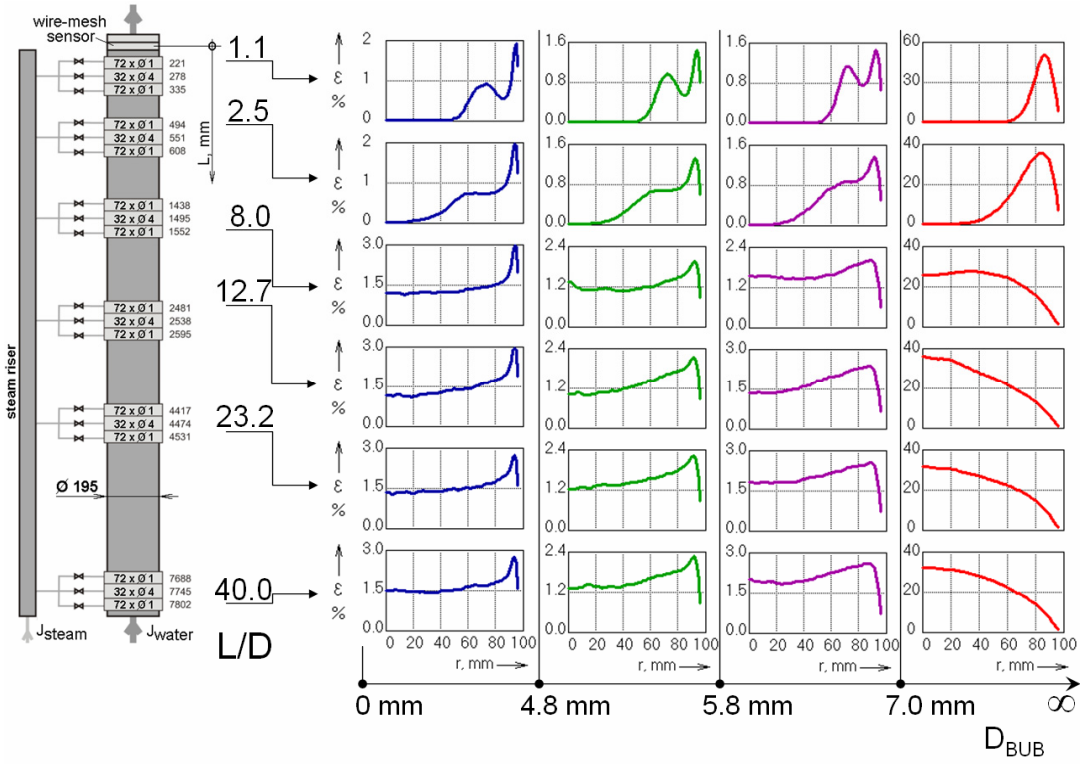

Fig. 4.4 Gas fraction profiles decomposed according to bubble size classes in the test pipe DN200 in an air-water experiment at J_L = 1.017 m/s and J_G = 0.534 m/s, T = 30 °C, p = 0.12 MPa at sensor position, gas injection orifices: D_{inj} = 1 mm

4.2 Analytical investigations

For effective analyses of models for the bubble forces the so-called Multi Bubble Size Class Test Solver was developed by Lucas et al. (2001a). It resolves the variables in radial direction and considers a number of bubble size classes. In its basic version equilibrium of the non-drag forces (lift-, wall-, deformation- and turbulent dispersion forces are considered) is assumed separately for each bubble class. In the result the decomposed radial volume fraction profiles are obtained and can be compared with the measured ones. Further on a summation weighted by the bubble size distribution allows to calculated radial gas volume fraction profiles. The equilibrium reflects the situation of fully developed flow and for these reason measured bubble size distributions for the largest L/D were used as an input for the solver to calculate the radial profiles. Comparison with according measured profiles allows assessing the quality and the range of validity of the non-drag force models used (see Fig. 4.5, Lucas et al., 2004b).

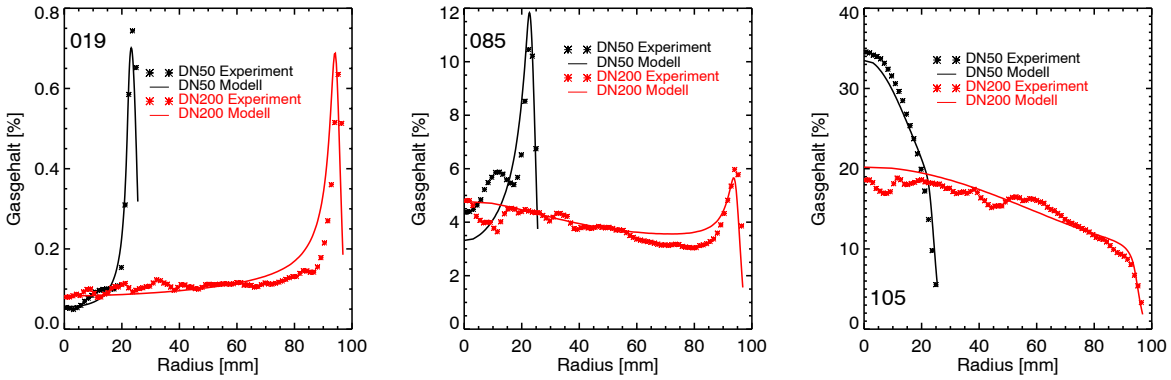

Fig. 4.5 Comparison of calculated and measured radial gas volume fraction profiles (**019**: J_L = 1.017 m/s, J_G = 0,004 m/s; **085**: J_L = 1.017 m/s, J_G = 0,057 m/s; **105**: J_L = 0,405 m/s, J_G = 0,140 m/s)

Later on this solver was extended to simulate the development of the flow along the pipe in an approximate way. The main simplification consisted in the assumption that the vertical gas velocity is independent on the radial position and bubble size (Lucas et al., 2007b). Instead equilibrium of bubble forces radial momentum equations including drag force and virtual mass force are solved separately for each bubble class. This allows simulating the radial bubble migration, which again can be compared with measured ones.

The radial gas volume fraction profiles, which can be observed as a result of the action of the bubble forces, can be divided in 3 groups: profiles with core peak, wall peak and intermediate peak. While the nature of the latter one, which occurs only at high liquid volume flow rates (~ 4 m/s), is not yet clear, the other ones can clearly be explained by the change of the sign of the lift force, which is discussed in the next section. Wall and deformation forces act only in the vicinity of the wall and the turbulent dispersion force flattens the profiles caused by mixing of the bubbles in consequence of turbulence. Scaling considerations are discussed by Lucas et al. (2004b) by comparing results for the DN50 and the DN200 pipes.

A detailed description of the test solver and its application to various pipe flows can be found in a separate report “CFD models for poly-dispersed bubbly flows” (see appendix A 5).

4.3 Lift force inversion in a poly-disperse bubbly flow

The lift force is a non-drag force experienced by a bubble that moves with a certain relative velocity compared to the local liquid velocity, if the liquid velocity field has a gradient. The force is non-zero, when the direction of the relative movement is not collinear with the liquid velocity gradient. Such situations are typical for bubbles rising in the shear field close to the wall of a vertical pipe. For spherical gas bubbles, the force is directed against the velocity gradient. It was shown by Tomiyama (1998, see also Tomiyama at al., 2002), that the lift force changes direction when the bubble size exceeds a certain critical equivalent bubble diameter. Tomiyama used an experimental set-up that allowed the observation of single bubbles in a well-defined shear field created by moving side walls in a vertical channel.

The MTLoop experiments (Prasser et al. 2003a) have shown the lift force reverse for the first time in a poly-disperse bubbly flow. Radial void fraction distributions show a wall peak for bubbles below the critical diameter, while bubbles with a bigger diameter form a central void fraction peak. This is independent from the general type of the profile of the total void fraction, i.e. a wall-peak for the small bubble fraction is found also in case of a pronounced central peaked void fraction profile.

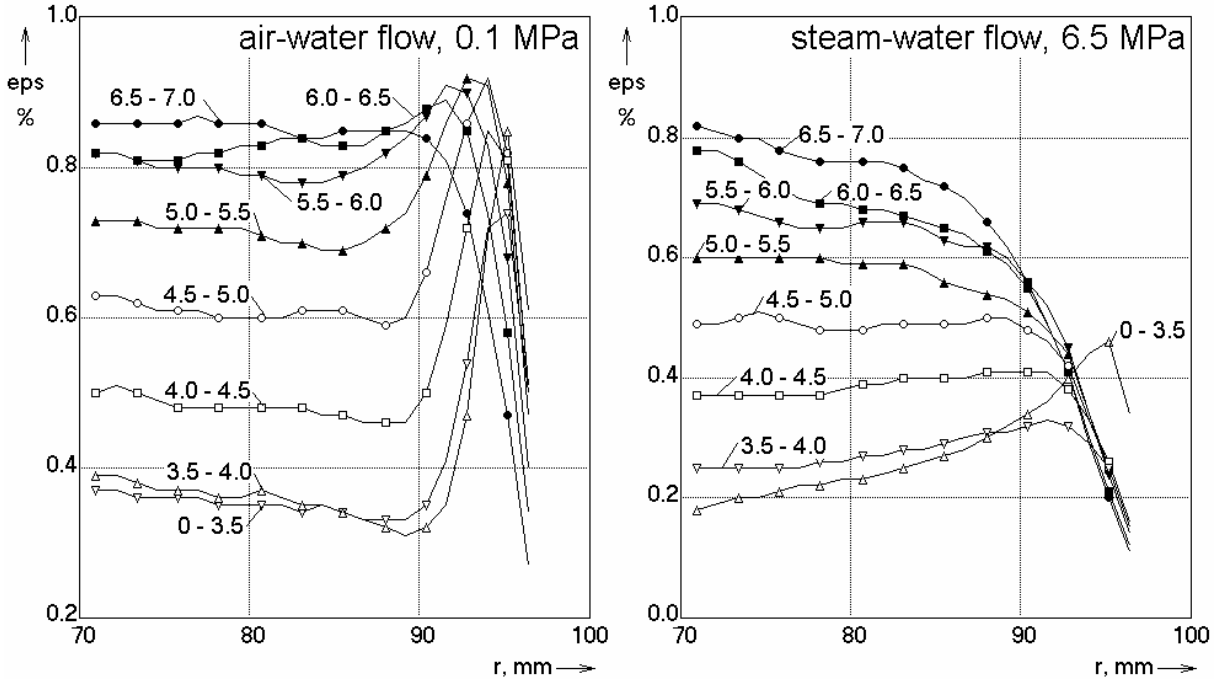

Fig. 4.6 Gas fraction profiles decomposed according to bubble size classes in the test pipe DN200 at J_L = 1.017 m/s and J_G = 0.219 m/s, L/D = 39.7, gas injection orifices: D_{inj} = 4 mm

TOPFLOW has significantly extended the experimental opportunities to study this effect. It was shown that the described effects are present also in a large diameter pipe. The vanishing of the wall peak in gas fraction profiles that are subdivided into narrow bubble-size classes of 0.5 mm class-width is observed at a diameter close to the value given by Tomiyama. For an air-water flow at ambient conditions, the equivalent critical bubble diameter is 5.5 mm. As shown in Fig. 4.6, bubble of this size still display a pronounced wall peak, which vanishes at about 6 - 6.5 mm bubble diameter. The fact that a wall peak is still present for bubbles slightly larger than the Tomiyama diameter results from their continuous production by coalescence events, which are frequent in the peak region between bubbles below the critical size.

An important merit of the TOPFLOW experiments is the possibility to check the correctness of the Tomiyama model at high pressures and temperatures. The critical diameter is scaled by increases with the modified Eötvös number:

$$Eo_d = \frac{g(\rho_l - \rho_g)d_h^2}{\sigma}, \qquad (2)$$

which is based on the horizontal bubble diameter d_h.

Keeping in view that the surface tension decreases with growing saturation temperature, the critical bubble diameter is expected to be lower for the steam-water tests. The dependency is given in Fig. 4.7. This was confirmed by the measurements, as shown in Fig. 4.6 (right side), where decomposed gas fraction profiles in the close-to-wall region are plotted for a saturation pressure of 6.5 MPa. A wall peak is only found for bubbles below 3.5 mm, which is in agreement with the dependency of the critical diameter from pressure in Fig. 4.7.

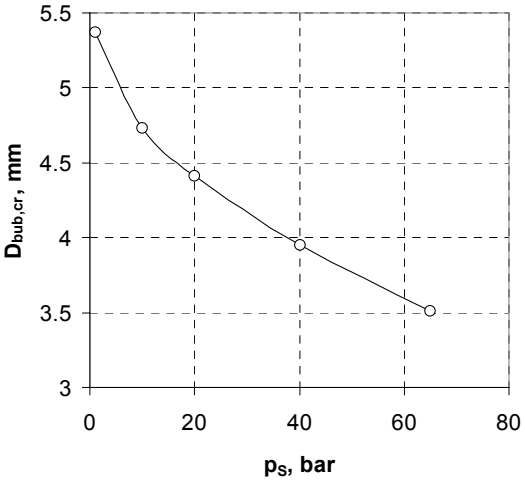

Fig. 4.7 Decrease of the critical equivalent bubble diameter of the lift force inverse with growing saturation pressure

4.4 Wall and deformation forces

The wall force simulates repulsion effects by the pipe wall. From point of view of modelling this force prevents the bubbles from a migration into the wall. The physical effect, which causes wall repulsion forces are the pressure distribution at the bubble surface resulting from the complicated liquid flow field around the bubble, which is characterized by strong velocity gradients close to the wall.

A second component is generated when there is direct contact between the bubble and the wall. Different models are available in literature for the long range lubrication forces, while models valid for the bubble-wall contact were not found. For this reason, a simple model for a deformation force has been developed in the frame of this project. It assumes that the bubble is deformed to a prolate ellipsoid as soon as the distance between the pipe wall and the centre of mass of the bubble is lower than the equivalent bubble radius. According to the increase of the bubble surface a repulsing force is generated. The action of this force can clearly be seen in the experiments and simulations on wall bouncing bubbles, in section 2.5.

4.5 Turbulent dispersion force

The turbulent dispersion of the bubbles is a result of interactions between individual particles of the dispersed phase and the continuous phase turbulence eddies. In the Eulerian frame, the effect of turbulent dispersion appears as a turbulent diffusion term in the scalar transport equations and the so-called turbulent dispersion force in the momentum equations. The further vanishes if the Favre (mass-weighted) ave-

raged velocity is adopted for the transport equation system. The latter is actually the total account of the turbulence effect on the interfacial forces.

In the frame of the project a new mathematical derivation for the turbulent dispersion force model for Eulerian multiphase flows was done. Starting point was the Lagrangian approach, which explains the physics in a straightforward way. The turbulent dispersion force was directly obtained from the fluctuating components of the drag force. Extensive model evaluations were made using the experimental data for bubbly flows in vertical pipes under various flow conditions. Poly-dispersed models were applied in the computations. Detail on this new derivation of the model and the model validation can be found in the special report “Turbulent dispersion of bubbles in poly-dispersed gas-liquid flows in a vertical pipe” (see appendix A 6).

5. Dynamics of the gas-liquid interface

5.1 Evolution of bubble size distributions, bubble coalescence and breakup

The data base for the modelling of bubble coalescence and breakup consists in the same experiments used for the development and validation of the relations for the interfacial moment transfer (comp. section 4.1). Depending on the superficial velocities of the liquid and the gaseous phases, the wire-mesh sensor data obtained in test with the variation of the distance between gas injection and sensor monitor more or less intensive changes of the bubble size distributions. These changing bubble-size distributions are sensible indicators for the correctness of coalescence and breakup models embedded into the CFD code (see Fig. 4.1 - Fig. 4.4). The influence of the fluid properties was studied by the comparison of air-water and steam water experiments, the latter performed at pressures up to 6.5 MPa (see Fig. 3.11).

As mentioned above, the Multi Bubble Size Class Test Solver was extended for the simulation of the evolution of the flow along the pipe. This comprises as well the solution of the momentum equation in radial direction, which is done separately for each bubble class to simulate the lateral bubble migration, as the consideration of bubble coalescence and breakup (Lucas et al. 2007b). The evolution of the flow is determined by a close interaction between local effects (spatial separation of bubbles depending on the bubble size, strong radial dependency of turbulence parameter and shear stresses) and bubble coalescence and breakup (Lucas et al., 2003).

Bubble coalescence and breakup are reflected by source terms for the single bubble classes. The coalescence rate and the breakup frequencies depend on the local bubble densities n_i for each bubble size class i and j as well as on the dissipation rate of the turbulent kinetic energy ε:

Coalescence rate: $\Gamma_{i,j} = K_c(d_i, d_j, \varepsilon) * n_i * n_j$

Breakup rate: $\Omega_i = K_b(d_i, d_j, \varepsilon) * n_i$

with the kernels for coalescence K_c and breakup K_b respectively. There are different models for these kernels available in literature, but their use seems to be limited to very special flow situations. Thus presently the predictions on the evolution of the flow are still unsatisfactory caused by the shortcomings of these closure models. This was shown using the test solver (Fig. 5.1) as well as by CFX simulations (see Chapter 6). Beside the limited quality of the models itself also uncertainties regarding

the prediction of the dissipation rate of turbulent energy may have an influence on the results, since they are necessary input parameters. An improved two-phase flow turbulence modelling is required for a more reliable prediction of bubble coalescence and breakup.

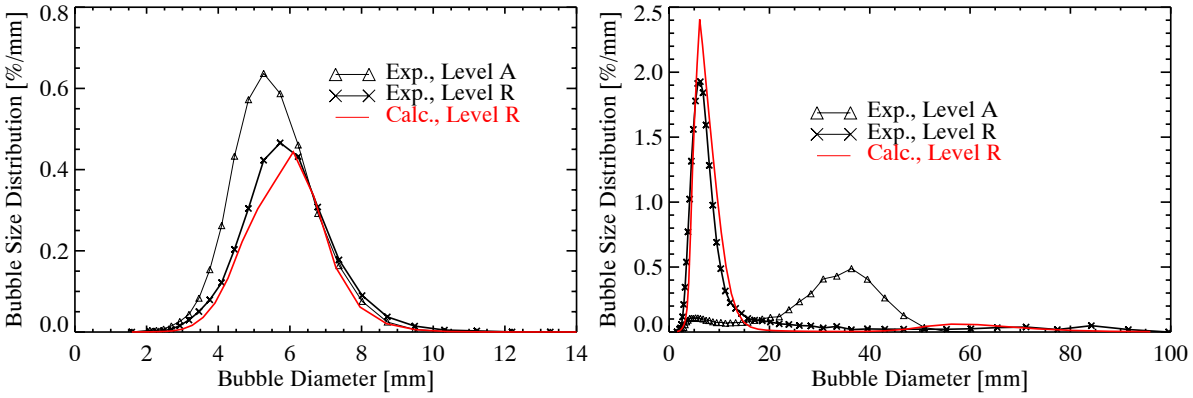

J_L = 1.611 m/s, J_G = 0.0235 m/s J_L = 1.017 m/s, J_G = 0.219 m/s

Fig. 5.1 Comparison of measured and calculated (test solver) bubble size distributions for Level R (7.8 m)

Another effect, which has to be considered regarding the evolution of the flow along the pipe, is connected with expansion of the gas bubbles due the pressure decrease with increasing height in the pipe. For dilute flows this effect may be more important than bubble coalescence and breakup (see Fig. 5.2).

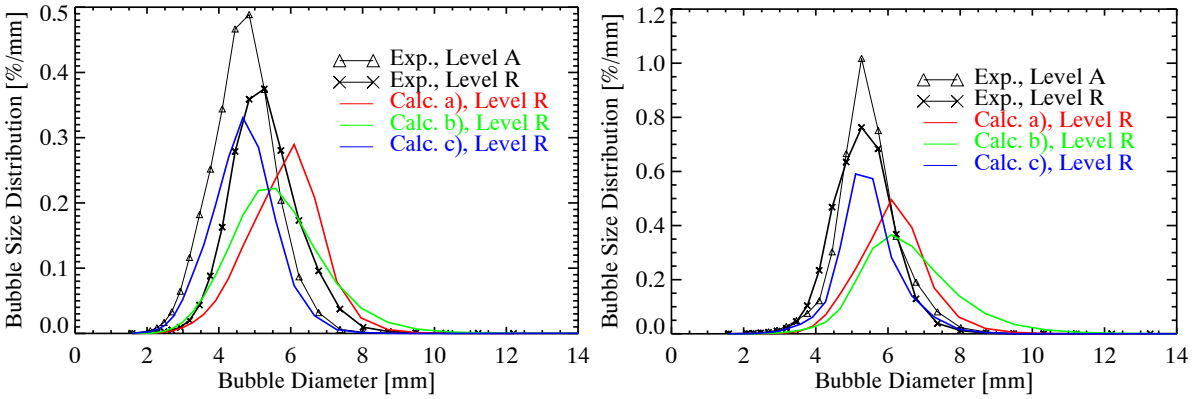

J_L = 1.017 m/s, J_G = 0.0096 m/s J_L = 1.017 m/s, J_G = 0.0151 m/s

Fig. 5.2 Comparison of measured and calculated (test solver) bubble size distributions for Level R (7.8 m):
Calc. a): with bubble coalescence and breakup,
Calc. b): bubble coalescence and breakup switched off and
Calc. c): in addition to Calc b) now also the bubble expansion caused by the pressure decrease is switched off

5.2 Interfacial area density

Within the project, the developed novel method to extract the interfacial area and the interfacial area density from the primary measuring data of wire-mesh sensors (section 2.6) was applied to a series of test points obtained at the DN200 test section with variable gas injection system. The results were released to GRS for the validation of models based on interfacial area conservation equations in ATHLET and

FLUBOX (Graf & Papadimitriou, 2006). An own theoretical analyses of the results was not performed by FZD.

The released data origins from the vertical test section DN200 of TOPFLOW with variable gas injection system (section 2.6). The inlet length between gas injection and mesh sensor was varied from 1.1 to 39.9. Both nozzle diameters were used, i.e. air was injected through either a ring of 72 orifices of 1 mm diameter or 32 orifices of 4 mm diameter, drilled in the pipe wall. The liquid was water at 20 °C at ambient pressure. In all presented tests, the liquid superficial velocity was kept constant at J_L = 1.017 m/s, while the gas superficial velocity was taken from the series J_G = 0.0094, 0.035, 0.086, 0.22, 0.53 m/s.

Since a pair of wire-mesh sensors with a matrix of 64x64 measuring points was used, both gas fraction and gas velocity profiles are available. The superficial air velocities cover the range from bubbly flow with a wall peaked gas fraction profile to values typical for slug flow with a central void fraction maximum (Fig. 5.3). The bubble-size distributions measured at about L/D ≅ 40 shown in Fig. 5.4 report the appearance of a peak in the range of very large bubbles at J_G = 0.53 m/s.

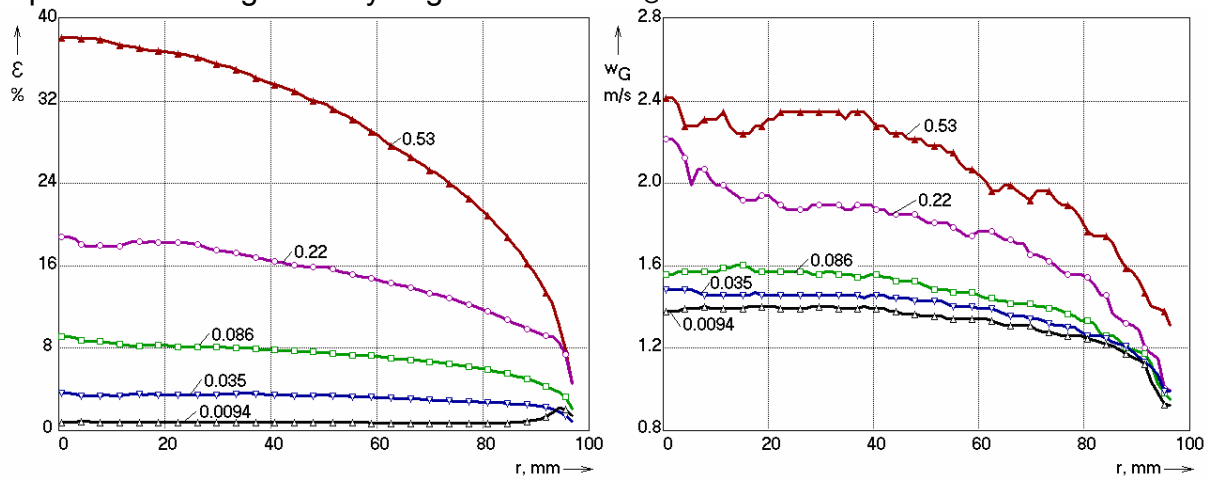

Fig. 5.3 Gas fraction and gas velocity profiles obtained by wire-mesh sensors in the pipe of 195.3 mm inner diameter at L/D ≅ 40 and J_L = 1.017 m/s for different gas superficial velocities J_G (parameter), gas injection: 72 orifices of 1 mm diameter

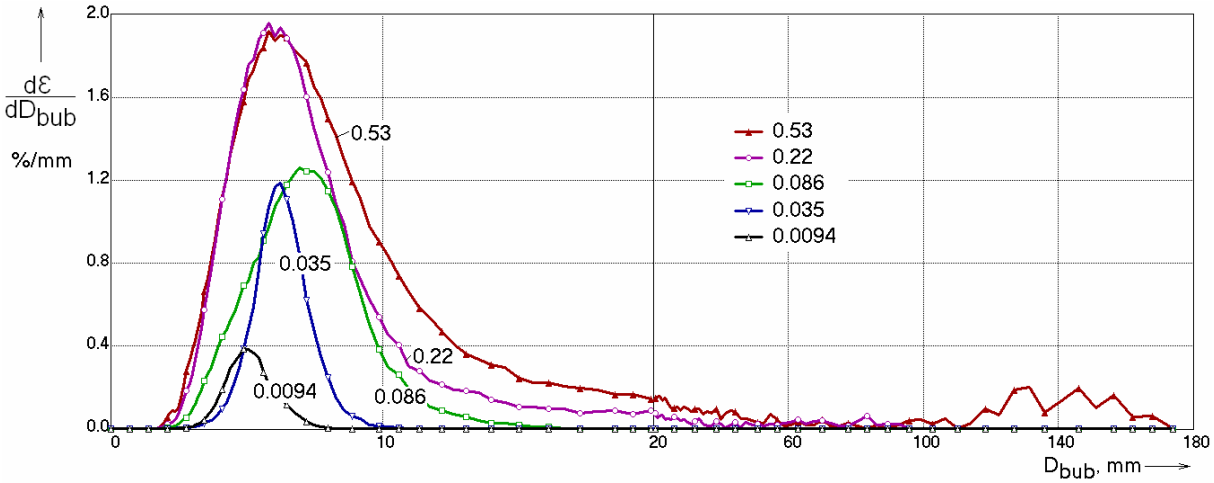

Fig. 5.4 Bubble size distributions obtained by the wire-mesh sensor in the pipe of 195.3 mm inner diameter at L/D ≅ 40 and J_L = 1.017 m/s for different gas superficial velocities J_G

The evolution of the interfacial area density along the pipe is shown in Fig. 5.5. In this figure, the results for both gas injection diameters are compared, too. There is a tendency of convergence between the results for 1 mm and 4 mm injection orifices with growing lengths.

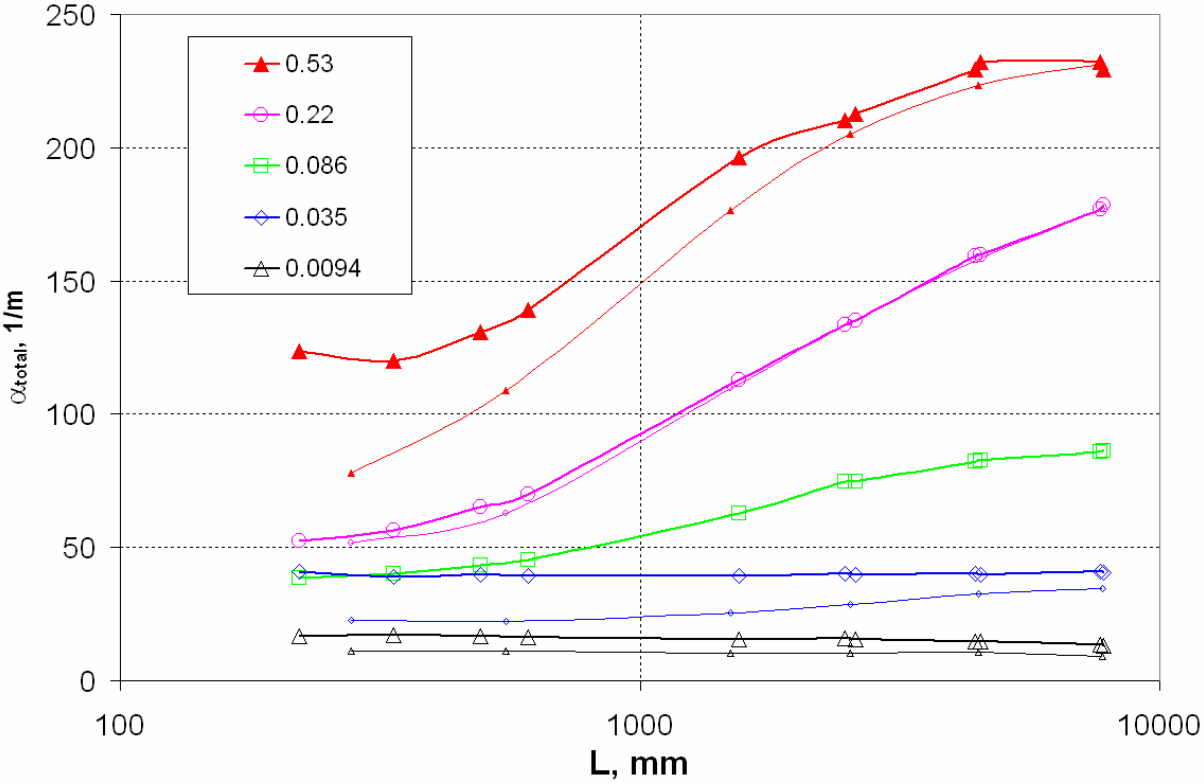

Fig. 5.5 Interfacial area density in the pipe of 195.3 mm inner diameter as a function of the distance between gas injection and measuring position L at J_L = 1.017 m/s for different gas superficial velocities J_G (parameter), Gas injection orifices: bold lines: 1 mm, thin lines: 4 mm

A growing interfacial area density along the pipe is observed at the superficial gas velocities of J_G = 0.086, 0.22, 0.53 m/s in case of both types gas injection orifices and also for J_G = 0.035 m/s for an injection through 4 mm orifices, which points at a preponderance of fragmentation processes in the flow, while the interfacial area density is slightly decreasing for the very small gas flow of J_G = 0.0094 m/s, which is due to bubble coalescence. It remains nearly constant for J_G = 0.035 m/s and an injection through 1 mm orifices.

6. Inhomogeneous MUSIG model

As discussed in the previous chapters, the interactions between the bubbles and the liquid clearly depend on the bubble size. For this reason an adequate Eulerian simulation of poly-dispersed flows requires the introduction of a number of bubble classes. In principle this can be done in the frame of a multiphase modelling, which introduces different bubble classes by different phases. Such a modelling is very expensive regarding the computational resources. For this reason simplifications are aspired. To reflect the interfacial area, which is important for mass and heat transfer between the phases the so-called MUSIG (**MU**lti bubbe **SI**ze **G**roup) model by Lo was implemented into CFX-4 (Lo 1996). In this model only the mass balance for the gas phase is sub-divided into a number of groups representing different bubble sizes.

This approach bases on a two-fluid model combined with a population balance. Bubble coalescence and breakup are considered as source and sink terms representing the mass transfer between the groups.

Nevertheless the separation of small and large bubbles caused by the lift force as discussed above can not be reflected by this model, since only one momentum equation for gas phase is solved, i.e. only one velocity field is representing the entire gas phase. In the result, all bubbles move with the same velocity, although in reality both value and direction of the velocity are dependent on their size. The investigations done by the Multi Bubble Size Class Test Solver proved that for poly-dispersed flows a number of bubble size groups is required (see special report: "*CFD models for poly-dispersed bubbly flows*"). Also the experimental results on vertical pipe flow discussed above show, that a spatial separation between small and large bubbles occurs. This only can be reflected in the simulation if the dispersed phase is represented by a number of momentum equations. At least two velocity groups are necessary. On the other hand, in general more groups are needed for an adequate reflection of the bubble size distribution and the simulation of bubble coalescence and breakup processes.

For this reason a new model concept was developed. In the so-called inhomogeneous MUSIG model (sometimes also called N * M MUSIG model), the dispersed phase is represented by N velocity groups, i.e. N "phases". Each velocity group can be sub-dived again into a number of subgroups for the conservation of mass. In principle the number of subgroups can be different for each velocity group. In that sense the appellation "N * M MUSIG model" may be misleading. A scheme explaining the concept is shown in Fig. 6.1. The justification of the model and details of the concept were published by Krepper et al. (2005). The inhomogeneous MUSIG model was developed in cooperation with ANSYS CFX and afterwards implemented into CFX-10 (see e.g. Shi et al. 2004, Frank et al., 2006).

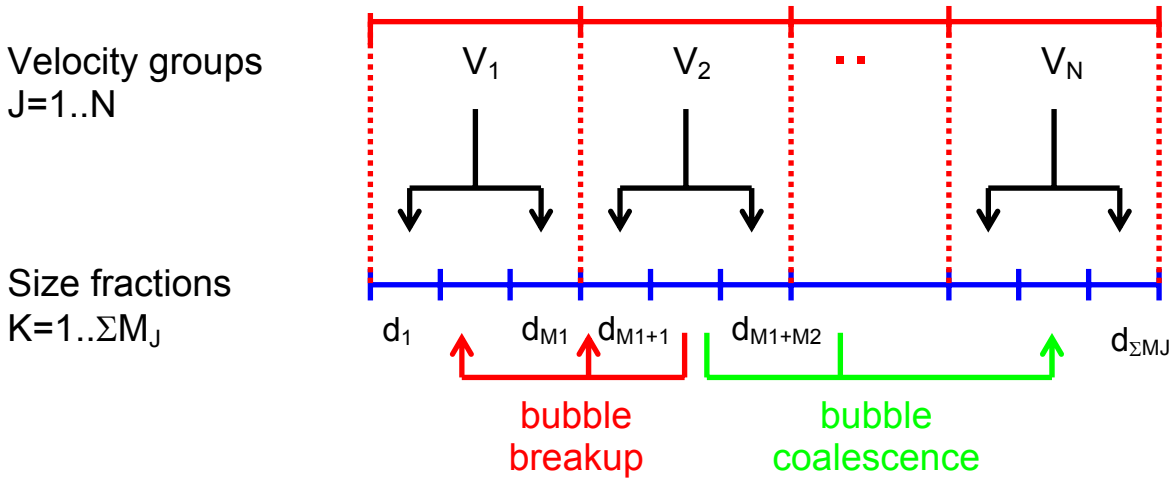

Fig. 6.1 Improvement of the poly-dispersed approach: The size fractions M_J are assigned to the velocity field V_J

Transfers between the bubble size groups in the mass conservation can occur due to bubble coalescence and breakup, expansion of the gas phase caused by pressure changes and mass transfer between gas and liquid as evaporation and condensation. In the present version of the model only source and sink terms accounting for bubble coalescence and breakup are implemented. The coalescence model by

Prince and Blanch (1990) and the breakup model by Luo and Svendsen (1996) are implemented in CFX-10 as standard models.

The concept of a multi bubble size group modelling as well as suitable models for the bubble forces and bubble coalescence and breakup were first extensively tested using the Multi Bubble Size Class Test Solver (see section 4.2). From the tests done for the assumption of fully developed flow (equilibrium of lift, wall, deformation and turbulent dispersion forces) was concluded, that a set of Tomiyama lift and wall forces (Tomiyama 1998, Tomiyama et al., 2002) together with the FAD model for turbulent dispersion force lead to satisfactory results. Similar results were obtained also by replacing the Tomiyama wall force by Hosokawa (2002) wall force and the deformation force. However these tests validate only the relation between these forces, not the relation to the drag and virtual mass forces, which become important only in developing flows. The simulations using the test solver showed that the radial bubble migration is too fast compared to experimental findings (Lucas et al., 2007b). This was also confirmed by simulations using CFX. The turbulent dispersion force was identified as the main reason. It seems to be too large, but a detailed investigation on this problem is still stands out.

The test solver was also used for the simulation of the evolution of the flow including bubble coalescence and breakup. No models for bubble coalescence and breakup were found, which can be used with the same model constants for a range of flow conditions. Instead it was necessary to tune the model constants for each combination of superficial velocities to obtain a satisfactory agreement with the experimental data.

For the validation of the Inhomogeneous MUSIG model experimental data for vertical pipe flow (air-water: MTLoop DN50 and TOPFLOW DN200, steam-water TOPFLOW DN200) as well as the flow around an obstacle (see Chapter 8) were used. The parameters of the selected tests are summarized in Tab. 6.1. The simulations done and the results are discussed in the technical reports: "*CFD models for poly-dispersed bubbly flows*" (see appendix A 5) and "*Validation of the Multiple Velocity Multiple Size Group (CFX10.0 N x M MUSIG) Model for poly-dispersed multiphase flows*" (see appendix A 7).

Tab. 6.1 Water and gas superficial velocities J_L and J_G of the tests used for validation of the Multi-MUSIG model

		J_G [m/s]			
		0.0368	**0.0898**	**0.140**	**0.219**
J_L [m/s]	**1.611**		097		
	1.017	074	096	107	118

The first question to be answered was the determination of the necessary number of velocity groups for an adequate simulation. From the numerical point of view the CFX solver was proven to cope with a large number of gaseous dispersed phases (cases with up to 8 phases were solved), although with increasing stability and convergence problems. In the report "*CFD models for poly-dispersed bubbly flows*", chapter 6.1, simulations with 2, 3 and 4 different dispersed phases were presented for the same test MTLoop 118. The relation of the different dispersed phases was adapted to the measured bubble size distribution of the developed flow. Considering only the different momentum exchange relations of the dispersed phases against the liquid phase, the total gas volume fraction distributions at the end of the tube was calculated and compared to the measurements. Between the three variants no

principal differences of the profiles were found. Also in the further calculations the simulation of only two different dispersed phases has been proven to be sufficient. Simulations using three or four velocity fields didn't improve the agreement to the measured values.

The next step was the simulation of the development of the bubble size distribution from the inlet to the top of the tube by bubble coalescence and fragmentation. A number of 20 up to 34 bubble size fractions representing an equidistant bubble size distribution was assigned to the two gaseous velocity classes. The size distribution at the inlet was adapted to the measurements. In the MTLoop tests 107 and 118 (J_L = 1.017 m/s, J_G = 0.140 m/s respective J_G = 0.219 m/s) starting with a quite narrow bubble size distribution a spreading out of the distribution at the end of the tube was found. For these tests the adaptation of the bubble breakup and coalescence coefficients to 0.25 respective 0.05 yielded the best agreement to the measurements. The development of the bubble size distribution could be reproduced. Consequently also the radial profiles of the total gas volume fraction corresponded to the experiments (see Fig. 6.2).

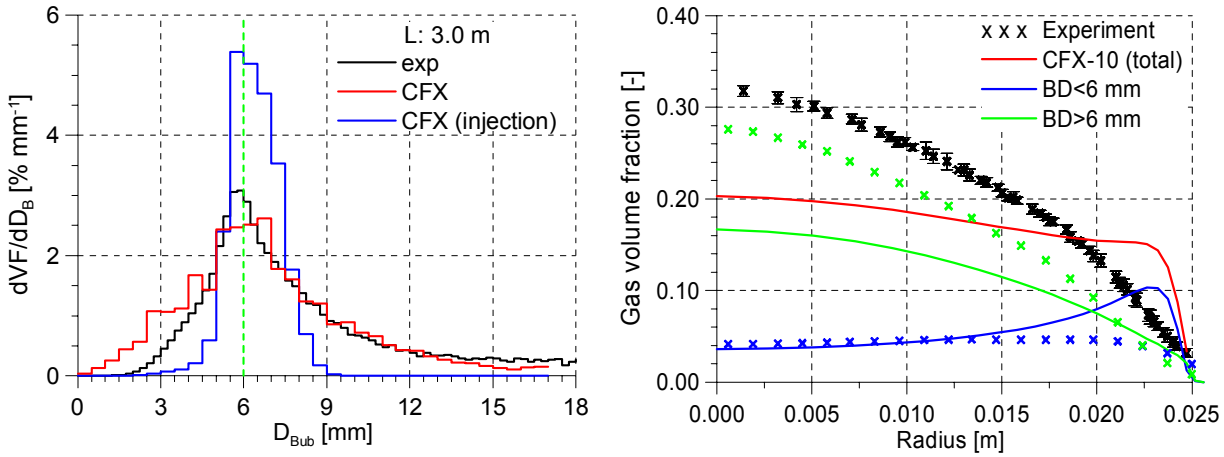

Fig. 6.2 Development of the bubble size distribution (left) and the radial gas fraction profiles (right) of the simulation of the test case MTLoop 118 (J_L = 1.017 m/s; J_G = 0.2194 m/s); F_B = 0.25, F_C = 0.05

This parameter set was also convenient for the TOPFLOW test 074, 107 and 118. During these tests gas was injected from the side walls by quite large valves. The initial bubble size distribution comprised a wide spectrum including large bubbles. During the flow the distribution shifted towards smaller values, i.e. in these tests the flow development was mainly determined by bubble fragmentation (see Fig. 6.3). In the calculations for the TOPFLOW test 074 and 107 also runs with reduced turbulence dispersion by 50% were performed. In the lower distance from the gas injection these calculations yielded better agreement of the radial gas profile.

Applying the same parameter set to steam-water tests at saturation conditions i.e. with limited phase transition the bubble fragmentation was strongly overestimated. For the comparison tests the highest applied pressure of 6.5 MPa was selected which minimizes the influence of the changing hydrostatic pressure along the test section on the saturation temperature. Only a further reduction of the breakup coefficient to a factor of 0.05 resulted in satisfying agreement to the experiments for the tests 107 and 118.

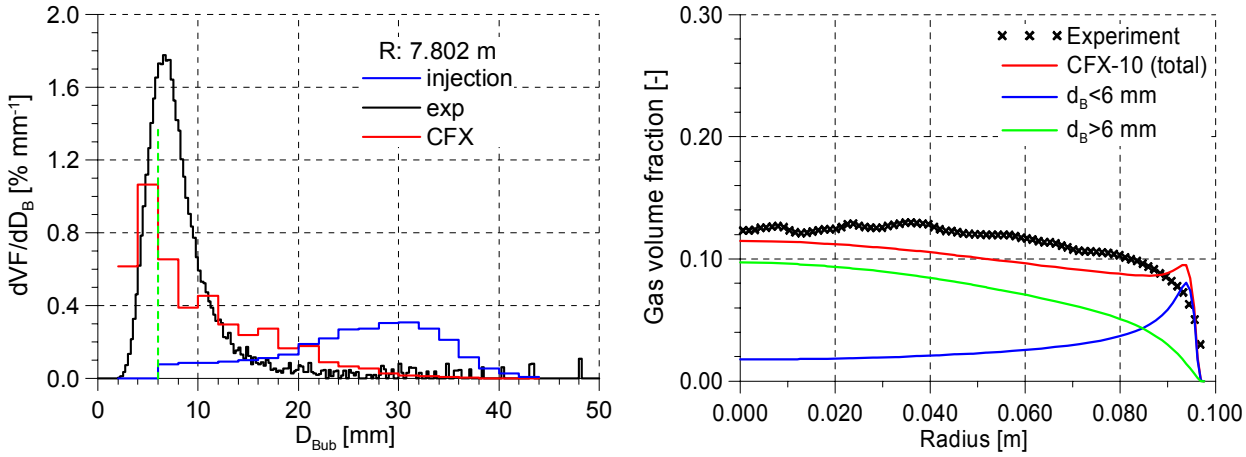

Fig. 6.3 Development of the bubble size distribution (left) and the radial gas fraction profiles (right) of the simulation of the test case TOPFLOW 107 (J_L = 1.017 m/s; J_G = 0.140 m/s); F_B = 0.25, F_C = 0.05

The inhomogeneous MUSIG model was applied for the simulation of a pronounced three-dimensional flow field (see chapter 8). With the actual model state the inhomogeneous MUSIG model not allows pretest predictions. But adjusting the bubble fragmentation and coalescence models the application of the inhomogeneous MUSIG model enables a deeper insight in the phenomena.

7. Evolution of a two-phase flow with phase transition

The condensation of saturated steam injected into a slightly sub-cooled water flow was studied at pressures of about 1 - 2 MPa (test runs see Tab. 7.1). The wire-mesh sensor purpose-built for steam-water tests at high pressure (section 2.2) was applied. It was used to record the evolution of the flow structure along the pipe, which is a result of the combined action of bubble coalescence and breakup together with the shrinking of bubbles due to the volume sinks caused by the condensation. The variation of the inlet length was performed using the variable gas injection system described in section 2.1.

Tab. 7.1 Conditions of test runs with sub-cooling and reference experiments

Run	Pressure			Superficial velocity		Temperature		Sub-cooling
	Sensor [MPa]	Steam drum [MPa]	Throttle [kPa]	Water [m/s]	Steam [m/s]	Water [°C]	Steam [°C]	Water [K]
1	1.07	1.00	70	1.017	0.534	177.8	182.8	5.0
2	1.10	1.00	100	1.017	0.534	177.8	184.0	6.2
3	2.08	2.00	80	1.017	0.534	210.5	214.4	3.9
4	2.16	2.00	160	1.017	0.534	210.5	216.3	5.8
Ref 1	1.00	1.00	0	1.017	0.534	177.8	179.2	1.4
Ref 2	2.00	2.00	0	1.017	0.534	210.5	211.2	0.7

The new detailed experimental data were used to check the complex interactions between the changes of local gas volume distribution, bubble size distribution and

local heat and mass transfer. To do this, the Multi Bubble Size Class Test Solver, first introduced by Lucas et al. (2001a) was extended to consider the phase transfer separately for each bubble class.

The pipe is supplied by water from the steam drum where saturation conditions are present (Fig. 1.1). Saturated steam comes from the electrical steam generator of TOPFLOW. A slight sub-cooling of the water (max. 6 K) was achieved by throttling a ball valve at the upper end of the vertical test section (Fig. 7.1). Behind this ball valve, saturation conditions are reached by expansion. Upstream the ball valve, the liquid phase is sub-cooled due to the head of the test section pump.

A visualization of the wire-mesh data (Fig. 7.2) is done by generating virtual side projections and side views of virtual central cuts from the mesh sensor data. For each mesh sensor data set, virtual side views and virtual centre cuts are combined in the same image. It is visible how bubbles injected at the periphery move towards the centre of the pipe in case of the reference experiment without sub-cooling, while in the experiment with condensation the bubble density decreases with growing distance from the injection device.

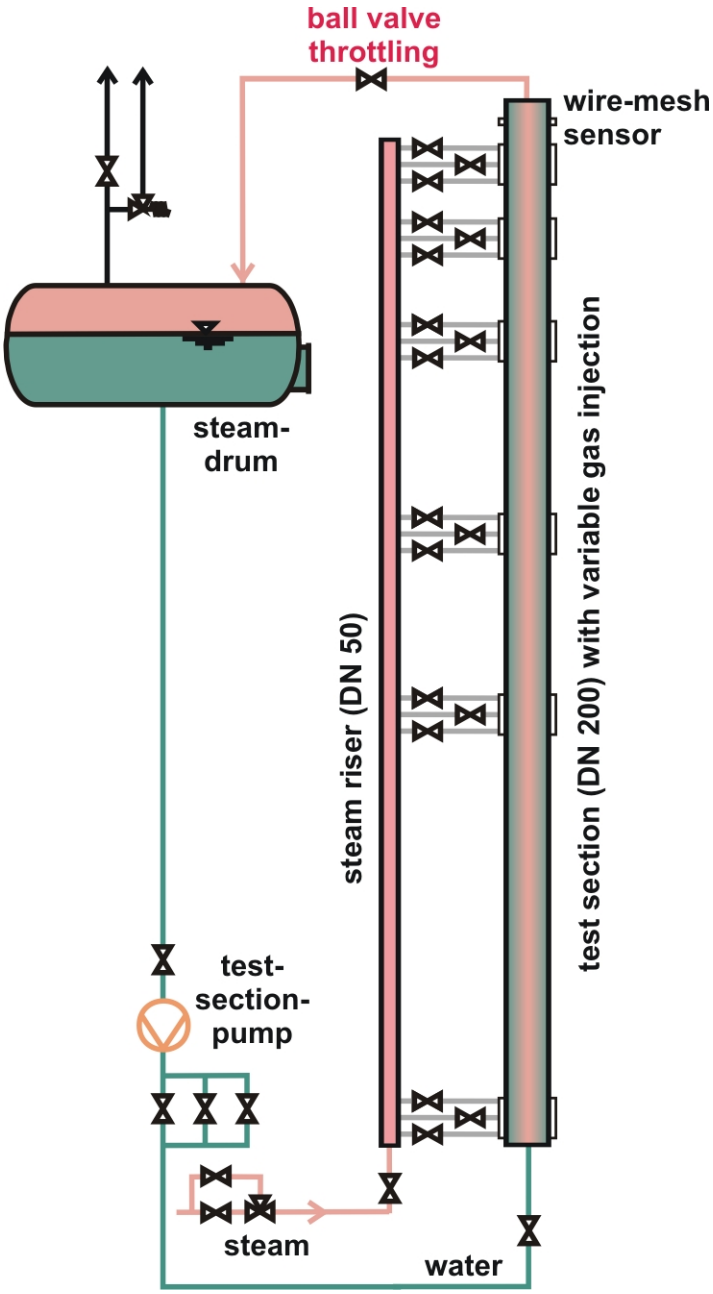

Fig. 7.1 Creation of a sub-cooling in the vertical test section with variable gas injection system by throttling the ball valve at the exit of the test pipe

Distributions of the extension of the bubbles in the horizontal measuring plane (i.e. in x-y direction) were used to characterize the bubble size. This technique was chosen instead of a calculation of equivalent bubble diameters, because for the latter information about the gas phase velocity is necessary, which was not measurable, since only one sensor was available. Without sub-cooling, the bubble-size distribution soon converges to an equilibrium, while an ongoing condensation disturbs the equilibrium, which can therefore not establish. In the consequence, bubble sizes at identical inlet lengths with condensation are significantly lower than without (Fig. 7.3).

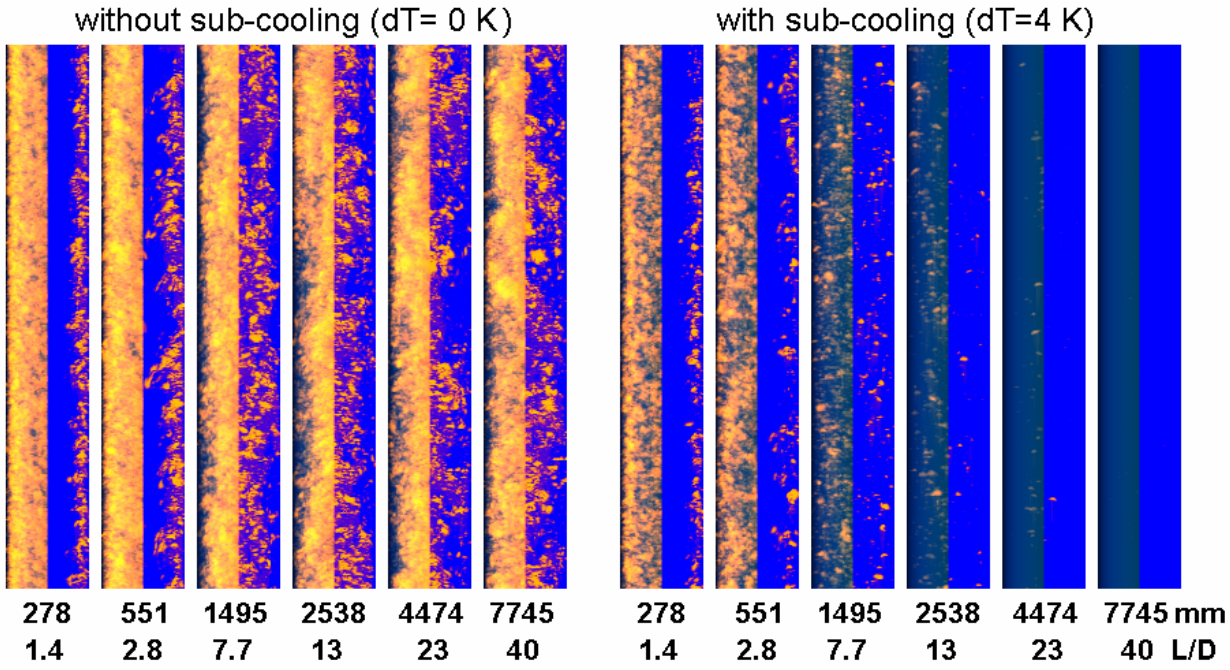

Fig. 7.2 Virtual side projections (left halves of the columns) and side views of virtual central cuts (right halves) of the mesh sensor data, test run 4, D_{inj} = 4 mm

The simplified test solver (Lucas et al., 2001a, 2001b and 2005b) was used to reproduce the measured radial profiles and bubble-size distributions. The simplified, one-dimensional model, which resolves the parameters in radial direction and which considers a large number of bubble classes was extended to support transient mass and heat transfer between the phases (Lucas & Prasser, 2005a).

The dynamics of the phase transfer is determined by the heat fluxes to or from the interface. It is assumed, that interface itself is on saturation temperature, which is function of the local pressure, while the bulk temperature of the liquid phases far from the interface differ from saturation. For the gaseous phase thermodynamic equilibrium is assumed. The interfacial heat transfer from the liquid phase to each bubble-size class was calculated according to the correlation given by Hughmark (1967), where the actual bubble size enters as an input parameter. The correlation was originally obtained for forced convection around a rigid sphere. It possibly under-predicts the heat transfer for gas liquid flows.

The interfacial area was calculated separately for each bubble class. To do that, an ellipsoidal shape of the bubbles according to the correlation from Wellek (1966) for the relation of horizontal and vertical axis of the ellipsoid bubble was assumed. The extrapolation of the Wellek correlation to very large bubbles is questionable since the bubble shape changes from ellipsoidal to spherical cap, but for the lack of more detailed information on the interfacial area it is used as a first approximation.

The mass transfer rate is calculated separately for each bubble class and each radial node. Afterwards, the changes of the liquid temperature for each node are calculated on basis of energy conservation. New vapour temperatures are obtained separately for each bubble class and node. To reflect the mass transfer, the changes of the vapour volume fraction are calculated for each bubble class and each radial node.

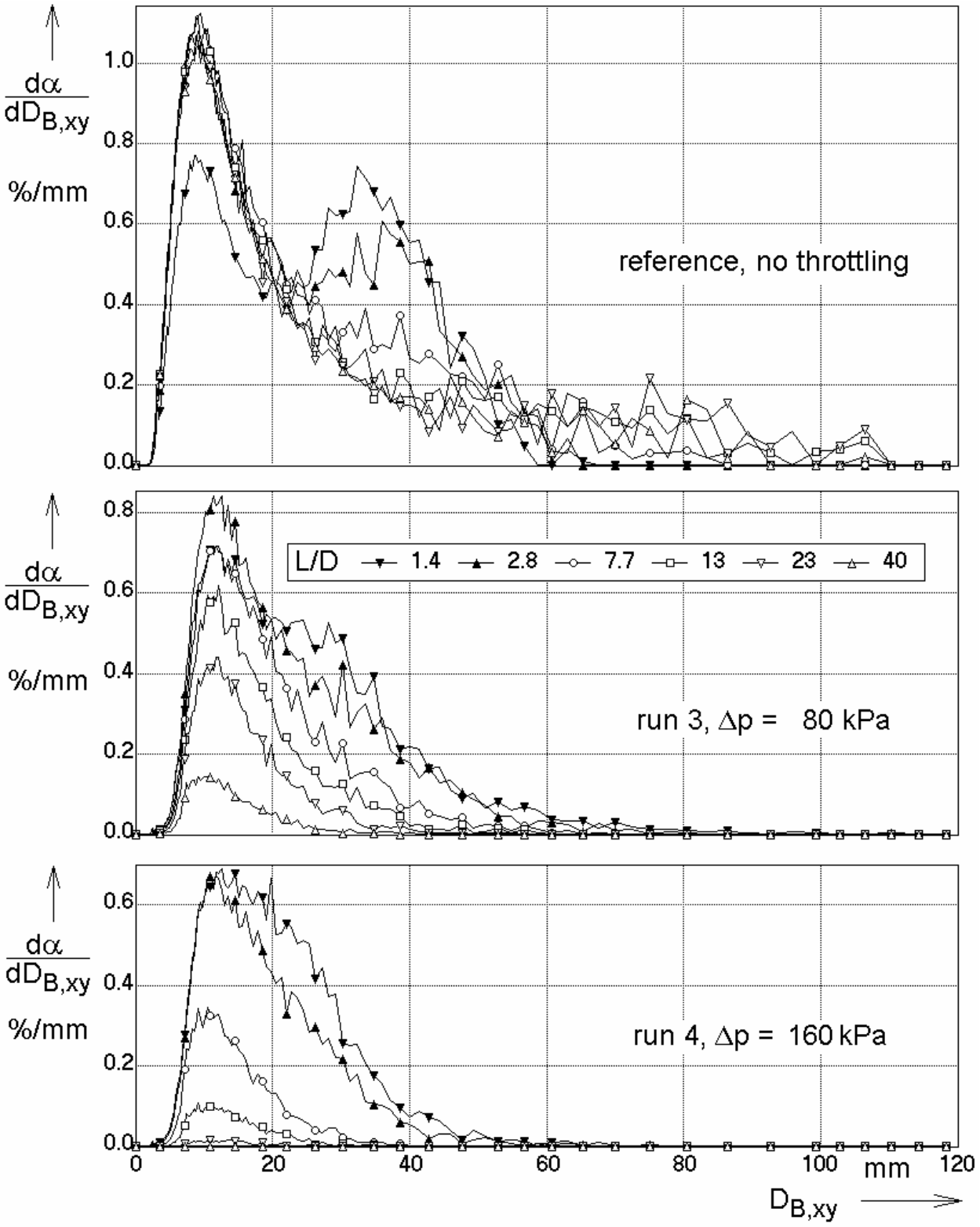

Fig. 7.3 Bubble-size distributions, test run 3 and 4, D_{inj} = 4 mm

The most substantial change compared to the modelling of a flow without phase transitions is the fact, that beside the decrease of the volume fraction caused by the condensation process, the shift in the local bubble size distributions towards smaller bubbles has to be considered. According to the changes in bubble size, source and sink terms are obtained and implemented into the conservation equations for all

bubble-size classes. The shift of the gas volume fraction to a group of smaller bubble size is demonstrated schematically in Fig. 7.4.

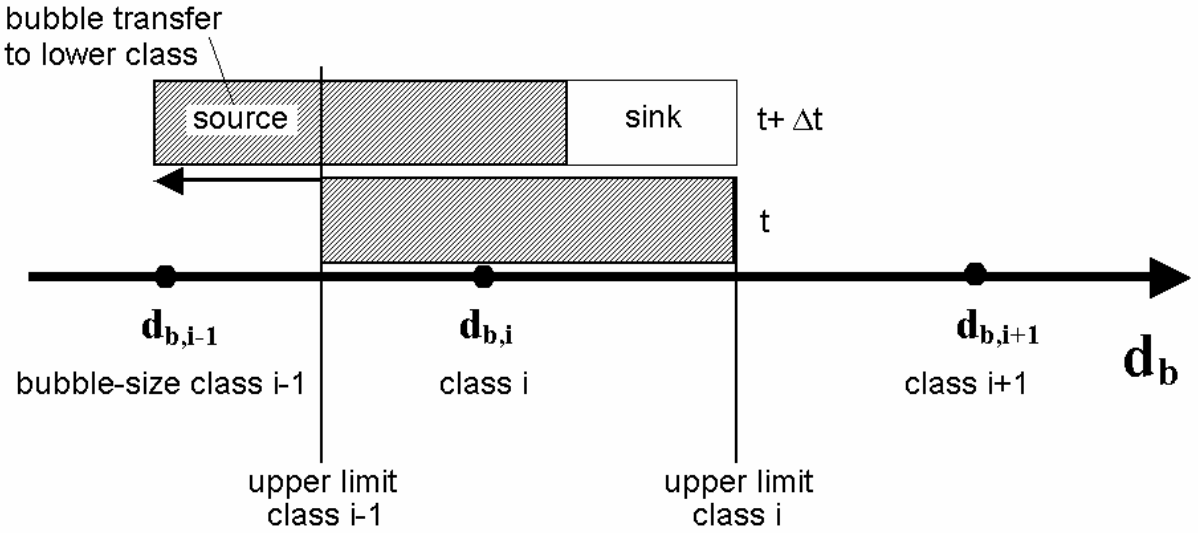

Fig. 7.4 Shift of volume fraction to lower bubble size group caused by the shrinking of the bubbles

To keep the model simple, a uniform vertical bubble rise velocity (according to the bubble velocity averaged over all the bubble classes and over pipe cross section) was assumed. In stationary flows, this simplification allows to use proportionality between rise time and travelling distance in vertical direction. In a real CFD simulation, the difference between the rise velocities of bubbles of different size can be taken into account using the Inhomogeneous MUSIG model (section 6). For the test of the bubble transfer terms due to condensation and the interfacial heat transfer correlations, the simplification is a good approximation, since forced circulation cases are studied, where the differences in the bubble rise velocity for different bubble sizes are much smaller than the dominating liquid velocity.

For the comparison of the model with the experimental results, an initial bubble size distribution, radial gas fraction profile and total gas volume fraction are necessary. They were taken from the measurement at the closest distance from the gas injection (L/D = 1.1 for injection via 1 mm orifices, L/D = 1.4 for injection via 4 mm orifices). It has to be kept in mind that measured bubble sizes represent the diameter of the circle equivalent to the maximum area of the measuring plane covered by the bubble during its passage through the sensor. For the input into the model, volume equivalent bubble sizes are needed. The use of the measured distributions as a boundary condition is therefore a compromise that has to be taken, since other data is not available.

The initial liquid temperature was set to the measured values. The pressure was set to the nominal pressure in the steam drum plus the overpressure generated by partially closing the ball valve. In addition the growing hydrostatic pressure and the resulting increase of the saturation temperature with increasing distance in the vertical pipe is considered in the simulation. The development of the flow was calculated for different distances between the gas injection and the wire-mesh sensor, available in the variable gas injection system (Fig. 2.3).

On the basis of a comparison with measured bubble-size distributions and void fraction profiles along the pipe, it was concluded that the proposed extension of the

multi-bubble class model to consider the phase transition due to condensation was successful. The calculated and measured axial void fraction curves and bubble size distributions for a selected test case are given in Fig. 7.5 and Fig. 7.6. The calculations were generally found to be in a good agreement with the experimental data. Some deviations are attributed to weaknesses of the applied bubble coalescence and breakup models and to uncertainties of the interfacial heat transfer model. The effect of the initial bubble size caused by the different diameter of the injection orifices is clearly reproduced in the simulations. A detailed presentation of the simulations can be found in Lucas & Prasser (2007a).

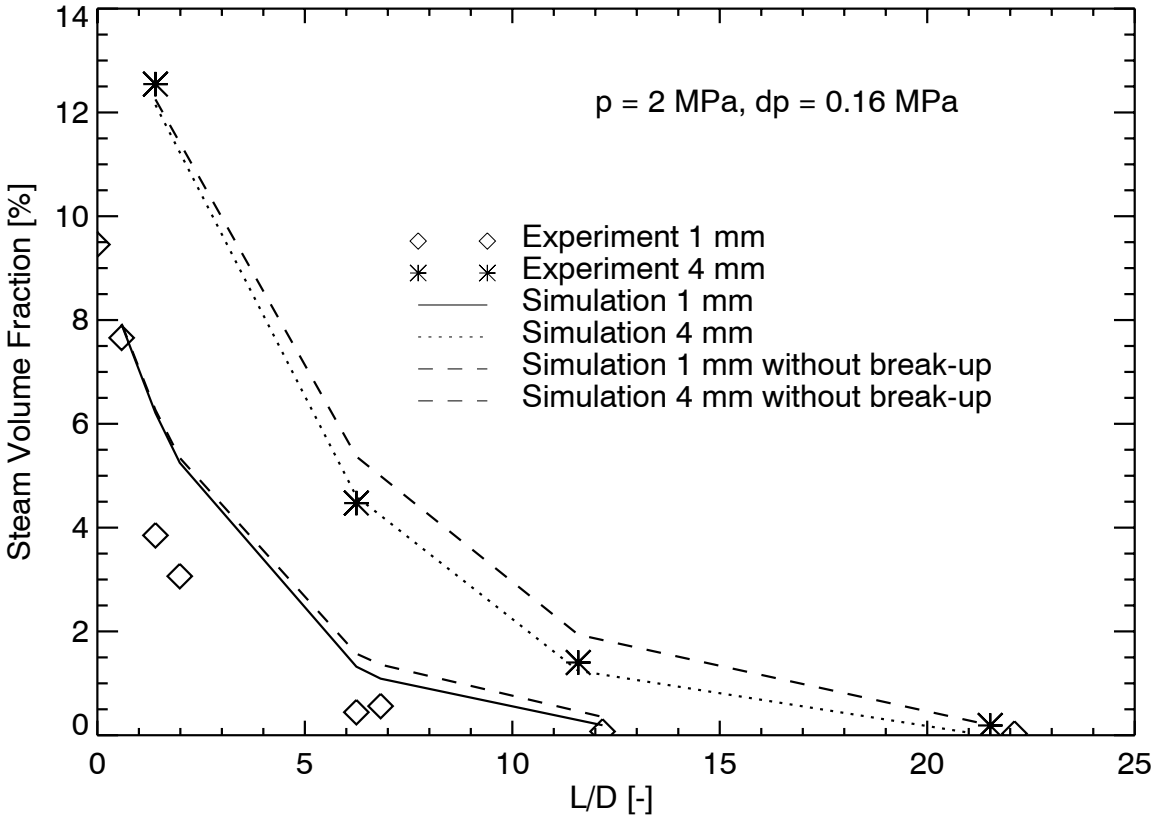

Fig. 7.5 Comparison of the calculated evolution of the cross section averaged steam volume fraction (with and without consideration of break-up) with experimental results

It is recommended to implement the tested model equations into the Inhomogeneous MUSIG model. Further attention has to be paid to the improvement of bubble coalescence and breakup correlations as well as to the description of the interfacial heat transfer. This is of particular relevance for future projects, since the available experimental material is still quite limited. It is restricted to a few parameter variations and, above all, to situations with a small sub-cooling of the liquid phase. Experiments with higher sub-cooling require an injection of sub-cooled water into the test section, which imply an extension of the TOPFLOW facility. Such tests were proposed for the successor project.

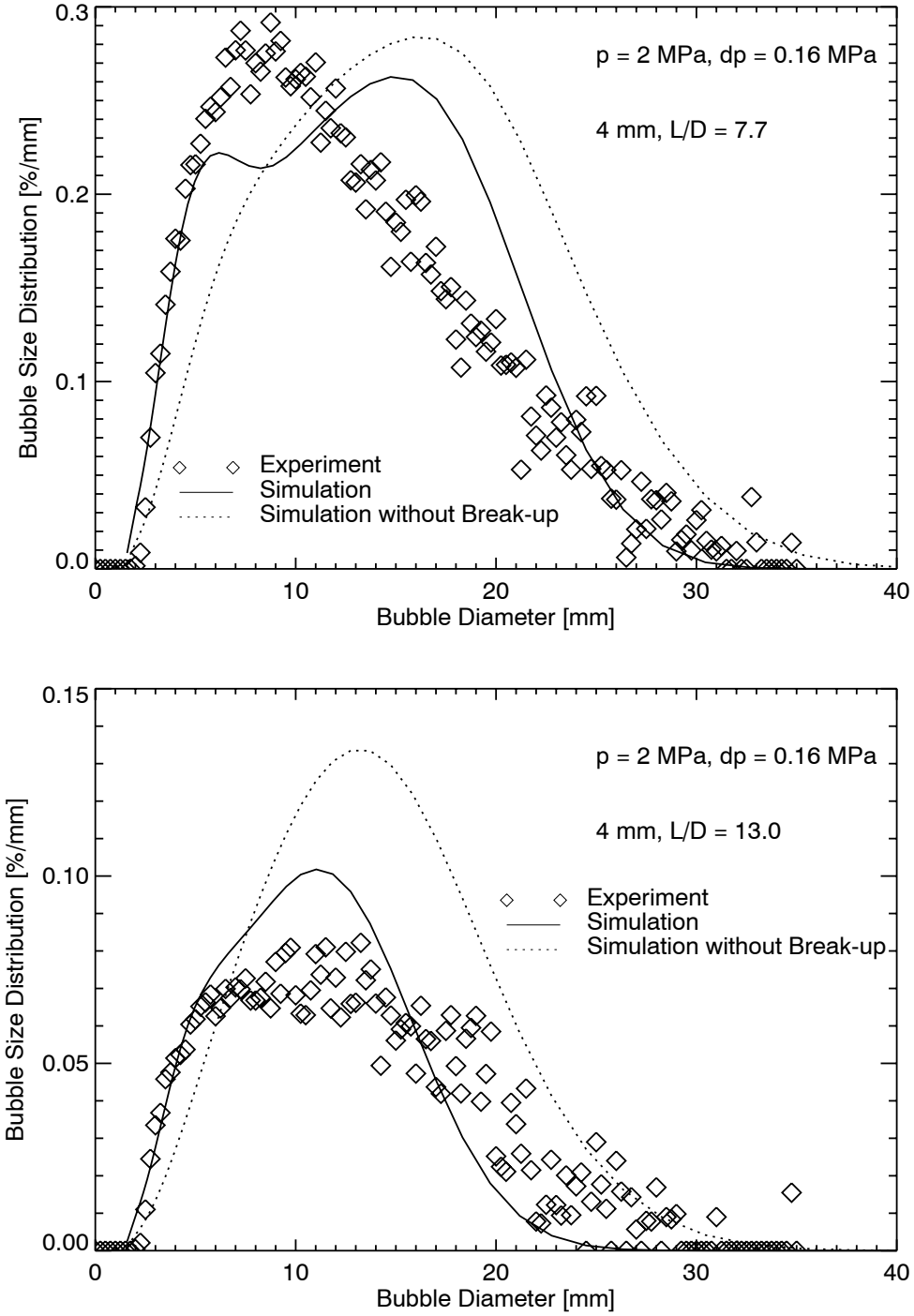

Fig. 7.6 Comparison of the calculated and measured bubble size distributions for 2 different L/D

8. CFD Validation for pronounced three-dimensional flow fields - experiments with movable obstacle

The assumption of the geometry-independence of new closure relations implemented into the CFD code as well as the postulated transferability of the models to different complex geometries that arise from the way CFD codes discretize the flow domain has to be proven by a validation against adequate experiments. For this purpose, the large test section with a nominal diameter of DN200 was used to study the flow field around an asymmetric obstacle. This is an ideal test case for the CFD code validation, since the obstacle creates a pronounced three-dimensional two-phase flow field. Curved stream lines, which form significant angles with the gravity vector, a recirculation zone in the wake and a flow separation at the edge of the obstacle are phenomena widespread in real industrial components and installations. It has to be shown that the CFD-code predicts these phenomena well, after it has been extended by new models, developed in simpler experimental geometries.

Tab. 8.1 Test matrix of the experiments with the movable obstacle, numbers: test run identifiers

		gas – superficial velocity							
	m/s	0,0368	0,0574	0,0898	0,14	0,219	0,342	0,534	0,835
water – superficial velocity	1,611	75	86	97	108	119	130	141	152
	1,017	74	85	96	107	118	129	140	151
	0,405	72	83	94	105	116	127	138	149
	0,102	69	80	91	102	113	124	135	146

One of the test series at the large vertical test section of TOPFLOW was dedicated to this kind of code validation in complex geometries. The technique of the movable obstacle was used, described in section 2.3. Test series were performed with an air-water flow at ambient conditions (temperature about 30 °C) as well as with a steam-water mixture at saturation pressure of 6.5 MPa and the corresponding temperature of 281 °C. Tab. 8.1 contains a section of the general measurement matrix of the FZD. The highlighted numbers correspond to the tests with the obstacle. Before the experiments were commissioned, an ANSYS CFX 10.0 pre-test calculation was carried out for one of the air-water tests (Prasser et al., 2006a).

The diaphragm (Fig. 2.8) is a half-moon shaped disk, the straight edge of which is arranged along the diameter of the pipe, while the circular edge is at a distance of 10 mm from the inner wall of the pipe. The distance between sensor and diaphragm was varied from 10 mm to a maximum distance of 520 mm for both cases: (1) sensor downstream of the obstacle and (2) sensor upstream of the obstacle.

The sensor data was used to calculate two-dimensional time-averaged void fraction distributions in the measuring plane. By combining the information from different distances between sensor and diaphragm, full three-dimensional void distributions around the obstacle were obtained. A centre cut along the axis of the test pipe in a vertical plane perpendicular to the straight edge of the half-moon diaphragm is a very illustrative way to visualize the void fraction field. Beside void fractions, time-averaged local liquid velocities can be extracted by evaluating the transit time of bubbles of a certain range of diameters. The lateral extension of each individual

bubble related to the transit time of a bubble is proportional to the bubble velocity. A local instantaneous value of the liquid velocity is available after subtracting the bubble rise velocity. The proportionality factor was found by integrating the liquid velocity and comparing the superficial water velocity reconstructed in this way with the injected liquid flow rate. Time-averaged profiles of the axial liquid velocity are calculated by averaging individual values from a manifold of analysed bubbles.

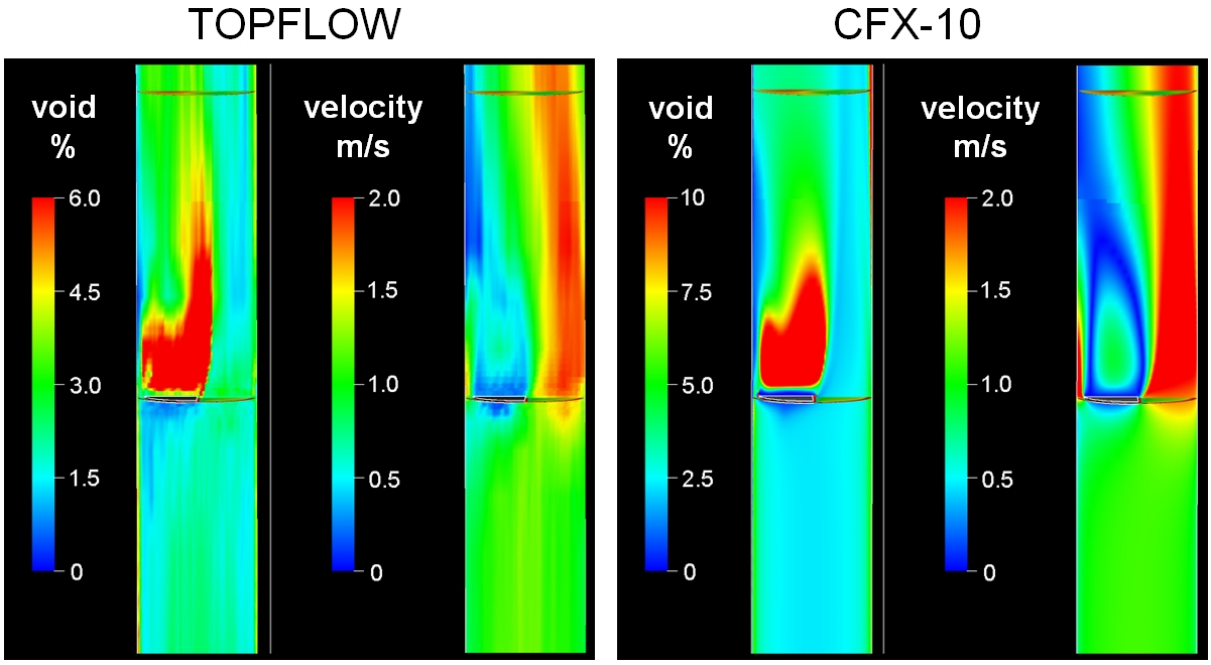

Fig. 8.1 Confrontation of experiment and CFX pre-test calculation by comparison of time averaged void fraction and absolute liquid velocity distributions up- and downstream of the obstacle in the air-water test run 074, J_L = 1.017 m/s, J_G = 0.0368 m/s

The void fraction and liquid velocity profiles for an air-water experiment with J_L = 1 m/s and J_G = 0.037 m/s are shown in Fig. 8.1 together with the results of a steady-state CFX-10 pre-test calculation. The latter was carried out using the two-fluid model with a mono-disperse bubble size of 5 mm and a two-equation turbulence model (SST) on a grid of 473000 hexahedral mesh elements. Calculation and experiment show the same global structures. There is a stagnation point in front of the diaphragm that is depleted from bubbles. Bubbles are pushed away from the stagnation point due to the curvature of the streamlines. The flow separates at the edge of the obstacle. Downstream, there is a stagnation zone with a recirculation area above the obstacle and a jet coming from the non-obstructed part of the cross-section. In the recirculation area, gas phase is accumulated. The local maximum of the velocity in the centre of this region corresponds to a downwards motion of the liquid phase. Negative velocities cannot be distinguished from positive one, since the measuring method described above is not sensible to the direction of the bubble passage through the measuring plane. For further information about the measuring method see the technical report: "*Experiments on two-phase flow in a vertical tube with a moveable obstacle*", appendix: A 2.

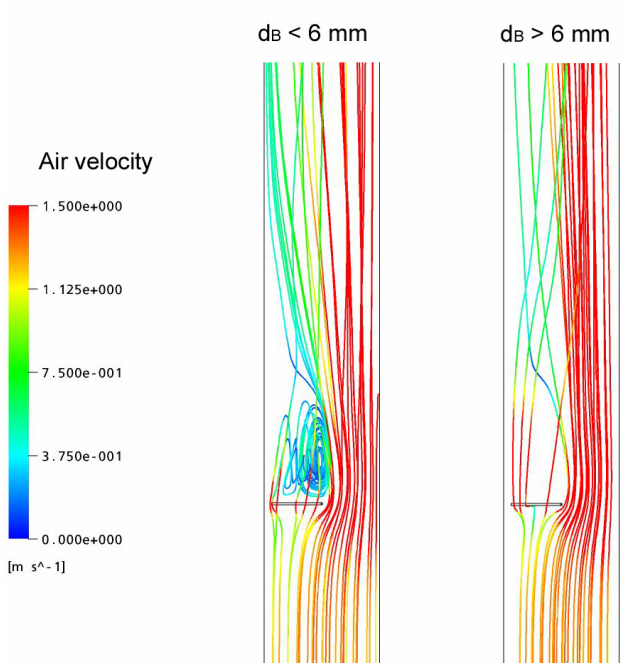

Fig. 8.2 Streamlines for small (left) and large (right) bubbles, run 096:
J_L = 1.017 m/s, J_G = 0.0898 m/s

With the actual model state the inhomogeneous MUSIG model not allows pretest predictions. But adjusting the bubble fragmentation and coalescence models the application of the inhomogeneous MUSIG model enables a deeper insight in the phenomena. So also for this application the capabilities of the model could be proven in principle. In the calculation, the accumulated gas in the recirculation area downstream the obstacle consists mostly of small bubbles (see Fig. 8.2). In the measurements, larger bubbles are found in this region (see Fig. 8.3). Obviously the bubble coalescence caused by gas accumulation dominates over the fragmentation caused by the turbulence effects. In the calculation the fragmentation is overestimated.

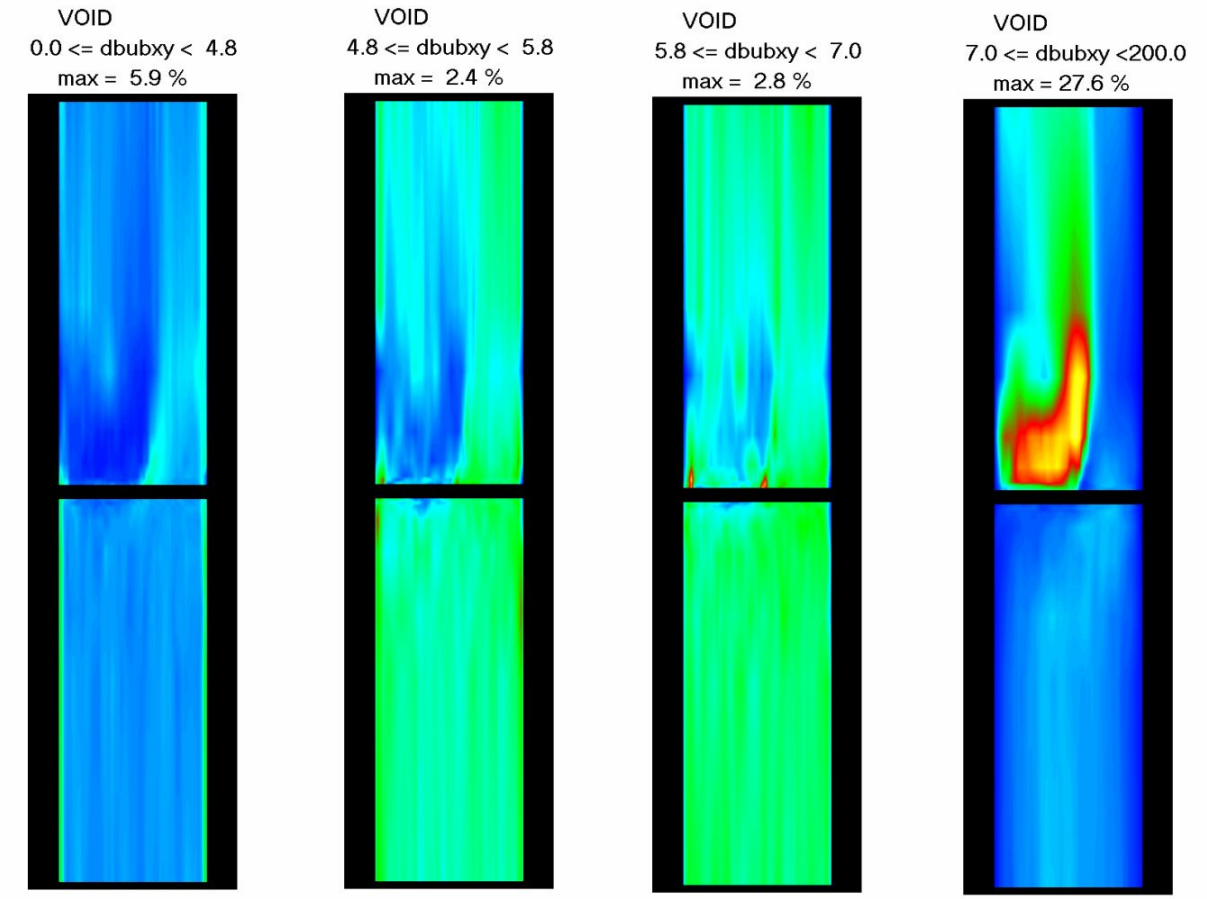

Fig. 8.3 Measured gas distributions resolved to bubble size regions;
run 096: J_L = 1.017 m/s, J_G = 0.0898 m/s

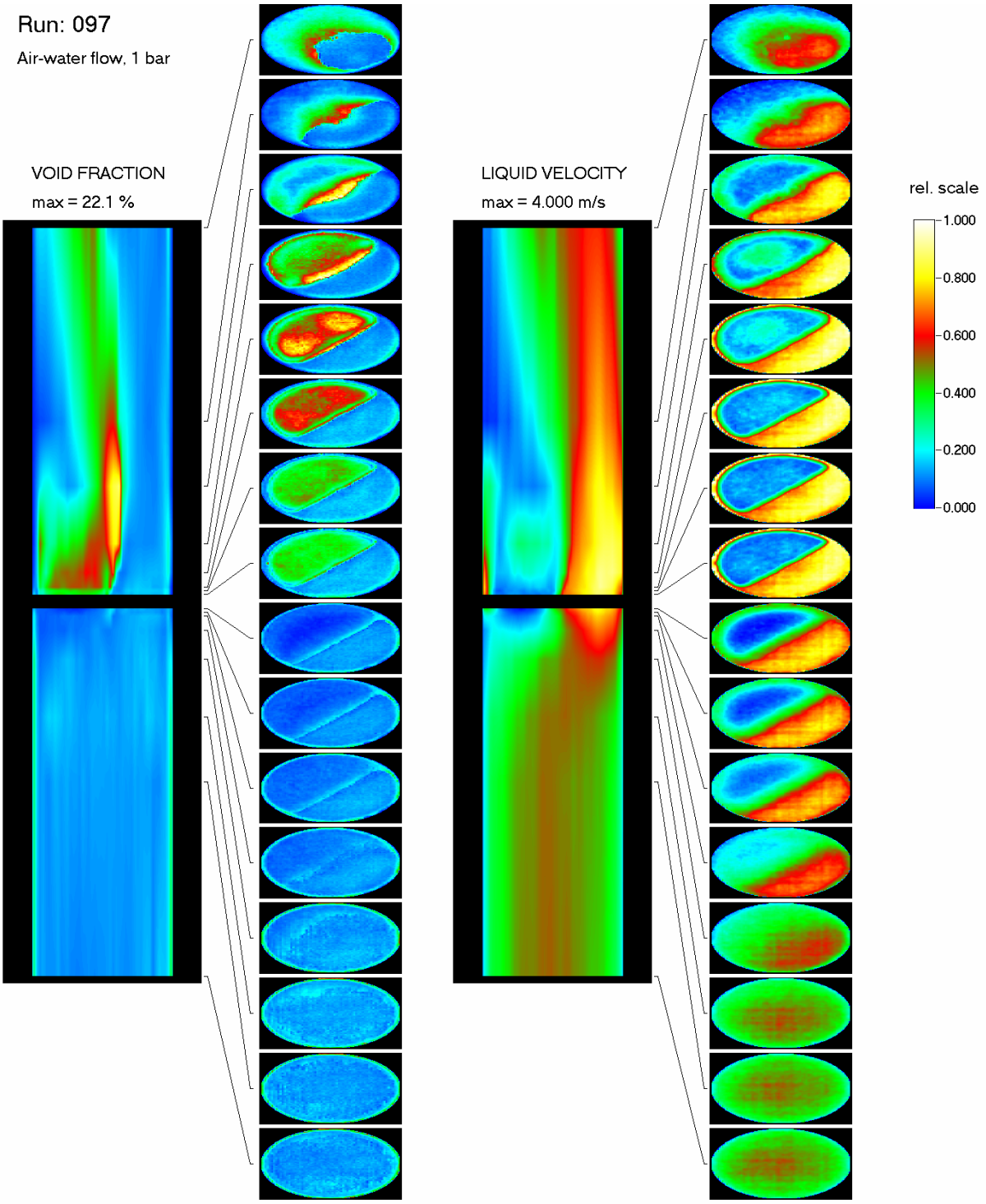

Fig. 8.4 Void-fraction and liquid velocity distribution upstream and downstream of the half-moon shaped diaphragm, air-water experiment 97; J_L = 1.611 m/s, J_G = 0.0898 m/s

A closer look to the void fraction distribution downstream of the diaphragm shows, that there is a clearly separated stable region of very low gas fractions in the jet that is coming from the non-obstructed part of the cross-section (Fig. 8.4). This effect was observed in air-water tests at ambient pressure and at superficial water velocities above 0.4 m/s. Bubbles are obviously hindered to enter the jet by the lift force. They crowd up at the boundary of the jet, where a local gas fraction maximum is found. In

the calculations this phenomenon can also be found for small bubbles (see Fig. 8.5). For the total values the phenomenon is partially compensated by the contributions of large bubbles (compare to Fig. 8.6). The calculated bubble size distribution has a strong influence on the integral gas distribution.

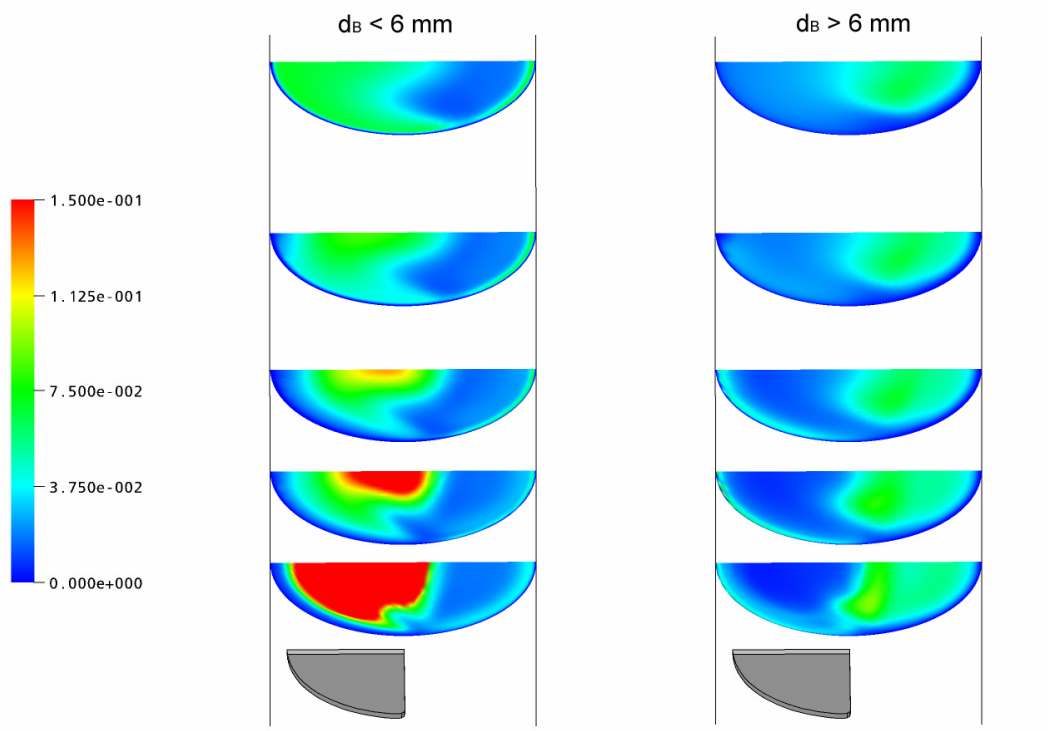

Fig. 8.5 Calculated gas volume fraction distributions for small and large bubbles 0.08 m, 0.16 m, 0.25 m, 0,37 m and 0,52 m downstream the obstacle; run 096

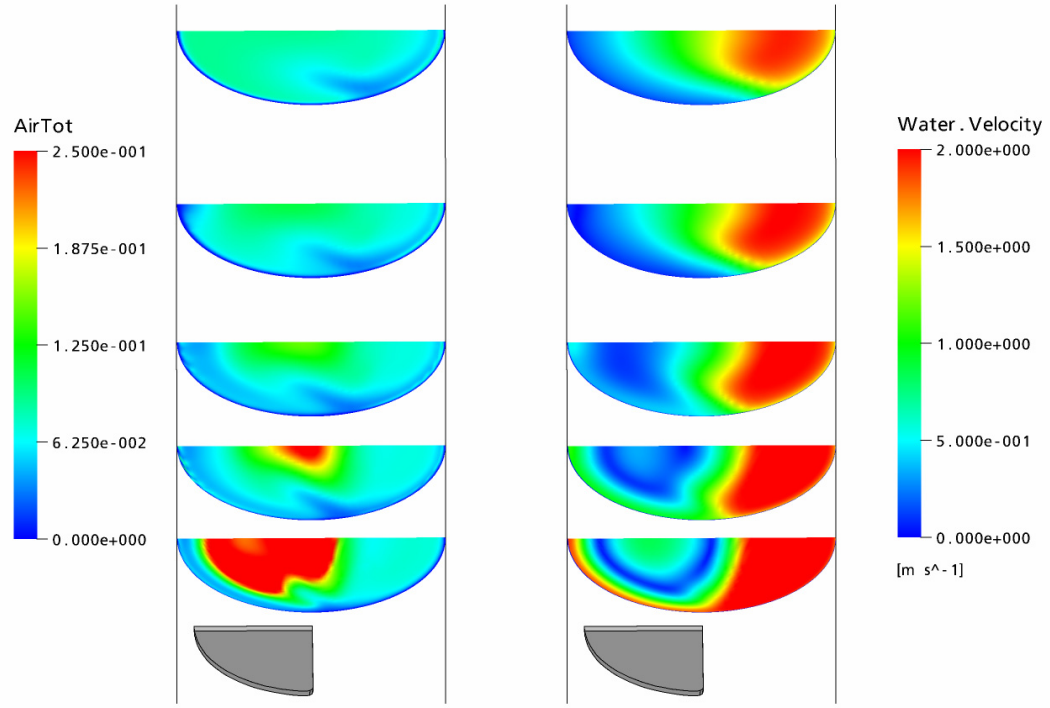

Fig. 8.6 Calculated integral gas volume fraction and water velocity distribution; run 096

The effect vanishes, when the fluid is changed to a high-pressure saturated steam-water flow, where the mentioned above coherent structure was not observed (Fig. 8.7).

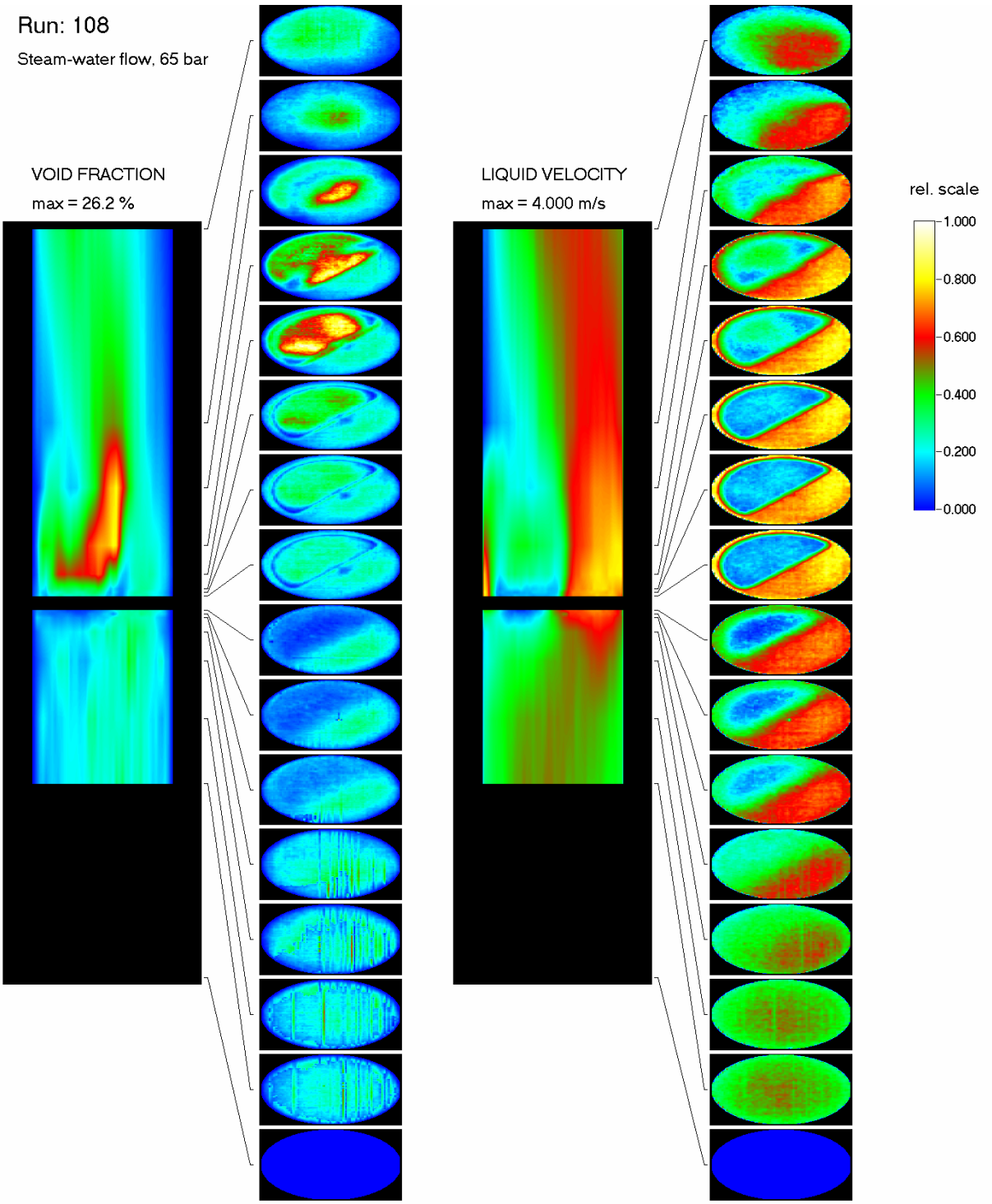

Fig. 8.7 Void-fraction and liquid velocity distribution upstream and downstream of the half-moon shaped diaphragm, steam-water exp. 108 at 6.5 MPa, J_L = 1.611 m/s, J_G = 0.14 m/s (void fraction at the sensor corresponds approximately to the air-water case shown in Fig. 8.4 due to partial condensation)

It is a future task to analyze this effect with the CFD code. It has to be expected that the smaller critical bubble diameter for the lift force reverse is the cause of the ob-

served phenomenon, which is therefore an ideal verification case for the Inhomogeneous MUSIG model in CFX.

A comparison with CFD calculations for a safety valve reveal, that all phenomena occurring e.g. in an industrial safety valve are reflected in the test geometry (Fig. 8.8). There is a topologic similarity between both geometries, although the geometry itself is different. This illustrates that a code validation against data from such kind of experiments contributes to the solution of industrially relevant problems despite of the simplifications that enable a very comprehensive acquisition of experimental data.

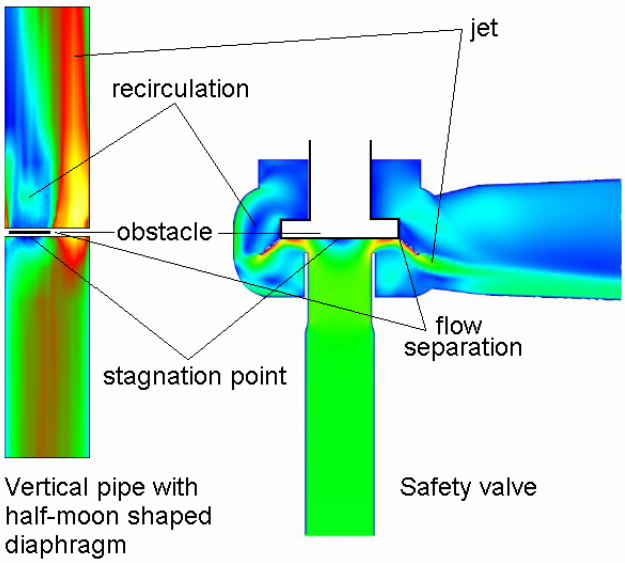

Fig. 8.8 Topologic similarity between the obstacle in the test pipe and an industrial safety valve

9. Dynamic free surface of stratified and slug flows

Slug flow as a stratified multiphase flow regime can occur in the main cooling lines of pressurized water reactors, for instance after a small break Loss of Coolant Accident (LOCA), and also in other fields, like chemical plants or oil pipelines. The slug flow regime is usually characterized by an acceleration of the gaseous phase and by the transition of fast liquid slugs, which carry a significant amount of liquid with high kinetic energy. It is potentially hazardous to the mechanical structure of the system due to the strong oscillating pressure levels formed behind the liquid slugs as well as the mechanical momentum of the slugs.

For the investigation of stratified two-phase flow, two horizontal channels with rectangular cross-section were built. The channels allow the investigation of air/water co-current flows, especially the slug behaviour, at atmospheric pressure and room temperature. The test-sections are made of acrylic glass, so that optical techniques, like high-speed video observation or particle image velocimetry (PIV), can be applied for measurements. The rectangular cross-section was chosen to provide better observation possibilities.

The first channel (Fig. 9.1) was built to perform preliminary tests for the planned hot-leg experiments. The straight channel is 2.35 m long and is mounted between two separators, which allows for co- and counter-current flows. Optical measurements were performed with a high-speed video camera. The images were analysed and an interface capture method was developed (Vallée et al. 2006). This allows extracting quantitative information from the image sequences (Fig. 9.2), for example the water level history in different cross-sections. These optical recordings were complemented by simultaneous dynamic pressure measurements. The latter shows that the order of magnitude of the pressure behind the slug is about a few kPa. The pressure increase is fast (2 to 10 ms) and the decrease starts when the slug is leaving the duct towards the outlet separator.

Furthermore, the velocity field of a slug was measured using PIV. It reveals the inner flow circulation of the slug around the point, where the slug is rolling over (Fig. 9.3).

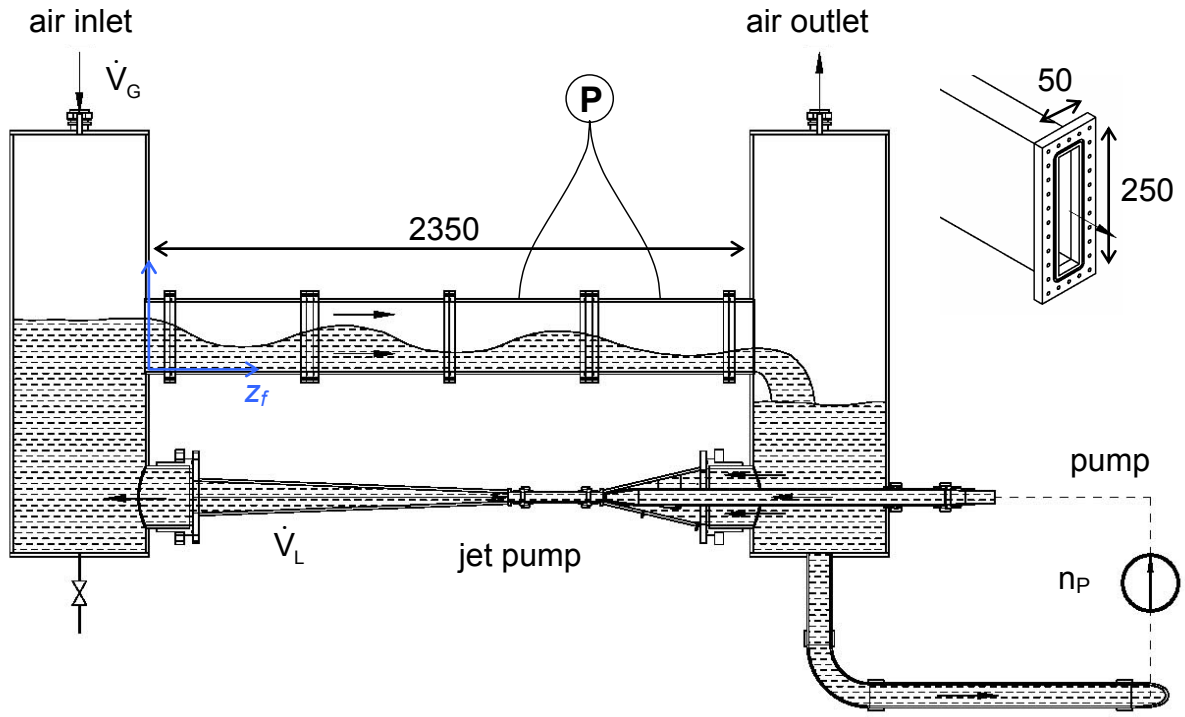

Fig. 9.1 Schematic view of the horizontal channel with inlet and outlet separators

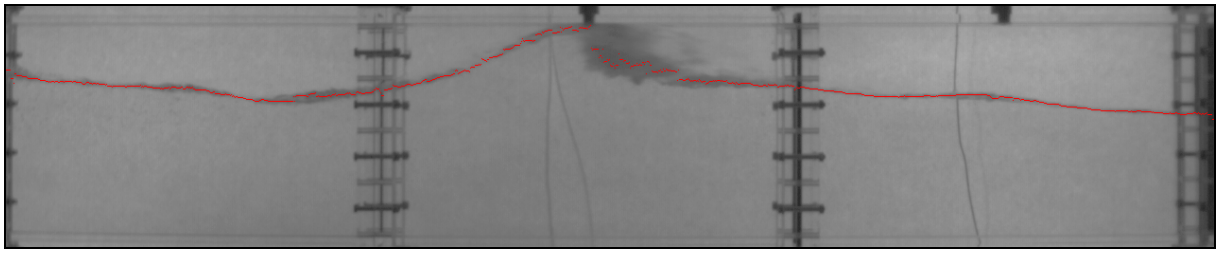

Fig. 9.2 Detected interface line (red) over original image from the high-speed camera during slug flow

The success of the first test channel motivated the construction of an improved test facility: the **H**orizontal **A**ir/**Wa**ter **C**hannel (HAWAC) dedicated to co-current flows (Fig. 9.4). The height of the rectangular cross-section was reduced to allow for velocity measurements with PIV over the entire height of the channel. In the HAWAC test facility, a special inlet device (Fig. 9.5) was designed to provide defined inlet boundary conditions by a separate injection of water and air into the test-section. Further, a blade separating the phases can be moved up and down to control the free inlet cross-section for each phase. These defined even so variable boundary conditions offer very good CFD-code validation possibilities. Last but not least, the 8 m long test-section, which corresponds to a length-to-height ratio *L/h* of 80, is enough to study the generation and evolution of the flow regime.

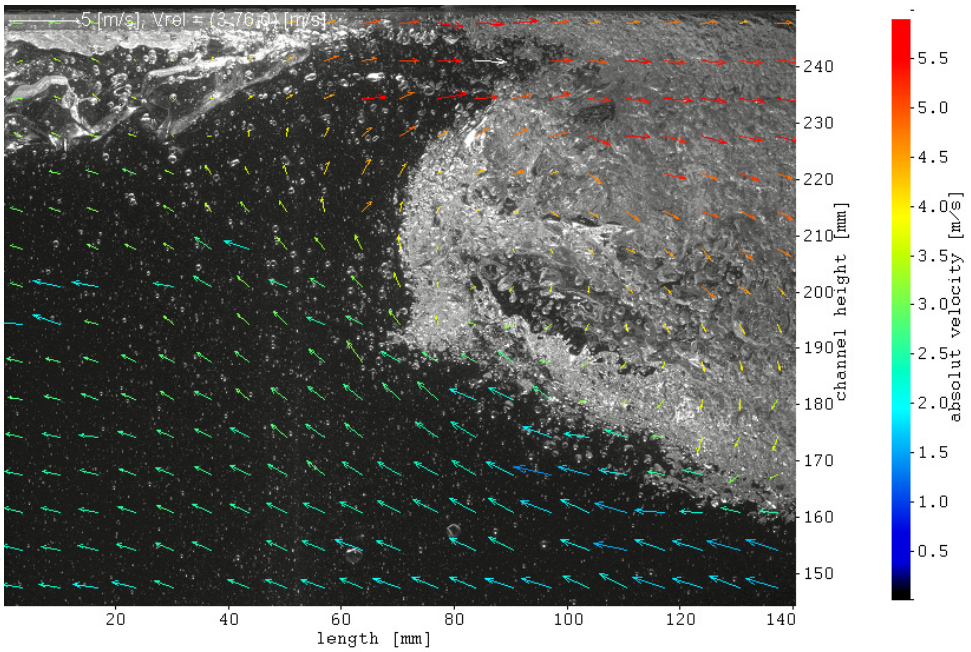

Fig. 9.3 Velocity field of the secondary flow inside of a slug (the vector colour shows the absolute velocity; the vector length and direction show the relative velocity after subtracting the propagation velocity of the slug)

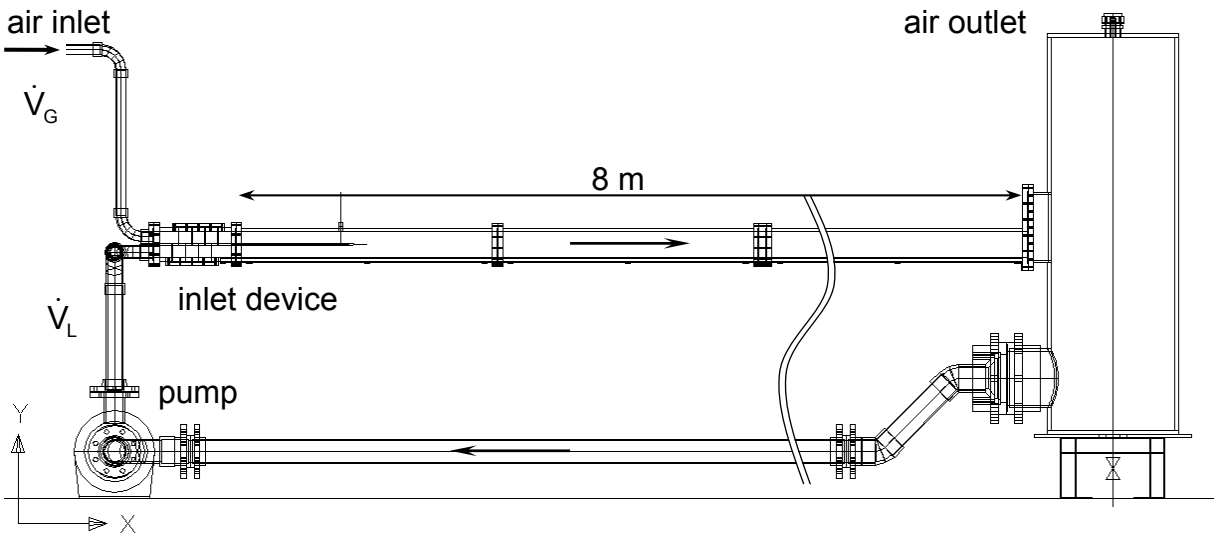

Fig. 9.4 Schematic view of the Horizontal Air/Water Channel (HAWAC)

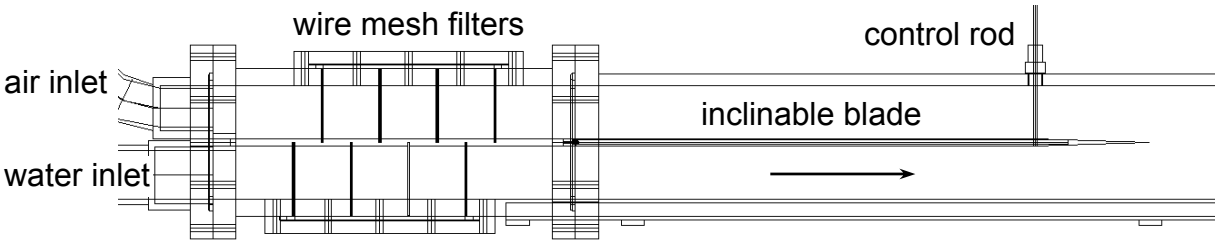

Fig. 9.5 The HAWAC inlet device

A flow pattern map was arranged and shows the potential of the HAWAC facility (Fig. 9.6): stratified smooth and stratified wavy flows were observed, as well as elongated bubble- and slug flow. Further, it was demonstrated that a variation of the inlet blade angle influences the generation of the two-phase flow regime. Especially at high water flow rates, and when the inlet blade is inclined down, a hydraulic jump can be realised in the test-section. This is an interesting phenomenon, particularly for CFD-validation purposes.

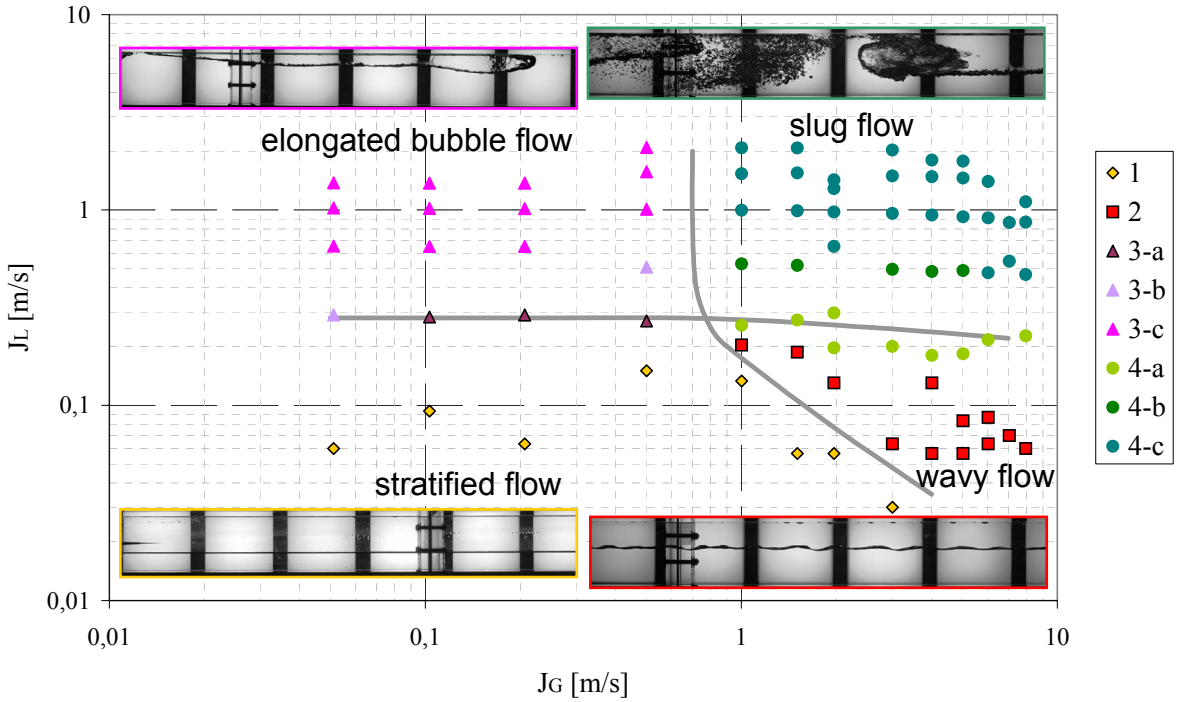

Fig. 9.6 Flow pattern map for the rectangular channel (inlet blade in horizontal position)

Parallel to the experiments, CFD calculations were carried out. The numerical simulations aim at the validation of prediction of the slug flow using the existing multiphase flow models built in the commercial code *ANSYS CFX*. Further, it is of interest to prove the understanding of the general fluid dynamic mechanism leading to slug flow and to identify the critical parameters affecting the main slug flow properties (like e.g. slug length, frequency and propagation velocity; pressure drop).

For the simulations, the Euler-Euler two fluid model with the free surface option was applied on grids of minimum $4 \cdot 10^5$ control volumes. The turbulence was modelled separately for each phase using the *k-ω* based shear stress transport (SST) turbulence model. In order to keep reasonable calculation times, just the horizontal test-section was modelled.

In the geometry of the HAWAC, the two-fluid model was applied with a special free surface treatment. Due to an interfacial momentum transfer, it was possible to generate slugs based on instabilities in this longer test-section (Fig. 9.7 and Vallée et al., 2007). A sequence of the volume fraction calculated with ANSYS CFX was compared with the camera frames recorded at equivalent boundary conditions (Fig. 9.8). The behaviour of slug generation and propagation at the experimental setup was qualitatively reproduced. Instabilities and small waves are generated by the interfacial momentum transfer randomly. As a result bigger waves are generated and some grow to slugs. Also the merging of waves was reproduced. However, quantita-

tive deviations were noticed, for example with the entrance length needed for slug generation. It was defined as the length between the inlet and the location nearest the inlet where a wave closes nearly the entire cross-section. This was observed at about 1.5 m in the experiment and 2.5 m in the calculation. These discrepancies require a continuation of the work.

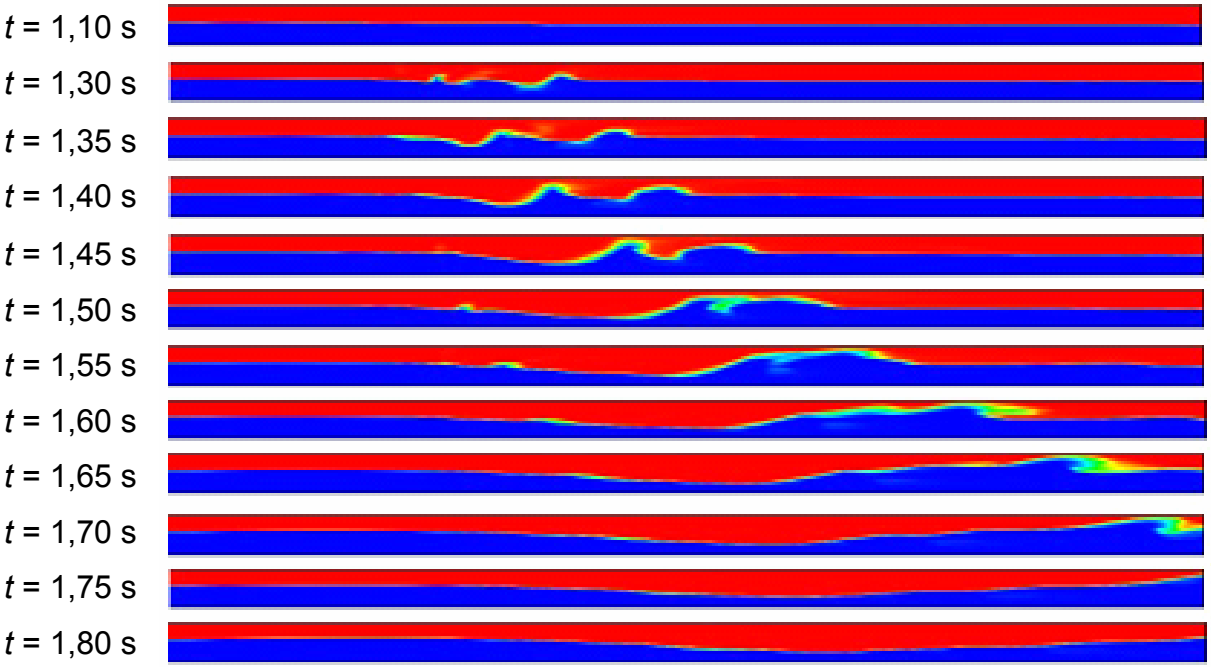

Fig. 9.7 Calculated picture sequence at J_L = 1.0 m/s and J_G = 5.0 m/s (depicted part of the channel: 1.4 to 4 m after the inlet)

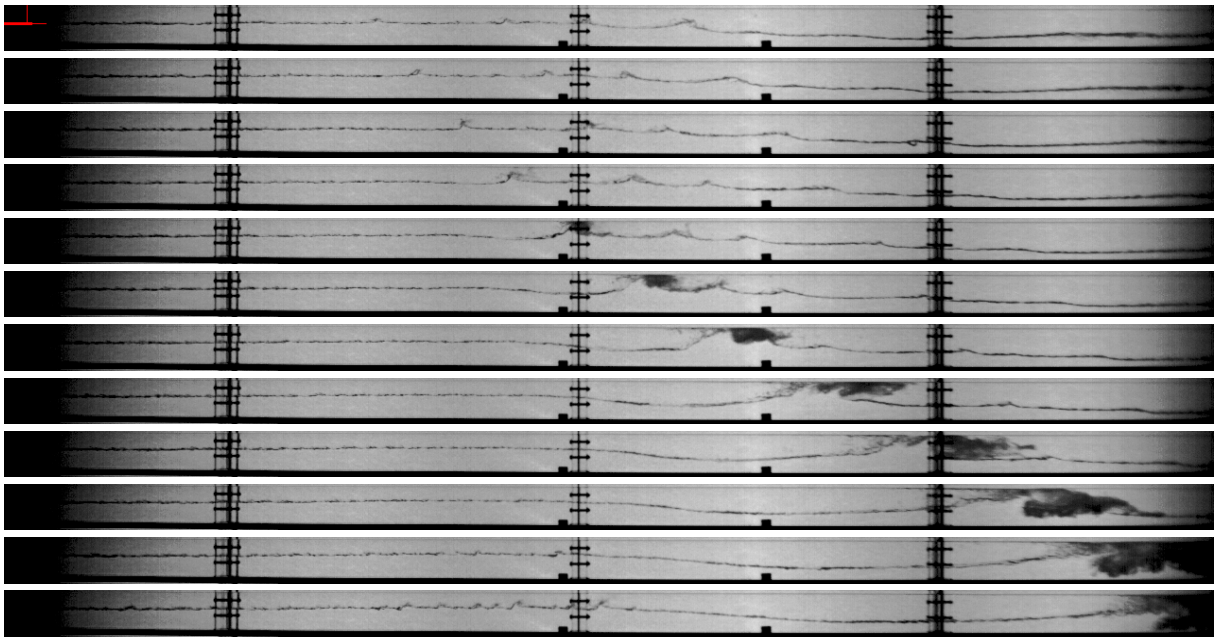

Fig. 9.8 Measured picture sequence at J_L = 1.0 m/s and J_G = 5.0 m/s with Δt = 50 ms (depicted part of the channel: 0 to 3.2 m after the inlet)

Furthermore, CFD pre-test calculations were done to show the possibility of slug flow generation in a real geometry and at relevant parameters for nuclear reactor safety.

The simulation was performed on a flat model representing the hot-leg of the German KONVOI-reactor at the scale of 1:3. The fluids were water and steam at a pressure of 50 bar and the corresponding saturation temperature of 263.9°C. The results of the CFD-calculation show first an upwards inclination of the stagnant water in direction of the steam generator, driven by the momentum exchange from the injected steam. Further, waves are generated randomly in the horizontal part of the hot-leg and grow to slugs in the region of the bend (Fig. 9.9).

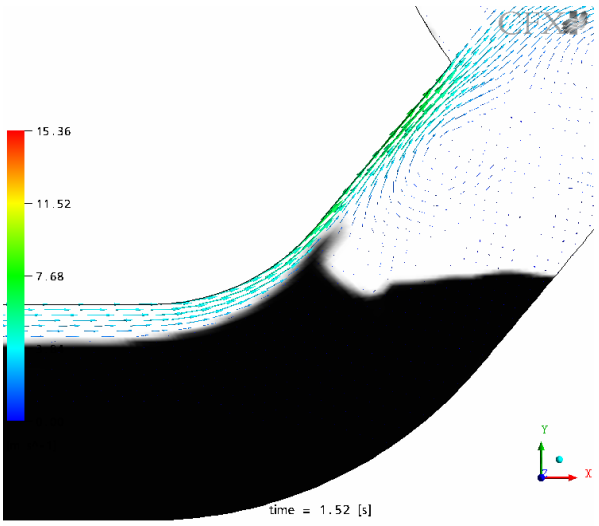

Fig. 9.9 Steam velocity distribution in the bended region of the hot-leg model calculated with ANSYS CFX (water: black labelled)

10. Experience with the hot leg model commissioning tests

The main infrastructure installation necessary for the planned hot-leg tests is the pressure tank for the pressure equilibrium. The TOPFLOW building was extended by an additional wing to accommodate the tank (see section 2.7), together with the auxiliary systems for pressurization, cooling, steam supply and handling of the test section. The commissioning work was started in March 2005 with the first pressurization of the tank with air, which was successfully completed after some amendments.

In parallel to the construction and commissioning of the pressure tank, the internals and the elements of the test section were developed and manufactured. Important infrastructure components for the hot-leg test, which are also important for other future steam-water experiments in the tank, are the movable mounting platform with the external support and the rail system to extract the platform from the tank to put it on the external support for construction and maintenance works on the test section, as well as the built-in condenser. The latter is responsible for the condensation of the exhaust steam from the test section. The cold end of the primary side of this heat exchanger is in permanent connection with the inner atmosphere of the tank, which ensures ideal pressure equilibrium.

For the commissioning experiments, the test section was built-up without the model of the steam-generator inlet chamber. A straight horizontal channel of rectangular cross-section (0.25 x 0.05 m, app. 3 m long) was used instead. The implementation of the transparent windows and the installation of the experimental instrumentation were planned for the time after a successful test of this preliminary test section. During the commissioning tests, there were 8 thermocouples placed at different positions in the tank and inside the built-in condenser to check its function.

Since all steam-confining equipment heats up until the temperature of saturated steam at 5 MPa, which is 264 °C, a sufficient thermal insulation of the outer surface

of the test section and the built-in condenser is necessary in order to keep the internal temperature in the tank below the design limit of 50 °C. A safety circuit is foreseen to disconnect the tank from the steam supply, if the temperature of the inner atmosphere rises above 70 °C. The inevitable heat flux from the test section into the tank is removed by an over-roof air cooler accommodated at the roof of an auxiliary wing of the building. The air is circulated by a pressure-proof electric fan installed in the circulation pipe.

The first steam tests performed have shown that the chosen material for the thermal insulation was insufficient. This is equally true for glass wool and mineral wool. The dynamic viscosity of air as a nearly ideal gas is approximately independent from the pressure. Due to the increasing density, the kinematic viscosity decreases with growing pressure and the air starts to perform intensive natural circulation within the fiber packages of the insulation mats. In the result, it was not possible to reach design parameters with this kind of thermal insulation. The first tests were terminated at a system pressure of about 8 bar (temperature in the test section app. 160 °C) due to a heat-up of the tank above 50 °C.

It was found that both insulation capability of the mineral wool and the heat removal capacity of the over-roof cooler were insufficient. The over-roof cooler was designed as a system of two finned U-tubes with natural convection on the secondary side. The achieved cooling power was between 0 and 4 kW heavily depending on the ambient air temperature. Therefore, the over-roof cooler was equipped with a forced circulation cooling on the secondary side. The air was driven by a radial ventilator working on suction. With this improvement, the power was increased by a factor of 3 approximately.

Nevertheless, the cooling problems remained. It was first tried to compact the mineral wool and to fill thermal bridges that were identified by additional amounts of insulation material. In the result a commissioning test was accomplished, where the facility reached nominal parameters. It was though not possible to keep the temperature inside the tank below 50 °C. In September 2005 a steam experiment at a mass flow rate up to 1.3 kg/s and a pressure of 5 MPa was accompanied by a temperature of the tank atmosphere of about 70 °C.

This experiment has shown that the hot-leg test is operable from the point of view of the thermodynamic boundary conditions in case the insulation problem can be solved. It was demonstrated that:

- the pressure equilibrium technique is fully operational, in particular the condenser is sufficient to remove the supplied steam at full heater power without a steam break-through into the tank via the cold end of the primary side of the condenser (it turned out that the condenser is significantly over-dimensioned, which was reflected by thermocouples sensing the progression of the density stratification between hot steam and cold air, i.e. the steam never needs more then 75 % of the available heat exchange surface for complete condensation), and
- the available mass flow rate of the steam supply was sufficient to achieve counter-current flow limitation in the preliminary test channel (test conditions: pressure: 2.36 MPa, full CCFL at a steam mass flow: 0.55 kg/s, see Fig. 10.1 and Fig. 10.2), as reported by Prasser et al., (2006b).

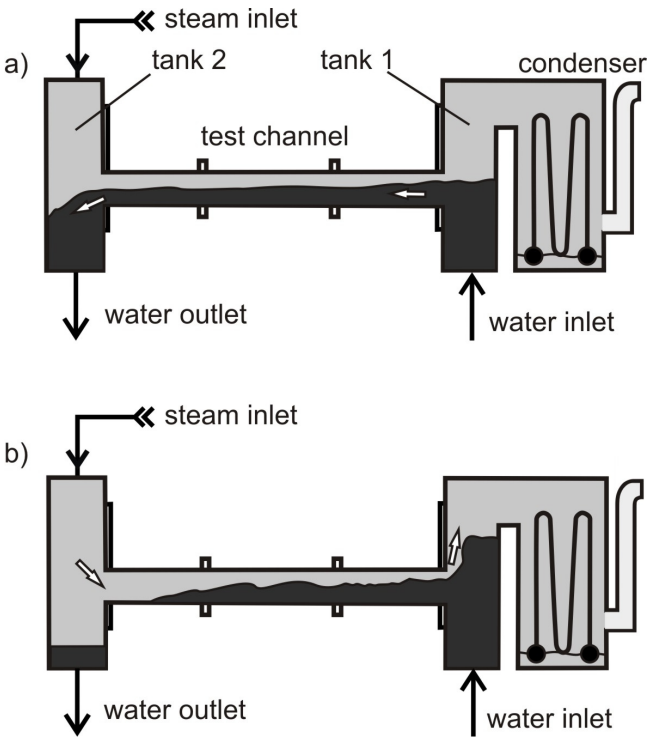

Fig. 10.1 Schematic illustration of the preliminary test: a) free liquid flow; b) counter current flow limitation

In parallel, the development of the sealing technique for the observation windows was progressing. At a small-scale mock-up, the function of the sealing as well as the fixing elements (lugs, bolts and springs) was successfully tested.

In order to identify an appropriate thermal insulation material for the test section, an autoclave was built and equipped with an electrical heater plate, which allowed testing samples of different materials under the design conditions of the hot-leg test. The insufficient properties of mineral wool were reproduced. After numerous series of tests with different materials, foam glass was found to be applicable. It showed excellent insulation properties, together with a full stability in air at 5 MPa and about 280 - 300 °C.

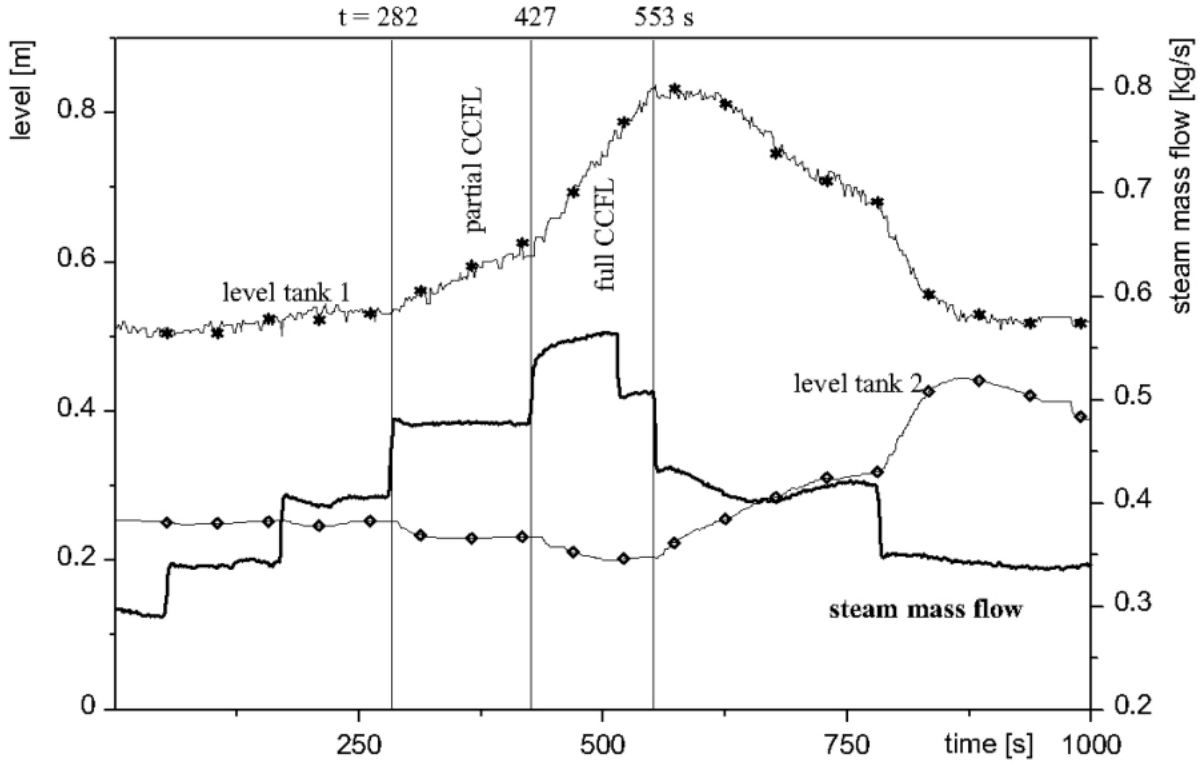

Fig. 10.2 Selected experimental results obtained during a preliminary test, which show the evaluation of counter current flow limitation

Relying on these positive results, the preliminary test section was insulated with bricks of foam glass, glued to the surface of the test section with a high temperature

silicon resin. In the first hot large-scale test inside the pressure tank, nevertheless, a large part of the foam glass bricks ruptured and disintegrated into debris at a pressure of 2.2 MPa and the corresponding saturation temperature inside the test section. The cause of this reaction was not understood, nor was it ever reproduced in autoclave tests. In the same time, the silicon resin used for fixing of the bricks showed no signs of degradation during this experiment.

A continuation of the search for an insulation material lead to the finding that a self-foaming two-component silicon resin after hardening is both insulating and stable under the test autoclave conditions. Additionally, the silicon resin foam is easy to handle if components of complicated geometry have to be covered, since the two-component mixture is a high-viscosity liquid that can be cast into forms put around the parts to be insulated. In this way, the entire preliminary test section together with the built-in condenser was insulated, using about 350 kg of silicon resin.

The test of this thermal insulation was performed in three steps. In step one the test section was heated up without pressurizing it. By this, it was intended to assure that the entire mass of the two-component resin arrived at fully polymerized conditions and residues of organic solvents were eliminated. In the second step, the tank was pressurized without heating-up to check the behavior of the insulation foam under pressure conditions.

The third experiment was a hot test with steam supply and a continuous pressure increase. It was planned to reach nominal parameters, both for pressure and temperature of the steam. The insulation properties of the silicon resin foam proved to be excellent until a system pressure of 4.7 MPa. The temperature in the pressure tank remained at maximal 44 °C. Eventually, at this stage of the pressurization and heat-up process, a sudden increase of the pressure and the temperature inside the tank happened, which was caused by the onset of a fast oxidation and decomposition process of the silicon resin. This fire lasted for about 4 minutes and lead to the nearly complete destruction of the thermal insulation. The safety valve of the pressure tank was activated at a pressure of about 5.5 MPa, but was not able to limit the pressure growth. A short time after the opening of the safety valve, the pipe connecting the tank with the valve broke and the discharging air uncovered a part of the roof of the building.

An inspection of the facility revealed that the silicon resin foam has turned into finely dispersed, white silicon oxide powder that covered all internals including the inner wall of the tank. Until the emergency stop the powder was transported by the circulating air through the cooling system and was found in the axial fan as well as in the over-roof cooler. After a careful analysis of the incident that included the examination of a material sample taking from the region of the nozzle connecting the broken pipe with the safety valve and an assessment of the maximum temperature the metallic structures were exposed to, it was found and confirmed by the technical surveillance organization TÜV that the pressure tank and the auxiliary equipment did not suffer from damages that would exclude a further operation under the following requirements:

- repair of the damaged pressure relief line,
- replacement of the nozzle connecting the pressure tank with the pressure relief line,
- installation of a larger safety valve (DN80-DN125),

- installation of a blow-off line with a bigger diameter (DN125) and
- pressure test of the tank up to 8.1 MPa with water.

The repair works included the removal of residua of the silicon foam, the cleaning of the internals of the tank and the cooling system as well as the reconstruction of the roof of the new wing of the building. In parallel, the over-roof cooling system was upgraded to 8 finned U-tubes with a cooling power up to 25 kW. Additionally to the requirements of the technical surveillance organization TÜV, the FZD took the following safety measures:

- installation of a nitrogen system for the inertisation of the tank atmosphere and
- identification of a pure inorganic oxidic insulation material.

A test program was foreseen to demonstrate the applicability of the new insulation material. Due to the delays caused by the incident, the completion of the hot-leg tests within the project duration was not achievable. Until Feb. 2007 these insulation tests with 2 new materials and the extended over-roof cooler were performed with very good results. During the third test at 5 MPa the temperature within the pressure tank remained at maximal 38 °C. Also the chemical properties checked by an external laboratory are correct.

11. Literature

Frank, Th., Zwart, P.J., Krepper, E., Prasser, H.-M., Lucas, D., (2006). Validation of CFD models for mono- and polydisperse air-water two-phase flows in pipes. International OECD/IAEA workshop CFD4NRS in Garching at 5 – 7 September 2006, Session B6, paper 32.

Fu, X. Y., Ishii, M., (2002a). Two-group interfacial area transport in vertical air/water flow, I. Mechanistic model. Nuclear Engineering and Design, 219(2002a) 143-168.

Fu, X. Y., Ishii, M., (2002b). Two-group interfacial area transport in vertical air/water flow, II. Model evaluation. Nuclear Engineering and Design 219, 169-190.

Giot, M., Seynhaeve, J.-M., (2004). Two-phase flow water hammer transients and induced loads on materials and structures of nuclear power plants. EU project WAHALoads, FIKS-CT-2000-00106, final report, May 2004.

Graf, U., Papadimitriou, P., (2006). Simulation of Two-Phase Flows in Vertical Tubes with the CFD Code FLUBOX. International OECD/IAEA workshop CFD4NRS in Garching at 5 – 7 September 2006, technical session A3, paper 13.

Hibiki, T., Ishii, M., (1999). Experimental study on interfacial area transport in bubbly two-phase flows. International Journal of Heat and Mass Transfer, 42(1999) 3019-3035.

Hibiki, T., Ishii, M., (2000). Two-group interfacial area transport equations at bubbly-to-slug flow transition. Nuclear Engineering and Design, 202(2000) 39-76.

Hosokawa, S., Tomiyama, A., Misaki, S., Hamada, T., (2002). Lateral migration of single bubbles due to the presence of wall. Proceedings of ASME Fluids Engineering Division Summer Meeting, Montreal, Ouebec, Canada.

Hughmark, G.A, (1967). Mass and heat transfer from a rigid sphere. AIChE Journal 13, 1219-1221.

Ishii, M., (1975). Thermo-Fluid Dynamic Theory of Two-Phase Flow. Eyrolles, Paris, 1975.

Kataoka I., Ishii M. and Serizawa A., (1986). Local formulation and measurements of interfacial area concentration in two-phase flow. Int. J. Multiphase Flow, Vol. 12, 1986, No. 4, pp. 505-529.

Kataoka, I., Ishii, M., (1987). Drift flux model for large diameter pipe and new correlation for pool void fraction. International Journal of Heat and Mass Transfer 30(1987), pp. 1927-1939.

Kim, S. et al., (2001). Bubble transport in small diameter pipe flow. 4th International Conference on Multiphase Flow, ICMF-200, New Orleans, La, USA, May 27 - June 1, 2001.

Kim, S., Ishii, M., (2001). Micro four-sensor probe measurement of interfacial area transport for bubbly flow in round pipes. Nuclear Engineering and Design, 205 (2001) 123–131.

Krepper, E., Lucas, D., Prasser, H.-M., (2005). On the modelling of bubbly flow in vertical pipes. Nuclear Engineering and Design 235, pp. 597-611.

Lo, S., (1996). Application of the MUSIG model to bubbly flows. AEAT-1096, AEA Technology, June 1996.

Lucas, D., Krepper, E., Prasser, H.-M., (2001a). Prediction of radial gas profiles in vertical pipe flow on basis of the bubble size distribution. International Journal of Thermal Sciences, 40(2001)217-225.

Lucas, D., Krepper, E., Prasser, H.-M., (2001b). Development of bubble size distributions in vertical pipe flow by consideration of radial gas fraction profiles. 4th International Conference on Multiphase Flow, New Orleans, May 27 - June 1, 2001, Conference-CD, Paper 378.

Lucas, D., Krepper, E., Prasser, H.-M., (2002). Experimental investigations and modelling on the transition from bubble to slug flow in vertical pipes. German-Japanese Workshop on Multiphase Flow, Karlsruhe, August 25-27, 2002.

Lucas, D., Krepper, E., Prasser, H.-M., (2003). Evolution of flow patterns, gas fraction profiles and bubble size distributions in gas-liquid flows in vertical tubes. Transactions of the Institute of Fluid-Flow Machinery 112(2003)37-46.

Lucas, D., Prasser, H.-M., (2004a). Scaling effects in vertical bubbly pipe flow. 5th International Conference on Multiphase Flow, ICMF'04, Yokohama, Japan, May 30–June 4, 2004, Paper No. 187.

Lucas, D., Shi, J.-M., Krepper, E., Prasser, H.-M., (2004b). Models for the forces acting on bubbles in comparison with experimental data for vertical pipe flow. 3rd International Symposium on Two-Phase Flow Modelling and Experimentation, Pisa, Italy, September 22-24, 2004, Paper ha04.

Lucas, D., Prasser, H.-M., (2005a). Simulation of condensation in a sub-cooled bubbly steam-water flow along a large vertical pipe. Archives of Thermodynamics 26(2005)49-59.

Lucas, D., Krepper, E., Prasser, H.-M., (2005b). Modelling of the evolution of bubbly flow along a large vertical pipe. The 11th International Topical Meeting on Nuclear Reactor Thermal-Hydraulics (NURETH-11) Avignon, France, October 2-6, 2005, Paper: 051.

Lucas, D., Prasser, H.-M., (2007a). Steam bubble condensation in sub-cooled water in case of co-current vertical pipe flow. Nuclear Engineering and Design 237 (2007)497-508.

Lucas, D., Krepper, E., Prasser, H.-M., (2007b). Modelling of the evolution of bubbly flow along a large vertical pipe. Nuclear Technology (May 2007).

Luo, H., Svendsen, H.F., (1996). Theoretical model for drop and bubble breakup in turbulent flows. AIChEJ, 42, 5, pp. 1225-1233.

Manera, A., Prasser, H.-M., Lucas, D., (2005). Experimental investigations on bubble turbulent diffusion in a vertical large-diameter pipe by means of wire-mesh sensors and correlation techniques. NURETH-11, Avignon, France, October 2-6, 2005, Paper: 091.

Manera, A., Ozar, B., Paranjape, S., Ishii, M., Prasser, H.-M., (2007). Comparison between wire-mesh sensors and conductive needle-probes for measurements of two-phase flow parameters. ICONE15-10312.

Ohnuki, A., Akimoto, H., (1996). An experimental study on developing air-water two-phase flow along a large vertical pipe: effect of air injection method. Int. J. Multiphase Flow 22(1996), 1143-1154.

Ohnuki, A., Akimoto, H., (2000). Experimental study on transition of flow pattern and phase distribution in upward air-water two-phase flow along a large vertical pipe. International Journal of Multiphase Flow, 26(2000)367-386.

Pietruske, H., Prasser, H.-M., (2005). Wire-mesh sensors for high-resolving two-phase flow studies at high pressures and temperatures. NURETH-11, 02.-06.10.2005, Avignon, France, CD-ROM, Paper 533.

Pietruske, H., Sühnel, T., Prasser, H.-M., (2006). Gittersensor. Patent DE 10 2005 019 739 B3 2006.10.26.

Prasser, H.-M., Böttger, A., Zschau, J., (1998). A new electrode-mesh tomograph for gas-liquid flows. Flow Measurement and Instrumentation, 9 (1998), 111-119.

Prasser, H.-M., Böttger, A., Zschau, J., (1999). Entwicklung von Zweiphasenmesstechnik für vergleichende Untersuchungen zur Beschreibung von transienten Strömungen in Rohrleitungen. Forschungszentrum Rossendorf, FZR-233 Februar 1999, ISSN 1437-322X, Abschlußbericht zum Vorhaben 11ZF9504/1.

Prasser, H.-M., (2000). High-speed measurement of the void fraction distribution in ducts by wire-mesh sensors. International Meeting on Reactor Noise, Oct. 11-13, 2000, Athens, Greece, proc. on CD-ROM, paper_7_1.

Prasser, H.-M., Scholz, D., Zippe, C., (2001). Bubble size measurement using wire-mesh sensors. Flow Measurement and Instrumentation, 12 (2001), 299-312.

Prasser, H.-M., Krepper, E., Lucas, D., (2002a). Evolution of the two-phase flow in a vertical tube - decomposition of gas fraction profiles according to bubble size classes using wire-mesh sensors. International Journal of Thermal Sciences, 41 (2002) 17-28.

Prasser, H.-M., Zschau, J., Peters, D., Pietzsch, G., Taubert, W., Trepte, M., (2002b). Fast wire-mesh sensors for gas-liquid flows - visualization with up to 10 000 frames per second. ICAPP 2002, Hollywood, Florida, paper #1055.

Prasser, H.-M., Lucas, D., Krepper, E., Baldauf, D., Böttger, A., Rohde, U., Schütz, P., Weiß, F.-P., Zippe, C., Zippe, W., Zschau, J., (2003a). Strömungskarten und Modelle für transiente Zweiphasenströmungen. Wissenschaftlich-Technische Berichte / Forschungszentrum Rossendorf, FZR-379, Juni 2003.

Prasser, H.-M., (2004). Influence of the Gas Injection on the Void Fraction Profiles and Bubble Size Distributions of an Air-Water Flow in Vertical Pipes. 5th International Conference on Multiphase Flow, ICMF'04, Yokohama, Japan, May 30–June 4, 2004, Paper No. 366.

Prasser, H.-M., Beyer, M., Böttger, A., Carl, H., Lucas, D., Schaffrath, A., Schütz, P., Weiß, F.-P., Zschau, J., (2005a). Influence of the pipe diameter on the structure of the gas-liquid interface in a vertical two-phase pipe flow. Nuclear Technology 152(2005)Oct, 3-22.

Prasser, H.-M., Misawa, M., Tiseanu, I., (2005b). Comparison between wire-mesh sensor and ultra-fast X-ray tomograph for an air–water flow in a vertical pipe. Flow Measurement and Instrumentation 16 (2005), 73-83.

Prasser, H.-M., Gregor, S., (2005c). Evolution of interfacial area concentration in a vertical air-water flow measured by wire-mesh sensors. NURETH-11, 2005, Avignon, France, October 2-6, 2005, paper 398.

Prasser, H.-M., Beyer, M., Carl, H., Gregor, S., Lucas, D., Pietruske, H., Schütz, P., Weiss, F.-P., (2005d). Evolution of the structure of a gas-liquid two-phase flow in a large vertical pipe. NURETH-11, 2005, Avignon, France, October 2-6, 2005, paper 399.

Prasser, H.-M., Frank, T., Beyer, M., Carl, H., Pietruske, H., Schütz P., (2006a). Gas-liquid flow around an obstacle in a vertical pipe - experiments and CFD simulation. JAHRESTAGUNG KERNTECHNIK 2006, Aachen, May 16 - 18, 2006, paper 218, proceedings 93-98.

Prasser, H.-M., Beyer, M., Carl, H., Manera, A., Pietruske, H., Schütz, P., Weiß, F.-P., (2006b). The multipurpose thermal-hydraulic test facility TOPFLOW: an overview on experimental capabilities, instrumentation and results. Kerntechnik 71(2006)4, 163-173.

Prince, M.J., Blanch, H.W., (1990). Bubble coalescence and breakup in air-sparged bubble columns, AIChEJ, 36, No 10, pp. 1485-1499.

Sato, Y., Sekoguchi, K., (1975). Liquid velocity distribution in two-phase bubble flow. *International Journal of Multiphase Flow*, 2, 79-95 (1975).

Sato, Y., Sadatomi, M., Sekoguchi, K., (1981). Momentum and heat transfer in two-phase bubble flow. *International Journal of Multiphase Flow*, 7, 167-177 (1981).

Schaffrath, A., Krüssenberg, A.-K., Weiss, F.-P., Hicken, E. F., Beyer, M., Carl, H., Schuster, J., Schütz, P., Tamme, M., (2001). TOPFLOW - a new multipurpose thermalhydraulic test facility for the investigation of steady state and transient two-phase flow phenomena. Kerntechnik, 66(2001)4, pp. 209-212.

Schaffrath, A., Krüssenberg, A.-K., Weiss, F.-P., Prasser, H.-M., (2002). Die Mehrzweck-Thermohydraulikversuchsanlage TOPFLOW des Forschungszentrums Rossendorf e.V. - Aufbau, Ziele und Perspektiven. Atomwirtschaft - Atomtechnik, 47(2002)6, pp. 383-388.

Shi, J.-M., Frank, T., Krepper, E., Lucas, D., Rohde, U., Prasser, H.-M., (2004). Implementation and validation of non-drag interfacial forces in CFX-5.6. 5th Int. Conf. on Multiphase Flow, ICMF'2004, Yokohama, Japan, Paper No. 400.

Sun, X., Smith T., Kim, S., Ishii, M., Uhle, J., (2002). Interfacial area of bubbly flow in a relatively large diameter pipe. Experimental Thermal and Fluid Science 27, 97–109.

Tomiyama, A., (1998). Struggle with computational bubble dynamics. Proceedings of Third International Conference on Multiphase Flow, ICMF 98, Lyon, France, June 8-12, 1998.

Tomiyama, A., Tamai, H., Zun, I., Hosokawa, S., (2002). Transverse migration of single bubbles in simple shear flows. Chemical Engineering Science 57 (2002) 1849–1858.

Vallée, C., Höhne, T., Prasser, H.-M., Sühnel, T., (2006). Experimental investigation and CFD simulation of horizontal air/water slug flow. Kerntechnik 71/3 (2006), 95-103.

Vallée, C., Höhne, T., Prasser, H.-M., Sühnel, T., (2007). Experimental investigation and CFD simulation of horizontal stratified two-phase flow phenomena. Nuclear Engineering and Design (accepted).

Wellek R.M., Agrawal A.K., Skelland A.H.P, (1966). Shapes of liquid drops moving in liquid media. AIChE Journal 12, 854-860.

Zaruba A., Krepper, E., Prasser, H.-M., Reddy Vanga, B.N., (2005a). Experimental study on bubble motion in a rectangular bubble column using high-speed video observation. Flow Measurement and Instrumentation 16(2005) 277–287.

Zaruba, A., Krepper, E., Prasser, H.-M., Schleicher, E., (2005b). Measurement of bubble velocity profiles and turbulent diffusion coeffcients of the gaseous phase in a rectangular bubble column using image processing. Experimental Thermal and Fluid Science 29(2005)851–860.

Zaruba, A., Lucas, D., Prasser, H.-M., Höhne, Th., (2007). Bubble-wall interactions in a vertical gas-liquid flow: Bouncing, sliding and bubble deformations. Chemical Engineering Science 62(2007)1591-1605.

Acknowledgement

The work presented in this report was founded by the BMWi (Federal Ministry of Economics and Technology of Germany) within the research project registered as No. 150 1265. Electronic equipment for wire-mesh sensors was developed in a close co-operation with TELETRONIC GmbH (www.tz-rotech.de/teletronic/). The authors thank the technical team of TOPFLOW, by name Klaus Lindner, Heiko Rußig, Marko Tamme and Steffen Weichelt for preparing the facility and the experiments.

12. Nomenclature and indexes

12.1 Symbols

Sign	Unit	Denomination
a	1/m	interfacial area concentration
D, d	m	diameter
D	m²/s	turbulent dispersion
D_c	m	capillary constant
Eo	-	Eötvös number
F	-	coefficient
g	m/s²	acceleration of gravity
h	m	height
i	-	index
J, j	m/s	superficial velocity
K	-	kernel
k-ω	-	two equation model based on turbulence kinetic energy (k) and specific dissipation (ω) applying the Reynolds averaging method

L	m	length
n	-	bubble density
p	MPa	pressure
r	m	radius
t	s	time
VF	%	gas volume fraction
w	m/s	velocity
x	m	coordinates
y	m	coordinates
z	m	coordinates
α	%	void fraction
α	1/m	interfacial area concentration
Δ	-	difference
ε	%	void fraction
ε	m^2/s^3	dissipation rate of the turbulent kinetic energy
Γ	$1/(m^3 s)$	coalescence rate
ρ	kg/m^3	density
σ	N/m	surface tension
Ω	1/s	break-up rate

12.2 Indices

Sign	Denomination
air	air
B, b	breakup, bubble
bub	bubble
bub,xy	bubble relating to the xy-plane (cross-section)
c	coalescence
cr	critical
eq	equivalent
G, g	gas
h	horizontal, relating to the cross-section
i, j	bubble size class
inj	injection
max	maximal
s	saturation
total	total
tr	threshold
L, l	liquid

12.3 Abbreviations

Abbreviation	Denomination
ACF	**A**uto **C**orrelation **F**unction
ANSYS	developer and distributor of CFX
ATHLET	thermal-hydraulic code (GRS)
BMWi	Federal Ministry of Economics and Technology of Germany
CCF	**C**ross **C**orrelation **F**unction
CCFL	**C**ounter-**C**urrent **F**low **L**imitation
CFD	**C**omputational **F**luid **D**ynamics
CFX	commercial CFD code
DN	nominal diameter
DNS	**D**irect **N**umerical **S**imulation
FAD	**F**avre **A**veraged **D**rag
FLOWMAP	research project for investigation of two-phase flows
FLUBOX	thermal hydraulic code (GRS)
FZD	**F**orschungs**Z**entrum **D**resden-Rossendorf e.V.
GRS	**G**esellschaft für **R**eaktor**S**icherheit mbH
HAWAC	**H**orizontal **A**ir/**WA**ter **C**hannel, test facility at FZD
KFKI	Hungarian Atomic Energy Research Institute
KONVOI	German pressurized water reactor
LOCA	**L**oss **O**f **C**oolant **A**ccident
MTLoop	**M**easurement **T**echnique **Loop**, former test facility on the FZD
MUSIG	**MU**lti bubbe **SI**ze **G**roup
PDF	**P**robability **D**ensity **F**unction
PIV	**P**article **I**mage **V**elocimetry
PMK-2	test facility of KFKI Budapest
PWR	**P**ressurized **W**ater **R**eactor
SST	**S**hear **S**tress **T**ransport
TOPFLOW	**T**ransient tw**O** **P**hase **FLOW** test facility
WAHALoads	**WA**ter **HA**mmer **Loads** (international research project)

12.4 Figures

12.5 Tables

Appendix A: Abstracts of the technical reports:

A 1: *Experiments on upwards gas-liquid flow in vertical pipes*

Two-phase flow experiments at vertical pipes are much suitable for studying the action of different constitutive relations characterizing the momentum exchange at the gas-liquid interface as well as the dynamic behaviour of the gas-liquid interface itself. The flow can be observed in its movement along the pipe and, in particular, within the shear field close to the pipe wall over a considerable vertical distance and, consequently, over a comparatively long time without the immediate separation of gas and liquid characteristic for horizontal flows.

Wire-mesh sensors, which were the working horse in the described experiments, supplied sequences of instantaneous two-dimensional gas fraction distributions with a high resolution in space and time. This allows to derive from the data not only void fraction and bubble velocity profiles, but also bubble size distributions, bubble-size resolved radial gas fraction profiles as well as the axial evolution of these distributions. An interfacial surface reconstruction algorithm was developed in order to extract the extension of interfacial area from the wire-mesh sensor data. The sensors were upgraded to withstand parameters that are close to nuclear reactor conditions. Most of the experiments were performed for both air-water flow at ambient pressure and steam-water flow of up to 6.5 MPa at identical combinations of the gas and liquid superficial velocities. This offers excellent conditions for studying the influence of the fluid properties.

A 1: *Experimente an aufwärtsgerichteten Flüssigkeits-Gas-Strömungen in senkrechten Rohrleitungen*

Zweiphasenmessungen in senkrechten Rohrleitungen sind gut geeignet, um die Wirkung verschiedener Konstitutivgesetze zu untersuchen, die den Impulsaustausch an der Phasengrenze sowie das dynamische Verhalten der Phasengrenze selbst beschreiben. Die Strömung wird in ihrer Bewegung entlang der Rohrleitung und im speziellen im Scheerfeld in Wandnähe über eine relativ große vertikale Lauflänge der Beobachtung zugänglich, ohne dass sofort eine Separation von Gas und Flüssigkeit erfolgt.

Gittersensoren, die das Arbeitspferd bei den beschriebenen Experimenten darstellen, lieferten Serien von momentanen, zweidimensionalen Gasgehaltsverteilungen mit hoher zeitlicher und räumlicher Auflösung. Sie erlauben nicht nur die Ermittlung von Gasgehalts- und Geschwindigkeitsprofilen, sondern auch die Bestimmung von Blasengrößenverteilungen und nach Blasengrößen aufgelösten Gasgehaltsprofilen sowie deren Entwicklung in Strömungsrichtung. Für die Messung der Zwischenphasengrenzfläche wurde ein neuartiger Algorithmus entwickelt. Die Sensoren wurden für einen Einsatz nahe den Betriebsparametern von Leichtwasserreaktoren ertüchtigt. Die meisten Versuche konnten so sowohl für eine Luft-Wasser- als auch für eine Wasser-Dampf-Strömung bei bis zu 6.5 MPa bei identischen Strömungsrandbedingungen durchgeführt werden, was die Möglichkeit bietet, den Einfluss der Stoffwerte zu ermitteln.

A 2: *Experiments on two-phase flow in a vertical tube with a moveable obstacle*

A novel technique to study the two-phase flow field around an asymmetric diaphragm in a vertical pipe is presented, that enables producing data for CFD code validation in complex geometries. Main feature is a translocation of the diaphragm to scan the 3D void field with a stationary wire-mesh sensor. Besides the measurement of time-averaged void fraction fields, a novel data evaluation method was developed to extract estimated liquid velocity profiles from the wire-mesh sensor data. The flow around an obstacle of the chosen geometry has many topological similarities with complex flow situations in bends, T-junctions, valves, safety valves and other components of power plant equipment and flow phenomena like curved stream lines, which form significant angles with the gravity vector, flow separation at sharp edges and recirculation zones in their wake are present.

In order to assess the quality of the CFD code and their underlying multiphase flow and turbulence models pre-test calculations by ANSYS CFX 10.0 were carried out. A comparison between the calculation results and the experimental data shows a good agreement in term of all significant qualitative details of the void fraction and liquid velocity distributions.

Furthermore, the report contains a method to assess the lateral components of bubble velocities in the form of a basic theoretical description and visualisation examples. The plots show the deviation of the flow around the obstacle in term of vectors represented the average velocities of the instantaneous cross-sections of all bubbles in the time interval when they pass the measuring plane.

A detailed uncertainty analyse of the velocity assessments finishes the presented report. It includes remarks about the comparison with a second method for calculating bubble velocity profiles – the cross-correlation. In addition, this chapter gives an overview about the influence of acceleration and deceleration effects on the velocity estimation.

A 2: *Experimente zur Zweiphasenströmung in einem vertikalen Rohr mit verschiebbarem Hindernis*

Der vorliegende Bericht beschreibt eine neue Methode zur Untersuchung von Zweiphasen-Strömungsfeldern in der Umgebung eines asymmetrischen Hindernisses innerhalb eines vertikalen Rohres, die Daten zur Validierung von CFD Codes für komplexe Geometrien liefert. Hauptmerkmal dieser Versuchsanordnung ist die Möglichkeit, das Hindernis gegenüber dem stationären Gittersensor zu verschieben und somit dreidimensionale Gasgehaltsfelder zu erfassen. Neben der Messung von zeitgemittelten Gasgehaltsverteilungen wird eine neue Methode zur Datenauswertung vorgestellt, die mittels Gittersensordaten Geschwindigkeitsprofile der flüssigen Phase abschätzt. Die Strömung im Umfeld eines Hindernisses mit der vorliegenden Geometrie hat viele topologische Ähnlichkeiten mit komplexen Strömungen in Rohrbögen, T-Stücken, Ventilen und Sicherheitsventilen sowie anderen in Kraftwerksanlagen verwendeten Komponenten. Gekrümmte und gegenüber dem Gravitationsvektor signifikant geneigte Stromlinien, Strömungsseparation an scharfen Kanten und Rezirkulationsgebiete im Nachlauf des Hindernisses sind Phänomene, die mittels dieser Versuchsanordnung analysiert werden können.

Um die Qualität von CFD Codes einschließlich der implementierten Mehrphasen- und Turbulenzmodelle einschätzen zu können, wurden mit ANSYS CFX 10.0 Vorausrechnungen durchgeführt. Ein Vergleich zwischen den Rechenergebnissen und

den experimentellen Daten zeigt eine gute Übereinstimmung bei allen signifikanten qualitativen Details sowohl für die Gasgehalts- als auch die Geschwindigkeitsverteilungen der flüssigen Phase.

Weiterhin enthält der Bericht eine Methode zur Abschätzung der lateralen Komponenten für Blasengeschwindigkeiten in Form einer kurzen theoretischen Beschreibung und Visualisierungsbeispielen. Die Bilder zeigen die Strömungsablenkung im Umfeld des Hindernisses mittels Vektoren, die die Durchschnittsgeschwindigkeiten aller Blasen an den jeweiligen Kreuzungspunkten während der Durchdringung der Messebene des Sensors repräsentieren.

Eine detaillierte Unsicherheitsanalyse zur Geschwindigkeitsabschätzung schließt den vorliegenden Bericht ab. Sie beinhaltet Informationen über den Vergleich mit der Kreuzkorrelation, einer zweiten Methode zur Ermittlung von Gasgeschwindigkeitsprofilen. Zusätzlich gibt dieses Kapitel einen Überblick über den Einfluss von Beschleunigungs- und Verzögerungseffekten auf die Geschwindigkeitsberechnungen.

A 3: *Experimental investigation of stratified air/water flows in a horizontal channel*

For the investigation of air/water flows, a horizontal Perspex duct with rectangular cross-section was build. The channel allows the investigation of air/water co- and counter-current flows at atmospheric pressure, especially the slug behaviour.

Optical measurements were performed with a high-speed video camera, and were complemented by simultaneous dynamic pressure measurements. A method for the image analysis was developed based on interface recognition and was tested for possible applications. The pressure measurements reveal that in case of a slug flow, the pressure increases by a few kilopascals and decreases when the slug leaves the duct. Moreover velocities were measured in the liquid phase using non intrusive techniques. The averaged velocity-profile at the duct inlet was measured with ultrasonic transducers. To access the velocity field in a slug, Particle Image Velocimetry (PIV) was applied.

A 3: *Experimentelle Untersuchung von geschichteten Luft/Wasser Strömungen in einem horizontalen Kanal*

Für die Untersuchung von Luft/Wasser-Strömungen wurde ein horizontaler Acrylglas-Kanal mit rechteckigem Querschnitt gebaut. Der Kanal ermöglicht Gleich- und Gegenstrom-Versuche bei Atmosphärendruck, insbesondere die Untersuchung der Schwallströmung.

Es wurden optische Messungen mit einer Hochgeschwindigkeits-Kamera durchgeführt, die durch synchronisierte dynamische Druckmessungen ergänzt wurden. Für die Analyse der Bilder wurde eine Methode zur Erfassung der Phasengrenze entwickelt und diese anhand möglicher Anwendungen getestet. Die Druckmessungen zeigten, dass der Druck bei Schwallströmungen um einige kPa ansteigt und wieder abfällt, sobald der Schwall aus dem Kanal austritt. Zudem wurden Geschwindigkeiten in der flüssigen Phase mittels nicht invasiver Verfahren gemessen. Das durchschnittliche Geschwindigkeits-Profil am Kanaleintritt wurde mit Ultraschall-Köpfen bestimmt. Die Ermittlung des Geschwindigkeitsfeldes in einem Schwall erfolgte mit PIV (Particle Image Velocimetry).

A 4: *Experimental investigation and CFD simulation of slug flow in horizontal channels*

For the investigation of stratified two-phase flow, two horizontal channels with rectangular cross-section were built at Forschungszentrum Dresden-Rossendorf (FZD). The channels allow the investigation of air/water co-current flows, especially the slug behaviour, at atmospheric pressure and room temperature. The test-sections are made of acrylic glass, so that optical techniques, like high-speed video observation or particle image velocimetry (PIV), can be applied for measurements. The rectangular cross-section was chosen to provide better observation possibilities. Moreover, dynamic pressure measurements were performed and synchronised with the high-speed camera system.

CFD post-test simulations of stratified flows were performed using the code ANSYS CFX. The Euler-Euler two fluid model with the free surface option was applied on grids of minimum 4·105 control volumes. The turbulence was modelled separately for each phase using the k-ω based shear stress transport (SST) turbulence model. The results compare well in terms of slug formation, velocity, and breaking. The qualitative agreement between calculation and experiment is encouraging and shows that CFD can be a useful tool in studying horizontal two-phase flow.

Furthermore, CFD pre-test calculations were done to show the possibility of slug flow generation in a real geometry and at relevant parameters for nuclear reactor safety. The simulation was performed on a flat model representing the hot-leg of the German Konvoi-reactor, with water and saturated steam at 50 bar and 263.9 °C. The results of the CFD-calculation show wave generation in the horizontal part of the hot-leg which grow to slugs in the region of the bend.

A 4: *Experimentelle Untersuchung und CFD-Simulation von Schwallströmung in horizontalen Kanälen*

Für die Untersuchung von horizontalen, geschichteten Zweiphasenströmungen wurden am Forschungszentrum Dresden-Rossendorf (FZD) zwei Kanäle gebaut. Diese Kanäle erlauben die Analyse von gleichgerichteten Luft-Wasser Strömungen, insbesondere die Entstehung von Schwallströmungen unter atmosphärischen Druck- und Temperaturbedingungen. Die Testsektionen sind aus Plexiglas gefertigt, so dass die Anwendung von optischen Messmethoden, wie etwa PIV-Technik bzw. die Verwendung einer Hochgeschwindigkeitskamera, möglich sind. Der rechteckige Querschnitt wurde ausgewählt, um diese Messmethoden optimal einsetzen zu können. Zusätzlich wurden noch dynamische Druckmessungen durchgeführt und mit der Hochgeschwindigkeitskamera synchronisiert.

CFD-Nachrechnungen dieser geschichteten Strömungen wurden mit dem kommerziellen Strömungsberechnungscode ANSYS CFX durchgeführt. Das Euler-Euler Zweifluid-Modell mit der Option für freie Oberflächen wurde auf einem Berechnungsgitter mit 4·105 Kontrollvolumen angewandt. Die Turbulenz konnte mit einem separaten Ansatz für die jeweilige Phase mit dem k-ω basierenden SST (shear stress transport) Modell beschrieben werden. Die Ergebnisse der Berechnungen stimmen gut im Hinblick auf Schwallentstehung und –geschwindigkeit überein. Diese qualitativ gute Übereinstimmung zeigt auf, dass CFD als nützliches Tool zur Beschreibung von horizontalen Zweiphasenströmungen eingesetzt werden kann.

Zusätzlich wurden Vorrausrechnungen mit ANSYS CFX unter Reaktorbedingungen durchgeführt, welche in der Sicherheitsanalyse von Bedeutung sind. Die Simulation beschreibt einen flaches Heißstrangmodell des deutschen Druckwassereaktors vom Typ Konvoi unter Störfallbedingungen mit einem Zweiphasengemisch Wasser bzw. Wasserdampf bei 50 bar und 263.9°C. Die Resultate dieser CFD-Berechnung zeigen die Entstehung von Wellenformationen im horizontalen Teil des Heißstranges und die Ausbildung von periodischen Schwällen im Bogen zur Dampferzeugerkammer.

A 5: *CFD models for poly-dispersed bubbly flows*

Many flow regimes in Nuclear Reactor Safety Research are characterized by multiphase flows, with one phase being a continuous liquid and the other phase consisting of gas or vapour of the liquid phase. In dependence on the void fraction of the gaseous phase the flow regimes e.g. in vertical pipes are varying from bubbly flows with low and higher volume fraction of bubbles to slug flow, churn turbulent flow, annular flow and finally to droplet flow. In the regime of bubbly and slug flow the multiphase flow shows a spectrum of different bubble sizes. While disperse bubbly flows with low gas volume fraction are mostly mono-disperse, an increase of the gas volume fraction leads to a broader bubble size distribution due to breakup and coalescence of bubbles. Bubbles of different sizes are subject to lateral migration due to forces acting in lateral direction different from the main drag force direction. The bubble lift force was found to change the sign dependent on the bubble size. Consequently this lateral migration leads to a de-mixing of small and large bubbles and to further coalescence of large bubbles migrating towards the pipe center into even larger Taylor bubbles or slugs. An adequate modelling has to consider all these phenomena. A Multi Bubble Size Class Test Solver has been developed to investigate these effects and test the influence of different model approaches. Basing on the results of these investigations a generalized inhomogeneous Multiple Size Group (MUSIG) Model based on the Eulerian modelling framework has been proposed and was finally implemented into the CFD code CFX. Within this model the dispersed gaseous phase is divided into N inhomogeneous velocity groups (phases) and each of these groups is subdivided into Mj bubble size classes. Bubble breakup and coalescence processes between all bubble size classes Mj are taken into account by appropriate models. The inhomogeneous MUSIG model has been validated against experimental data from the TOPFLOW test facility.

A 5: *CFD Modelle für polydisperse Blasenströmungen*

In vielen für die Reaktorsicherheitsforschung relevanten Untersuchungen werden Mehrphasenströmungen betrachtet, bei denen eine kontinuierliche Flüssigkeitsphase und eine gasförmige Phase als Dampf der Flüssigkeit vorliegen. Je nach dem Volumenanteil der Gasphase bilden sich z.B. in vertikalen Rohren Strömungsformen heraus, die von Blasenströmungen mit geringem oder hohem Gasanteil über Pfropfenströmungen, aufgewühlt turbulenten Strömungen, Ringströmungen bis hin zu Tropfenströmungen variieren können. In den Bereichen der Blasen- und Pfropfenströmungen gibt es ein breites Spektrum von Blasengrößen. Während Blasenströmungen bei geringem Gasgehalt meist monodispers sind, führt eine Erhöhung des Gasanteils auf Grund von Blasenkoaleszenz und –zerfall zu breiteren Blasengrößenverteilungen. Zusätzlich zur Widerstandskraft, die der Relativbewegung der Blase zur Flüssigkeit entgegenwirkt, müssen laterale Kräfte berücksichtigt werden.

Eine dieser Kräfte, die Liftkraft, wechselt ihr Vorzeichen mit zunehmender Blasengröße. Das führt zu einer Separation großer und kleiner Blasen, die wiederum starken Einfluss auf die Entwicklung der Strömung hat und z.B. einen Übergang zu einer Pfropfenströmung bewirken kann. Die Modellierung muss all diese Phänomene berücksichtigen. Ein Mehrblasenklassen-Testsolver wurde zur Untersuchung der Effekte und zum Test unterschiedlicher Modellansätze entwickelt. Basierend auf den Ergebnissen dieser Untersuchungen wurde ein Konzept für ein Mehrblasenklassenmodell, das Inhomogene MUSIG Modell vorgeschlagen und schließlich in den CFD Code CFX implementiert. In diesem Modell erfolgt eine Unterteilung der dispersen Phase in N Geschwindigkeitsgruppen (Phasen). Jede dieser Gruppen kann wiederum in Mj Blasenklassen unterteilt werden. Durch geeignete Modelle werden Übergänge zwischen diesen Gruppen durch Blasenkoaleszenz und –zerfall modelliert. Das inhomogene MUSIG-Modell wurde an Hand von TOPFLOW-Daten validiert.

A 6: *Turbulent dispersion of bubbles in poly-dispersed gas-liquid flows in a vertical pipe*

Turbulence dispersion is a phenomenon of practical importance in many multiphase flow systems. It has a strong effect on the distribution of the dispersed phase. Physically, this phenomenon is a result of interactions between individual particles of the dispersed phase and the continuous phase turbulence eddies. In a Lagrangian simulation, a particle-eddy interaction sub-model can be introduced and the effect of turbulence dispersion is automatically accounted for during particle tracking. Nevertheless, tracking of particle-turbulence interaction is extremely expensive for the small time steps required. For this reason, the Lagrangian method is restricted to small-scale dilute flow problems. In contrast, the Eulerian approach based on the continuum modelling of the dispersed phase is more efficient for densely laden flows. In the Eulerian frame, the effect of turbulence dispersion appears as a turbulent diffusion term in the scalar transport equations and the so-called turbulent dispersion force in the momentum equations. The former vanishes if the Favre (mass-weighted) averaged velocity is adopted for the transport equation system. The latter is actually the total account of the turbulence effect on the interfacial forces. In many cases, only the fluctuating effect of the drag force is important. Therefore, many models available in the literature only consider the drag contribution. A new, more general derivation of the FAD (Favre Averaged Drag) model in the multi-fluid modelling framework is presented and validated in this report.

A 6: *Turbulente Blasendispersion in einer polydispersen Rohrströmung*

Die turbulente Dispersion ist ein wichtiges Phänomen in Mehrphasenströmungen. Sie hat starken Einfluss auf die lokale Verteilung der dispersen Phase. Die physikalische Ursache der turbulenten Dispersion liegt in der Wechselwirkung der einzelnen Partikel der dispersen Phase mit den Turbulenzwirbeln der kontinuierlichen Phase. In einer Lagrange'schen Betrachtungsweise kann ein entsprechendes Modell für die Wechselwirkung eingebaut und separat für jedes Partikel berücksichtigt werden. Dafür ist allerdings eine sehr hohe Orts- und Zeitauflösung erforderlich, die solche Simulationen auf kleinskalige Probleme mit wenigen dispersen Partikeln beschränkt. Daher wird für Strömungen mit höherer Partikelbeladung i.a. eine Eulerscher Betrachtungsweise benutzt. In diesem Fall wird die turbulente Dispersion in Form eines turbulenten Diffusionsterms in der Massenerhaltungsgleichung und

einer turbulenten Dispersionskraft in der Impulserhaltungsgleichung berücksichtigt. Der Diffusionsterm verschwindet im Fall einer Favre-Mittellung (massengewichtete Mittelung) der Geschwindigkeit in den Transportgleichungen. Die turbulente Dispersionskraft ergibt sich hingegen aus dem Turbulenzeffekt der Kräfte an den Phasengrenzflächen. Oft ist dabei nur der Schwankungsanteil der Drag-Kraft wichtig. Daher berücksichtigen viele der in der Literatur verfügbaren Modelle nur diesen Anteil. Im vorliegenden Bericht wird eine neue und allgemeinere Form der turbulenten Dispersionskraft abgeleitet und validiert.

A 7: *Validation of the Multiple Velocity Multiple Size Group (CFX10.0 N x M MUSIG) Model for poly-dispersed multiphase flows*

To simulate dispersed two-phase flows CFD tools for predicting the local particle number density and the size distribution are required. These quantities do not only have a significant effect on rates of mixing, heterogeneous chemical reaction rates or interfacial heat and mass transfers, but also a direct relevance to the hydrodynamics of the total system, such as the flow pattern and flow regime. The Multiple Size Group (MUSIG) model available in the commercial codes CFX-4 and CFX-5 was developed for this purpose. Mathematically, this model is based on the population balance method and the two-fluid modelling approach. The dispersed phase is divided into N size classes. In order to reduce the computational cost, all size groups are assumed to share the same velocity field. This model allows to use a sufficient number of particle size groups required for the coalescence and breakup calculation. Nevertheless, the assumption also restricts its applicability to homogeneous dispersed flows. We refer to the CFX MUSIG model mentioned above as the homogeneous model, which fails to predict the correct phase distribution when heterogeneous particle motion becomes important. In many flows the non-drag forces play an essential role with respect to the bubble motion. Especially, the lift force acting on large deformed bubbles, which is dominated by the asymmetrical wake, has a direction opposite to the shear induced lift force on a small bubble. This bubble separation cannot be predicted by the homogeneous MUSIG model. In order to overcome this shortcoming we developed an efficient inhomogeneous MUSIG model in cooperation with ANSYS CFX. A novel multiple velocity multiple size group model, which incorporates the population balance equation into the multi-fluid modelling framework, was proposed. The validation of this new model is discussed in this report.

A 7: *Validierung des N x M MUSIG Modells für polydisperse Mehrphasenströmungen*

Zur Simulation disperser Zweiphasenströmungen werden CFD Codes zur Berechnung der lokalen Partikeldichte und ihrer Größenverteilung benötigt. Diese Größen beeinflussen sowohl die Vermischung, die Reaktionsraten im Fall heterogener chemischer Reaktionen oder den Massen- und Energietransfer zwischen den Phasen als auch die Dynamik der Strömung. Für diesen Zweck wurde ein Mehrblasenklassenmodell (MUSIG) entwickelt. Es ist in den CFD Codes CFX-4 und CFX-5 verfügbar. Das Modell basiert auf einer Populationsbilanz und einem Zwei-Fluid-Ansatz. Die disperse Phase wird dabei in N Gruppen unterteilt. Zur Begrenzung des Rechenaufwands wird nur ein Geschwindigkeitsfeld für alle Blasenklassen berücksichtigt. Dieses Modell gestattet die Berücksichtigung einer genügend großen Anzahl

von Blasenklassen für Blasenkoaleszenz und –zerfall. Allerdings ist die Anwendung dieses Ansatzes auf homogene Strömungen begrenzt und wird daher als homogenes MUSIG-Modell bezeichnet. Es versagt, wenn eine heterogene Partikelbewegung simuliert werden soll. In vielen Strömungen sind die s.g. Non-Drag-Kräfte für die Partikelbewegung von Bedeutung. Insbesondere hat die Lift-Kraft im Fall großer, deformierbarer Blasen, die durch Asymmetrien der Nachlaufströmung einer Blase bestimmt wird das entgegengesetzte Vorzeichen der scherinduzierten Lift-Kraft bei kleinen Blasen. Die Separation der kleinen und großen Blasen kann mit dem homogenen MUSIG-Modell nicht simuliert werden. Um diese Beschränkung zu überwinden wurde in Zusammenarbeit mit dem Codeentwickler ANSYS ein effizientes inhomogenes MUSIG-Modell entwickelt. Dieses neue Modell mit mehreren Geschwindigkeitsgruppen für die disperse Phase beruht auf einem Multi-Fluid-Ansatz unter Einbeziehung einer Populationsbilanz. Im vorliegenden Bericht wird die Validierung des Modells diskutiert.